TRANSIENT LIQUID PHASE BONDING OF AEROSPACE SINGLE CRYSTAL RENE-N5 SUPERALLOY

By

JAMES TOLULOPE ADU

A thesis submitted to the faculty of Graduate Studies in partial fulfillment of the requirements for the degrees of

MASTER OF SCIENCE

Department of Mechanical Engineering,
University of Manitoba, Winnipeg
Canada

ACKNOWLEDGEMENT

In the first instance, my profound gratitude goes to my able advisor, Dr. M.C. Chaturvedi for giving me the rare opportunity to work on this notable project as well as provided me with the needed financial resources. Also, I would like to express my heartfelt appreciation to my co-advisor, Dr. Olanrewaju Ojo, for his patience, encouragement, valuable time, scholarly contributions, and most importantly, his mentorship. He has taught me more than I could ever give him credit for here. For this, I am most grateful.

I would like to thank the University of Manitoba for the award of IGSES and NSERC for their financial support. Special appreciation goes to the following persons: Mr. Gbenga Asala, Mallikarjuna Thammaiah, Dr. L.N. Zhang, Dr. Kunle Oluwasegun, and Dr. L.O. Osoba for their constant needful guidance during this work. It is a great pleasure to acknowledge the technical support from Mike Boswick and Trevor Smith as regards the use of facilities available for this research work.

I want to thank all my friends and colleagues: Oluyemi Aina, Emmanuel Adejumo, Oluwasanmi Oguntuase, Jamiu Mogbolagbe, Chidinma Anyanwu, Deborah Michael, Taiwo Dada, Nnaemeka Ugodilinwa, Ajayi Oluwatomisin, Francis Amushi, Hamid Reza Abed, Olusola Bamidele and Osamudiamen Olaye for their support throughout this MSc program.

I am grateful to Aina Johnson, Mr. Muyiwa Atoyebi, Dayo Wilson, Mr. & Mrs. Omigbodun, Barrister Davidson, Dr. D.A. Adetan, Dr. H.A. Owolabi, Hon. Niyi Owolade and family, Hon. Muyiwa and family, Ven S.W. Ojelade and the entire congregation of All Souls' Ang. Church, Osogbo as well as Dr. D.K. Olukoya and MFM (Nigeria and Winnipeg) for their immense contributions towards the realization of this program.

I deeply appreciate the love of my family members: 'Tosin Adu, Dr. 'Tomide Adu, Dr. Temitope Adu, Mr. & Mrs. Adu and my fiancée, Adesewa Abigail Owoeye

Lastly, I wish to reference my heavenly God for all that He has done to beautify my life.

LIST OF ACRONYMS

AC: Alternating Current

AEW: Average Eutectic Width

OSZ: On-cooling Solidified Zone

DAZ: Diffusion Affected Zone

FCC: Face Centered Cubic

GMAW: Gas Metal Arc Welding

GTAW: Gas Tungsten Arc Welding

HAZ: Heat Affected Zone

ISW: Isothermal Solidified Width

ISZ: Isothermal Solidified Zone

MPD: Melting Point Depressant

OM: Optical Micrograph

PX: Poly Crystal

SAW: Submerged Arc Welding

SX: Single Crystal

TCP: Topologically Close-Packed

TLP: Transient Liquid Phase

DEDICATION

I dedicate this dissertation to the Almighty God and my friends whom God had used in divers ways to get me to this stage of my life.

ABSTRACT

Due to a major concern of susceptibility of single crystal weld to solidification cracking, transient liquid phase (TLP) bonding has been developed as an attractive alternative method for the repair of these single crystal superalloys. In this research, the effect of process parameters on the joint microstructure of TLP bonded single crystal Nickel-base superalloy, Rene-N5 using the conventional filler, Nicrobraz 150 is investigated. The bonding experiments are performed at the bonding temperatures, 1090^{o}C to 1200^{o}C for bonding times ranging from 1 to 50 hours. The results show a variable isothermal solidification rate constant, which can be attributable to atomic diffusion coefficient that is varying with concentration and time. Furthermore, an increase in the bonding temperature is observed to result in a decrease in isothermal solidification rate constant (slope), which is in contrast to what is expected based on a binary system. The reduction in isothermal solidification rate constant may be due to difference in phase relationship in simple Ni-B binary system compared to that in multi-component Rene-N5 alloy system. Moreover, the experimental results show that the addition of additive powder material to a conventional filler alloy powder reduces the processing time compared to the use of only conventional filler, which can enhance the effectiveness of the bonding process for commercial application.

TABLE OF CONTENT

LIST OF FIGURES

LIST OF TABLES

CHAPTER 1 - INTRODUCTION

1.1 Background Information

The development of the first single crystal (SC) turbine blade for aircraft jet engines in recent times has paved the way for the continued use of Nickel-based SC superalloys for high temperature applications. These superalloys are advanced materials that have single grain owing to the processing technique employed for their production known as directional solidification [1], [2], [3], [4]. The engine manufacturers opt for the second generation Nickel-based SC superalloys as raw materials (see Figure 1.1) for hot section components since they demonstrate excellent resistance to high-temperature oxidation and corrosion, exceptional mechanical properties and phase stability while subjected to service conditions at elevated temperatures [2], [5], [6]. Rene-N5 is classified as a second generation alloy having rhenium concentration at about 3-4 wt. % among the Nickel-based SC superalloys developed at General Electric [2], [7], [8]. The strengthening effect in this alloy is governed by two mechanisms, namely solid solution and precipitate hardening [8], [9].

The harsh operating conditions encountered by superalloys particularly single crystal superalloys (including Rene-N5) after a protracted period of service conditions often lead to abrupt degradation of the inherent thermo-mechanical behaviors. This degradation is attributed to creep, fatigue, and aggressive processes of oxidation-corrosion [8], [10], [11], [12]. Generally, replacement and repair actions are considered as a remedy to this problem of damaged parts. Repair action is widely utilized relative to replacement because it has been shown to be cost-effective [13]. Welding and brazing have been successfully applied on superalloys with remarkable successes. However, these joining techniques have some major drawbacks such as stress-induced cracks when applied on gamma prime strengthened alloys [9], [10], [11]. It is observed that materials, such as Rene-N5, contains γ'-promoting alloying

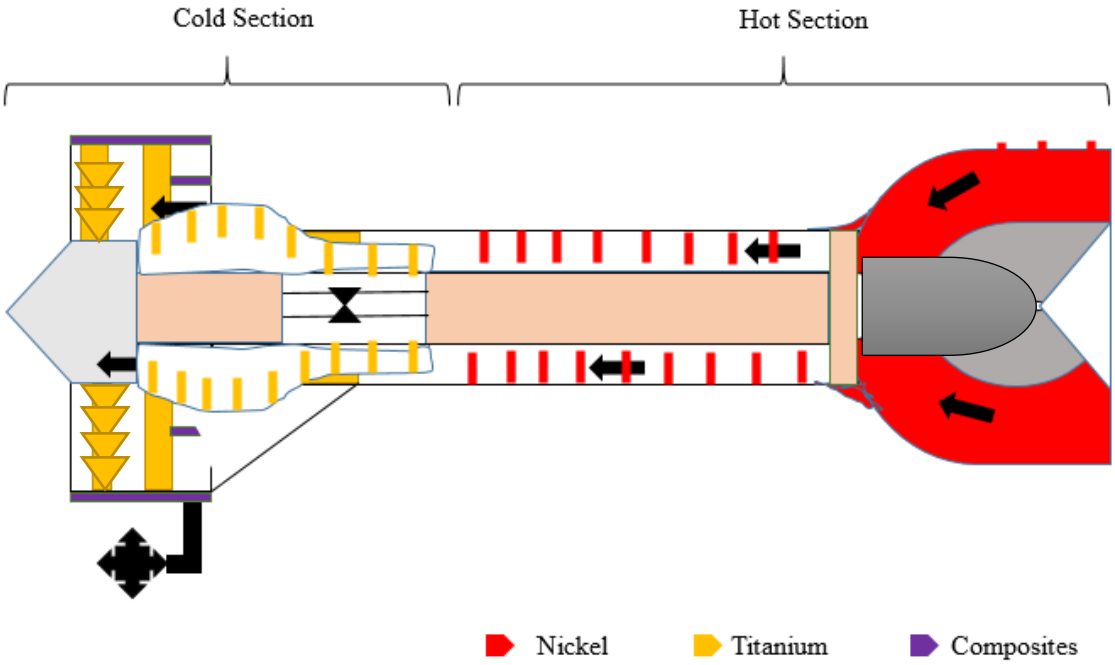

Figure 1.1: Schematic diagram of materials application in a gas turbine [20]

elements in an amount that is substantial to cause stress-induced cracks especially within the heat-affected zones (HAZ) [8], [9], [11], [12], [14], [15]. This noticeable difficulty is the reason for the name, "difficult-to-weld" for these alloys, as shown in Figure 1.2 [10], [16]. A developed method that could be used as an attractive alternative due to its peculiarity of combining the characteristic benefits of brazing and diffusion bonding is transient liquid phase bonding (TLP). Other advantages of this method are cost-effectiveness and excellent joint integrity [10], [12], [17], [18].

During TLP bonding, a filler alloy which contains melting point depressants (MPD) is properly located between the surfaces of the materials to be joined (base metal) and arranged accordingly to make the joint assembly. The assembly is heated in a vacuum furnace to a pre-determined bonding temperature which is usually between the solidus of the base metal and liquidus of the filler alloy. The process proceeds with the melting of the filler alloy, which prompts dissolution of the base metal to establish local equilibrium. Activation of the isothermal solidification is as a result of the vacancy diffusion of the MPDs into the base metal as the assembly is retained at the bonding temperature for a specific holding time [14], [15], [17], [18].

Since it is the commonest practice to use single crystal turbine blade instead of polycrystalline turbine blade [19], the efficient joining of single crystal superalloys is crucial towards extending the service life of hot-section components. This joining is not only meant for post-service repairs but also for fabrication demands. Due to the limitations on the use of third generation single crystal superalloys, there is a need to optimize the applications of various second generation single crystal alloys. This is to satisfy the drive for overall efficiency in aero-engines and land-based turbines in terms of cost reduction and performance. Consequently, it is essential to fully explore the benefits of TLP, with respect to traditional repair methods, for satisfactory joining of similar difficult-to-weld alloys. This would be achieved by adequate control of the kinetics of TLP through the governing process parameters such as bonding

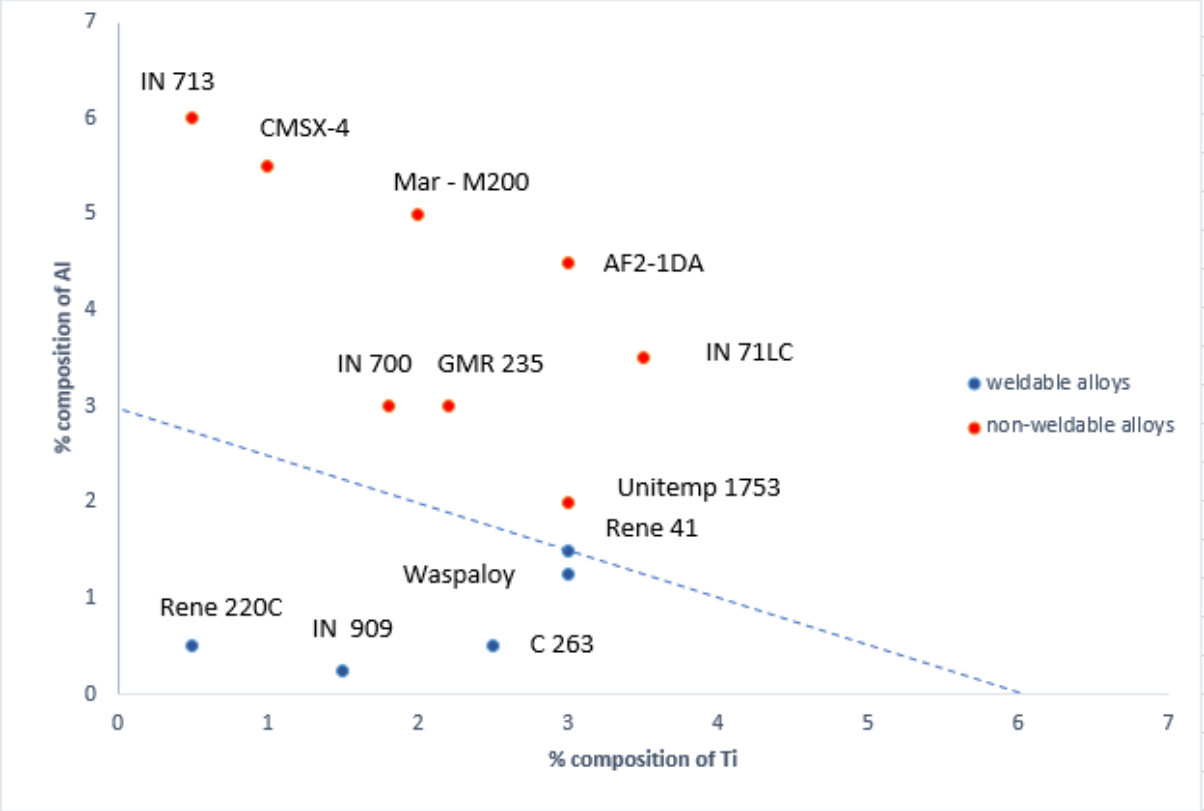

Figure 1.2: Diagram showing weldability assessment of superalloys [21]

temperature, bonding time and filler composition so as to obtain a joint that exhibits microstructural features indistinguishable from that of the base metals and can perform to fulfill service requirements.

Several studies had been done on TLP bonding of single crystal Ni-base superalloys [6], [7], [22], [23], [24], [25], [26]; however, further work still need to be done to add to the existing knowledge as regards the interrelationship between process parameters and joint microstructure, particularly single crystal (SX) Rene-N5. Therefore, this study has been carried out to investigate the effect of process parameters on joint microstructure during TLP bonding of SX aerospace Rene-N5.

1.2 Research Objectives

The objective of this research work is to investigate the influence of process parameters, specifically, holding time, bonding temperature and filler alloy on the joint microstructure produced by TLP bonding of single crystal Rene-N5.

1.3 Summary of Work Done

Samples of Rene-N5 were bonded at temperatures between 1090^{o}C and 1200^{o}C inclusive for bonding times of 1 hour, 5 hours, 10 hours, 15 hours, 25 hours, and 50 hours using 200 µm gap size and filler, NB-150, to achieve the research objective. To study the effect of temperature and time, experiments were conducted at bonding temperatures of 1090^{o}C, 1120^{o}C, 1150^{o}C, and 1180^{o}C at the above-stated bonding times. The effect of filler alloy on the microstructure of single crystal Rene-N5 was studied. Two types of filler alloy were used, namely: 100% conventional filler and powder mixture (which is a combination of conventional filler and additive powder). The effects of certain factors on the extent of melting of the additive powder were investigated by conducting surface deposition at temperatures of 1180^{o}C and 1200^{o}C for 1 hour. These factors investigated are temperature, mix ratio, powder size, and type of additive.

This is to obtain the condition of complete melting of the additive powder so as to avoid formation of stray grains. Lastly, experimental work was performed to investigate the effect of using additive powder mixture instead of conventional filler on the processing time.

1.4 Major Findings

Microstructural analysis performed on the bonded joint reveals that it is comprised of three regions, namely: Isothermal Solidified Zone (ISZ), On-cooling Solidified Zone (OSZ), and Diffusion Affected Zone (DAZ). There is formation of centerline eutectic along the bonded joints owing to insufficient holding time to achieve complete isothermal solidification. The average width of the eutectic is observed to reduce with the increase in holding time. This follows a linear relationship between the width of the isothermal solidified zone and the square root of holding time up to a certain time before deviation is observed. Hence, there is variable isothermal solidification rate constant (slope), which is in contrast to the expected constant slope based on standard TLP bonding models. This observation may be attributed to the diffusion coefficient that is varying with concentration and time. Also, the numeric value obtained from computing activation energy for the diffusion of boron in Rene-N5 is high, which implies that longer processing time is required during the TLP bonding of single crystal Rene-N5.

The experimental result, obtained by increasing the bonding temperature from 1090^{o}C to 1120^{o}C, shows increase in the rate constant of isothermal solidification as the bonding temperature was increased. However, additional increase in the bonding temperature from 1120^{o}C to 1200^{o}C results in decrease in the isothermal solidification rate constant, which is in contrast to slope increment in a binary system This could be due to solidus and liquidus concentrations in a multicomponent system being different from that of binary system and are in forms, which cause the reduction in slope as the temperature increases.

Furthermore, some parameters are found to influence the extent of melting of the filler alloy. These include: temperature, powder size, mix ratio and filler alloy composition. It is observed that the extent of melting increases as powder size and mix ratio reduces. However, the extent of melting increases as temperature increases. This observation could be because the liquidus concentration reduces as the bonding temperature increases, based on the Ni-B phase diagram. Complete melting of the filler alloy containing additive powder is necessary for single crystal so as to avoid the formation of stray grains. In this part of the current work, it is observed that the use of an alloy, such as IN-738, as an additive powder is better than pure Nickel to achieve complete melting. Hence, the reason the IN-738 powder melted more than Nickel powder may be attributed to the fact that alloying elements in IN-738 reduces the melting point of Nickel.

Lastly, the experimental results show that the use of filler mixture containing 40% fine IN-738 additive powder and 60% conventional filler resulted into complete melting at 1200^{o}C and caused a considerable reduction (23.16%) in the processing time of a single crystal joint during TLP bonding when compared to the use of 100% conventional filler, NB-150. This can enhance the effectiveness of the bonding process for commercial application.

1.5 Thesis Format

Chapter 1 is an overview of the work with an ordered arrangement of subsections as background information, research objective, work done, major findings, and thesis format.
Chapter 2 contains the review of the literature on relevant concepts relating to superalloys and joining techniques. The various types of superalloys, as well as the strengthening mechanisms, are discussed. The major part of this chapter focused on the principle of operations, advantages, and disadvantages of each joining technique. The scope of this work is paraphrased to conclude this chapter.

Chapter 3 is the presentation of the materials used and experiments performed, which include sample preparations, TLP bonding, and post-bonding operations. Also, the analyses conducted on metallographic equipment are listed.

In chapter 4, the investigations on the microstructural analyses of Rene-N5 prior and after TLP bonding are reported. The detail discussions on the influence of time, temperature, and filler alloy compositions on the TLP bonded Rene-N5 are also presented. The calculation of the percentage reduction in processing time achieved with the help of additive powder is included.

Chapter 5 is the conclusion on the findings in this research work and recommendation for future work.

CHAPTER 2 - LITERATURE REVIEW

2.1 Historical Background of Superalloys

The name “superalloy” is believed to be used firstly in the middle of 1940s to designate a class of alloy with high performance at elevated temperatures [27]. This class of alloy was meant for use in gas turbine engines of military aircraft at that time. The development of the nickel-base alloys and cobalt-base alloys for turbochargers or superchargers of aircraft engine seems to originate the name “superalloys” [27]. There was speculation regarding the origin of “super-alloys” that it was initially referred to the group of stainless steel alloys. The advent of superalloys can be traced to the challenges of thermal degradation encountered in the use of aero-engines and gas turbines before World War II [28]. This was due to the delay in the technology of the aero-engines and gas turbines in the 20^{th} century. The restrictions on the applications of stainless steels [29] resulted in a need for materials that can operate at very high temperatures without failure of degradation. This started with the development of heat resistant steels during the periods of industrial revolution [27]. The craving for solutions to this problem over time led to the development of superalloys through the improvement of the pre-existing alloys to make iron-based alloys and cobalt-based alloys. Hence, superalloy is used to describe this class of iron-based alloys and cobalt-based alloys. The first set of these alloys were produced using vacuuming melting process [27]. The word ‘super’ is used to describe the excellent behavior of this class of alloys at elevated temperatures, which makes the name to be established for the class of iron-base alloys by the year 1960. This was even before adequate information about the required compositions, structure, and procedures for heat treatment needed for the successful development of these superalloys [27]. Generally, superalloys can be defined as a group of high-performance alloys with heat resistance capability and can operate at a range of temperatures of 0.7 to 0.85 of their melting temperature [27], [30], [31], [32].

These alloys have been applied in the hot sections of gas turbines and aircraft engines due to their resistance to oxidation as well as excellent creep strength from the period preceding World War II [30], [33], [34]. During the 1930s and 1950s, the progress in the development of superalloys was on microstructure optimization and process optimization [35]. The first known superalloy developed is called Nichrome [29], [35], [36] and the first successful gas turbine engine was jointly produced for aircraft in the year 1937 by Hans von Ohain and Max Hahn [35].

2.2 Types of Superalloys

Superalloys are generally known as a class of nickel alloys [37]. The two main criteria used in the classification of superalloys are:

1. The chief element in the superalloy
2. The grain structure

Based on the chief elements in the superalloy, we have three classes of the superalloy, which are nickel-based superalloy, cobalt-based superalloy, and iron-based superalloy. Based on the grain structure of the superalloy, we have three classes of superalloys which are single-crystal superalloy, polycrystalline superalloys, and directionally solidified polycrystalline superalloys. Grain boundaries serve as weak points in polycrystalline superalloys [27]. To improve the performance and mechanical properties of these alloys, a method was devised to produce columnar structures such that the grains and component axis are in parallel alignment [27]. These resulting alloys are referred to as directionally solidified superalloys. Then, single crystals were developed to suitably eliminate problems of grain boundary effect in superalloys.

2.3 Nickel-Based Superalloys

Certain corrective methods, including coating, cooling, and use of thermal resistance superalloys, have been devised to ensure thermal efficiency of aero-engines. Nickel-based

superalloys are known to be made up of alloying elements to the maximum of thirteen (13) such that their weight composition is to be about 40 percent [34], [38], [39], [40], [41]. The principal element is taken to be Nickel, which has an austenitic face-centered cubic (FCC) crystal lattice structure in the matrix phase[33], [38]. Franklin and Betteridge studied and explained the nature of gamma prime in the matrix of a superalloy by using x-ray diffraction technique [27]. Nickel-based superalloys have certain properties (such as creep strength, hot corrosion resistance, stability, etc.) that have contributed to the increase in the demand of these alloys for industrial uses. Superalloys can be produced and supplied as either cast or wrought forms. Wrought forms have high ductility, strength, and toughness [42] while the cast alloys exhibit good creep strength [33]. Cast superalloys can be further categorized into three, namely directionally solidified, conventionally cast, and single crystal. Single Crystal superalloys possess relatively excellent mechanical properties at high temperature due to the absence of grain boundaries. This has influenced the occurrence of high demand of single crystal in the manufacture of components like turbine blades of aero-engines, land-based gas turbine, and land-based natural gas-fired power generators [32], [34], [39], [32], [41], [43]. Single Crystal superalloys are alloyed with refractory elements such as rhenium, molybdenum, tungsten so as to improve the creep resistance as well as rupture properties [44], [45]. Based on the content of ruthenium and rhenium, there are six (6) classes of these alloys called generations of single crystal superalloys [33] as represented in Table 1. Despite the vital roles of these refractory elements in strengthening the matrix, there is great danger of topologically close-packed (TCP) phases being formed if subjected to long service conditions under elevated temperatures [34], [46], [47]. Rhenium is known to promote the precipitation of TCP-phases [48] that can invariably cause adverse effects on the phase stability and mechanical properties of these superalloys [49] and it is a major concern as regards the mechanical properties of polycrystalline alloys [33].

Table 2.1: Examples and classification of superalloys according to generations [33].

Classification	Elements / Alloys	Cr	Co	Mo	W	Al	Ti	Ta	V	Nb	Hf	Re	Ru
First Generation	AM1	8.0	6.0	2.0	6.0	5.2	1.2	9.0	-	-	-	-	-
	AF56	12	8.0	2.0	4.0	3.4	4.2	5.0	-	-	-	-	-
	CMSX-6	10	5.0	3.0	-	4.8	4.7	2.0	-	-	0.1	-	-
	Rene-N4	9.0	8.0	2.0	6.0	3.7	4.2	4.0	-	0.5	-	-	-
Second Generation	CMSX-4	7.0	9.0	0.6	6.0	5.6	1.0	7.0	-	-	0.1	3.0	-
	Rene-N5	7.0	8.0	2.0	5.0	6.2	-	7.0	-	-	0.2	3.0	-
Third Generation	CMSX-10	2.0	3.0	0.4	5.0	5.7	0.2	8.0	-	-	0.1	6.0	-
	Rene-N6	4.2	13	1.4	6.0	5.8	-	7.2	-	0.1	0.2	5.4	-
Fourth Generation	PWA1497	2.0	17	2.0	6.0	5.6	-	8.3	-	-	0.2	6.0	3.0
Fifth Generation	TMS 162	3.0	5.8	3.9	5.8	-	5.6	-	-	0.1	4.9	6.0	-
Sixth Generation	TMS 238	4.6	6.5	1.1	4.0	5.9	-	7.6	-	-	0.1	6.4	5.0

This problem is reduced with the development of fourth and fifth generation nickel base superalloys relative to lower generation classes of superalloys [48] by the disruption of precipitation of TCP phases due to the addition of ruthenium into the composition of these superalloys [50]. Long-time service use at high-temperature applications is assisting the formation of these phases within the microstructure of single crystal superalloys despite all the efforts made at the production stage of manufacturing single crystal superalloys to eliminate TCP-phases precipitation.

2.4 Strengthening Mechanism and Metallurgy for Superalloys

Strengthening mechanisms are means by which essential properties of the superalloys are improved such that they can perform efficiently in their various applications, particularly aero-engine. This makes it a necessity to use quality materials in the manufacture of the components that make up these power-unit engines. The term "quality material" refers to having inherent properties that meet these engine service conditions which are regarded to be harsh and a great deal of efficiency, as well as safety, is required [10]. Different materials have different microstructures [28]. It is the chemical composition that dictates the constituents of the phase, and the phases make up the microstructure that is formed [28]. The microstructures determine the properties as well as the performance of the materials [28], [10]. For instance, grain sizes play vital roles in determining the mechanical properties of metals and their alloys. A fine grain results in excellent mechanical properties like tensile and fatigue life properties, whereas the coarse grain improves the creep and crack growth, especially at high temperatures [51]. Failure of materials is inevitable over the service conditions after a certain time, but it can be reduced by taking adequate preventive measures. The superalloys are used in the manufacture of the components of these engines due to their reliability, phase stability, excellent performance at elevated temperatures, and cost efficiency [10].

The strength of metals and their alloys can be improved majorly in two ways, namely, methods of alloying and processing, which could be mechanical, thermal, or thermomechanical processes [51]. The essence of strengthening mechanism is to impede the dislocation glide, and this can be achieved by lattice resistance, solid solution strengthening/hardening, precipitation of intermetallic phases or strengthening [51], [38], [52] and grain boundary strengthening. The latter is only applicable to polycrystalline superalloy. The FCC crystal lattice of nickel enables these superalloys the greater ability to dissolve many other elements [38] in the form of interstitial and substitution solute atoms. The purpose is to impede the dislocation glide at high temperatures [51], [53] and thus increase the yield strength of superalloys via solid solution strengthening. Nickel-base superalloys are generally known to have face center cubic structure, which is a gamma matrix comprising of nickel, chromium, cobalt, molybdenum, and iron [54]. Nowadays, the alloy optimization process is commonly adopted to strengthen the matrix of nickel-base superalloys by the addition of substitutional elements into the solid solution due to the electronic configuration of nickel [51], [55].

Elements like titanium and aluminum are considered essential solutes relative to microstructural properties of nickel-based superalloys and they are usually with a total concentration that is not greater than ten atomic percent [28], [56], [57]. They produce a two-phase equilibrium microstructure which consists of evenly distributed gamma-prime (γ') in a gamma (γ) face center cubic matrix of nickel base superalloy [34], [39], [47], [58]. The quantity of gamma prime (γ') is determined by temperature and chemical composition [57] which controls their volume fraction in the matrix. The gamma prime is an ordered hardening precipitate, and its crystallographic inter-relationship with the gamma matrix contributes to the high strength and creep resistance of superalloys [40], [54], tensile strength and fatigue life at elevated temperatures. The size and forms of these hardening precipitate are controlled by the formation processes using standard heat-treatment procedure [59]. The sizes of the gamma

prime contribute to the yield strength of the material through the interaction between these intermetallic phases and the dislocation [54]. The composition of the gamma prime affects their ability to resist shearing [34], [38], [58] and their respective volume fraction is influenced by their chemical compositions. The low volume fraction with large inter-spacing particle and coarse precipitates can cause the matrix dislocation to bend around the precipitate with regards to Orowan mechanism [28], [38], [54]. Otherwise, there is dislocation cutting in the case of coarse grains [28], [54]. Hence, the efficient performance of nickel-base superalloys can be attributed to their microstructure and chemical compositions [59]. These are essential factors, among others, such as the size of the precipitate, forms, and phase composition, that are considered in alloy optimization [34], [38], [58].

2.5 Microstructure of Nickel-Base Superalloy

The microstructure of Nickel-based superalloys contains the following phases described below:

- ✓ Gamma Matrix: This is denoted by a Greek letter with this symbol, γ. It is a continuous nonmagnetic phase matrix of FCC Nickel [28]. As an austenitic solid solution phase [56], it can dissolve certain solutes such as tungsten, cobalt, iron, molybdenum, and chromium.
- ✓ Gamma Prime: This is denoted by this symbol, γ'. It contains solute atoms such as titanium and aluminum as chief of others. This phase is responsible for superior strength at high temperature as well as creep resistance [28]. The constituent element ratio is Ni_3Al, and the microstructure contains ordered L12 crystal [41]. The schematic diagram of the microstructure is shown in Figure 2.1.
- ✓ Gamma Double Prime: This is denoted by this symbol, γ''. Solute atom like niobium combines with nickel form body-centered tetragonal Ni_3Nb in the presence of iron. This

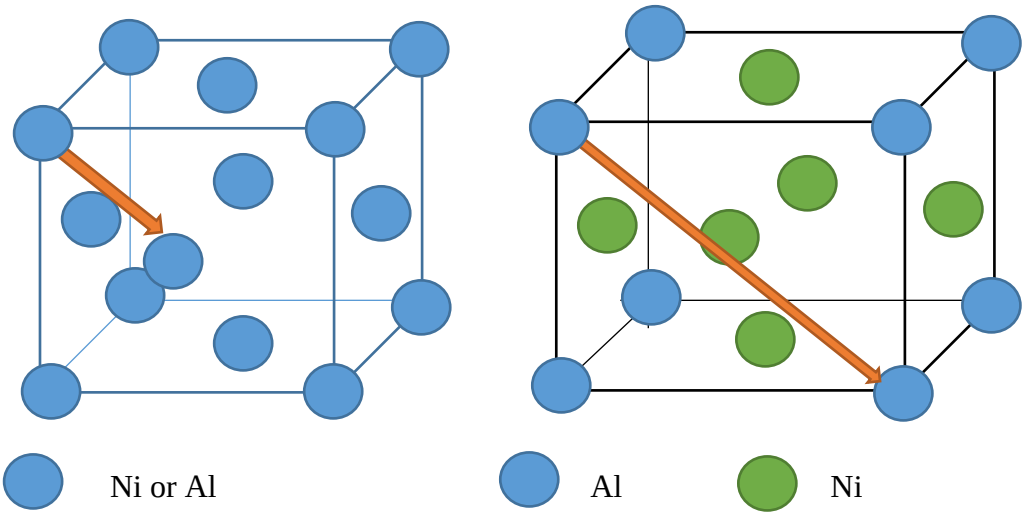

Figure 2.1: Schematic representation of the gamma structure and gamma prime structure [56].

phase is responsible for very suitable strength within temperature ranges from low to intermediate [28].

- ✓ Borides: These are formed when the diffusing boron solutes exceed their solubility in Nickel.
- ✓ Grain Boundary γ': The combined effect of service condition and heat treatments produce this phase at grain boundaries. They are responsible for better rupture properties [28], [56].
- ✓ Topologically close-packed (TCP) Type Phase: These phases are in the form of plates and needles. Examples are σ and μ, which are brittle phases. They lower the rupture strength and ductility [28].
- ✓ Carbides: Carbon reacts with certain metals to form carbides. They are very good for strengthening the grain boundaries.

2.6 Aerospace Single Crystal Rene-N5

Rene-N5 is a second generation Nickel-based superalloy and was produced at General Electric about three decades ago [60], [61]. The composition by weight of each constituent elements is shown in Table 2.2 and contains about 3-4% concentration of rhenium [7]. Rene-N5 has a stable microstructure and strength that is capable of resisting the effect of high-temperature degradation [7]. It has a better creep strength by 30^{o}C greater than the first generation superalloys [62]. The density of Rene-N5 is 8.63g/cm^{3} [62], [50], [63] and its young modulus is found to be between 140-150 GPa [64]. The absolute melting range for this alloy is found to be between 1651 K and 1653 K [65] and suitably strengthened by gamma prime formers with the addition of solute elements such as tungsten, tantalum, and chromium [66]. The mechanical properties are greatly improved by the ratio of two vital constituent elements, which are aluminum and titanium. For instance, this alloy has excellent creep strength as a result of the

Table 2.2: Percentage composition by weight of elements in Rene-N5 [41], [61], [62]

Elements	% wt composition
Ni	balance
Cr	7.0
Co	7.5 – 8.0
Mo	1.5 – 2.0
W	5.0
Ta	6.5 – 7.0
Re	3.0
Nb	-
Al	6.2
Ti	-
Hf	0.15 – 2.0
C	0.05
B	0.00 – 0.04
Y	0.01

presence of aluminum [63] but limited in its applications because of its susceptibility to the formation of crack and the cost of producing them by process of casting is very high [60]. Since this alloy retains a considerable amount of residual stresses (due to the high concentration of Ti and Al) if joined by welding (especially fusion welding), it is considered to be difficult to weld [16], [67].

2.7 Roles of Alloying Elements in Rene-N5

The excellent properties of this alloy are obtained from the individual contributions of each constituent elements. The elements and their respective roles are discussed below [56]:

i. Chromium:

- It ensures strengthening of the gamma matrix
- It ensures strengthening of the gamma prime
- It impairs the lattice mismatch
- It diminishes the energy of the antiphase boundary
- It amplifies the extent of resistance to corrosion and oxidation
- It safeguards the surface by the oxide film

ii. Cobalt:

- It ensures strengthening of the gamma matrix
- It raises the energy of the antiphase boundary
- It ensures the easy formation of the strengthening precipitate

iii. Molybdenum:

- It ensures strengthening of the gamma matrix
- It ensures strengthening of the gamma prime
- It impairs the lattice mismatch
- It raises the energy of the antiphase boundary

- It ensures the gamma prime that is stable

iv. Tungsten:

- It ensures strengthening of the gamma matrix
- It ensures strengthening of the gamma prime
- It impairs the lattice mismatch
- It ensures the gamma prime that is stable

v. Tantalum:

- It ensures strengthening of the gamma prime
- It raises the lattice mismatch
- It enhances the formation of strengthening precipitates

vi. Aluminum:

- It ensures strengthening of the gamma matrix
- It diminishes the energy of the antiphase boundary
- It amplifies the extent of resistance to corrosion and oxidation
- It safeguards the surface by the oxide film
- It enhances the formation of strengthening precipitates

vii. Hafnium:

- It builds up the grain boundary

viii. Carbon:

- It promotes the formation of phases at the grain boundary.

ix. Boron:

- It forms the borides.

2.8 Methods of Repair and Metal Joining of Superalloys

The purpose of joining of alloys such as superalloy can be categorized into three (3), namely maintenance repair, component fabrication, and joining of dissimilar metals [56]. In the first instance, high working efficiency in the use of engines is very paramount for optimum operation of these engines such as gas turbines, aero-engines at elevated temperatures. Despite the advantage of high efficiency, there is aftermath danger in running these engines at such temperatures since it can lead to quick degradation of the parts of these engines. Hence, methods of joining are required to prolong the service life as well as reduce the cost of maintenance of the engine parts with various shapes ranging from simple to complex or intricate ones. For the purpose of accomplishing a successful production process, several simple parts can be made and joined so as to obtain any complex shape assembly. Similarly, different materials with different crystal structure may be joined, e.g., a combination of single crystal and polycrystalline alloys into a single component part.

It is important that a joining process must be neat aesthetically, cheap, and ensure the structural integrity of the joint [10]. Due to major reasons of fabrication and repair as a result of the failure, there are already existing methods of joining which can be divided into the following categories highlighted below [10], [68], [69]:

i. Physical methods
ii. Mechanical methods
iii. Chemical methods.

Mechanical joining methods are said to be localized because they are point-like attachments of parts to be joined and make use of fasteners like rivets, screws, bolts, nails, etc. This method is known for its cost-effectiveness and reliability in making joints, and the components of the joints are firmly held together by either tensile residual stresses or compressive residual stresses. This method has found applications in joining plates of ships, flanges of both high and

low-pressure vessels, interlocking seams to mention but few.

A suitable chemical reaction, involving adhesives as the commonest materials, is required to make a joint in chemical methods which can cause residual stresses in the parts to be bonded. Unlike in mechanical joints, these developed stresses are detrimental and can jeopardize the structural soundness of the bonded joint. These adhesives are either solvent-based or reaction-based [10], [69], and a major example of adhesives is epoxy resin.

Another method of joining materials is achieved by the physical method in which the joining is done by a change of state from the liquid phase to the solid phase. Examples of these methods are welding, brazing, diffusion bonding, and transient liquid phase bonding [10].

Generally, the superalloys are used in an unfriendly environment which subjects them to various failure mechanisms. Upon failure, the choice of a replacement or obtaining a newly-produced part as corrective maintenance do not justify cost and time. The feasible alternative is to repair. The physical methods of joining are vastly used more than any other method of joining to produce structurally good joints for superalloys depending on the suitability of each method as regards the parts to be joined. The highlights of these methods will be discussed further.

2.8.1 Welding

Forge welding was just a primitive method of joining metals until some inventions and discoveries were made, as far back as 2000 B.C., which are believed to give birth to the current-day welding processes. In, 1836, Edmund Davy uncover the use of acetylene gas and resistance welding was discovered in the eighteenth century, but it was not used until the early nineteenth century. Landmark progress was made in 1800 as regards the development of suitable welding techniques. The various factors considered to be vital to the use of welding processes are nature of metal that is to be joined, cost (capital) implications, types of components to be produced, job location and manufacturing methods, materials, availability of equipment and wealth of

experience of the welder [70]. The principle of operations involved in the course of welding will be discussed next.

2.8.1.1 Fusion welding

Fusion welding is a collective name for every welding technique whereby a source of heat is used locally to cause heating and melting of the parent metal to be joined. This simultaneously solidifies and cools thereafter such that the parts of the metals to be joined surrounding heat affected zone are at about room temperature [68], [71]. Fusion welding process takes simply two stages, namely [68], [72]:

- Melting of the parts to be joined
- Solidification of the welded joint.

In the course of melting, a molten pool is formed which then grows into the required dimensions [73], stabilized and maintained until solidification is completed. Additions of filler metal(s) into the pool may be done, but it is not generally used while joining metals using available welding processes. Any weld in which filler metal is not used is called autogenous weld [70]. The beads of the weld are formed with every individual pass of the source of heat during the welding process and the thickness of the component parts to be joined determines the number of beads to be formed. Various applications of fusion welding are in the following industries: construction, aerospace, chemical and petrochemical, vehicle designs and production, electronics, and power generation [74]. By carefully examining the surface of a welded joint, three separate zones can be seen, as shown in Figure 2.2, namely [10], [74]:

- ✓ The fusion zone.
- ✓ The Heat Affected Zone (HAZ) that do not melt [75].
- ✓ The parent metal or base metal zone.

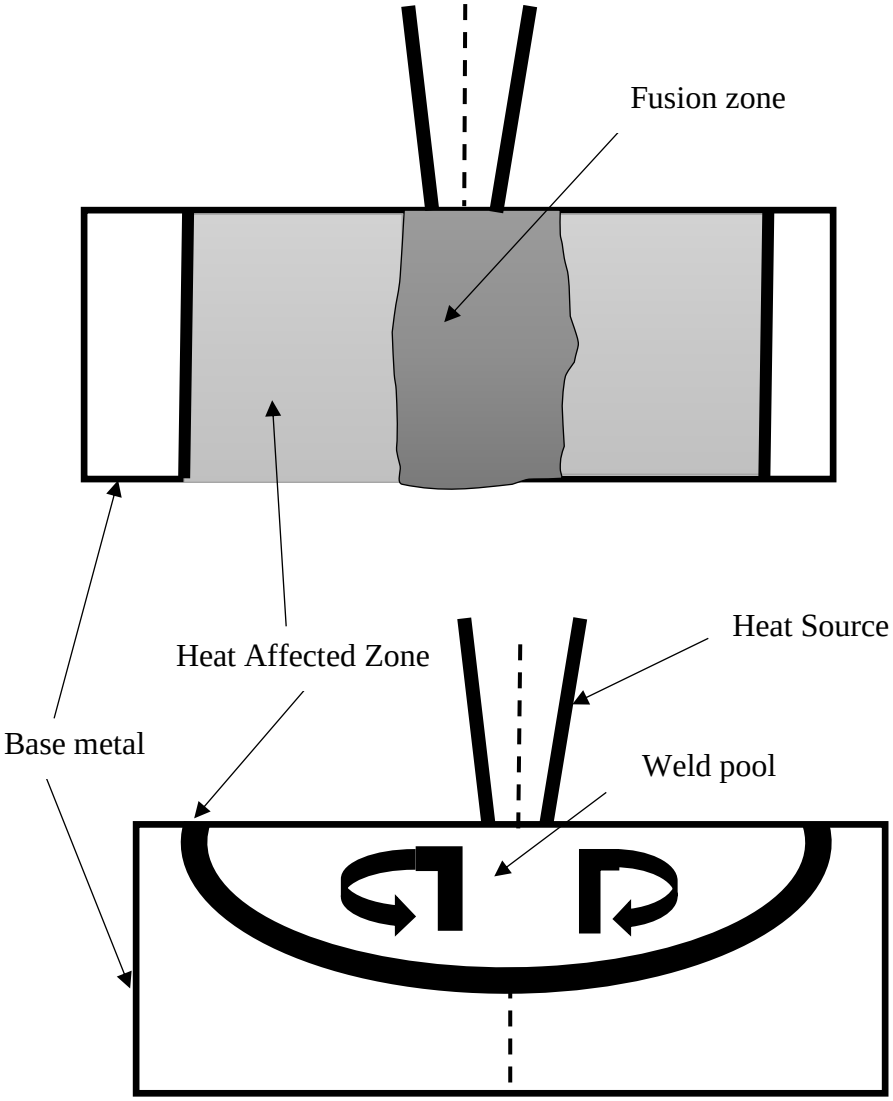

Figure 2.2: Schematic diagram of a welded component [74].

Upon the application of the heat source to the parts to be joined, there is accelerated heating, melting, and effective spread of the liquid (molten) metal in the weld pool [76]. This is as a result of fluid pressure by buoyancy, surface tension and/or electromagnetic forces if electrical energy is applied [10], [74], [76]. The subsequent transfer of heat and fluid flow control a lot of factors listed below [74], [77]:

- Weld pool size as well as shape.
- Cooling rate.
- Kinetics of various transformation reactions which occurs within the fusion zone as well as heat affected zone.

The shape of the weld determines the dendrite and grain growth selection processes [74]. Also, the partitioning of some elements such as hydrogen, nitrogen, and oxygen within the weld pool and immediate weld surroundings together with the change of state of alloying elements greatly affects the properties, microstructure, and composition of the welded joint. The sources of heat are an electric arc, high energy beams (laser or electrons) and fuel (gas flame). The power density is highest for the high energy beam (approximately 10^9 W/cm^2) and least in gas flame [73], [71]. There is great gain in increasing the power density of the source of heat. Among the benefits are the suitable depth of weld penetration, greater welding speeds, and excellent quality of the weld with damage to the parts to be welded reduced to a minimum [71]. Based on the source of heat used to accomplish a welding process, fusion welding can be sub-divided into three (3) categories. The first category comprises of gas metal arc welding (GMAW), submerged arc welding (SAW) and gas tungsten arc welding (GTAW). The second category includes electron-beam and laser beam welding. The third category includes gas welding. Though electroslag welding does not use electric arc, it is classified under arc welding for easy discussion of the types of welding processes [71]. These three major types of fusion welding processes are highlighted below [10], [70]:

I. **Gas welding:**

Oxyacetylene welding: This welding process employs the use of a fuel gas called acetylene while the required heat of welding is obtained from the burning of combustible gas in air (oxygen).

II. **Arc welding:**

Shielded metal arc welding: In this method of welding, there is the formation of a shielded arc which is achieved by the breaking down of the coating of the electrode. It is used in the construction of machines, bridges, buildings, etc.

Gas–tungsten arc welding: The electrode used for this welding is made from tungsten. In this method of welding, there is provision for the protection of the arc between the electrode and the materials to be welded by a shielding gas. It is used for tubes and pipe joints.

Plasma arc welding: The principle of operation could employ either a non-transferable arc or transferable arc, which is formed between a non-consumable electrode (made from tungsten) and weld pool. It is used virtually for all metals.

Gas–metal arc welding: In this method, it is not required to change electrode since it is continuously fed as a wire during welding. The arc is between the non-discontinuous wire electrode and weld area. It is used for all general purposes in manufacturing.

Flux-cored arc welding: The electrode has tube geometry with the flux embedded in its core. It is used for certain grades of steel as well as cast iron. It can be used for all general purposes of shop and field fabrications.

Submerged arc welding: The electrode is a bare metal, and the arc is effectively produced between the bare metal and the weld pool. A granular flux is poured on the surface of the parent metals to be welded which invariably submerged the arc, the electrode, and the weld pool. It is chiefly used for heavy steel plates.

Electroslag welding: The required heat for this type of welding is produced by the opposition to the flow of electric current. This method can be used for steels, dissimilar metals, and aluminum.

III. **High-energy beam welding:**

Electron beam welding: The required heat is generated by moving electrons with high velocity while the atmosphere for this welding must be a vacuum. This is mostly used for metals such as titanium [78], [70].

Laser beam welding: The required heat is generated by a laser beam, and it is used in power plants, ship-building, and pipelines [73].

2.8.1.2 Limitation of fusion welding

Certain elements that made up superalloys have placed restrictions on the use of available joining technique such as fusion welding since there is a strong affinity between these elements (aluminum and titanium) and oxygen [79], [21]. Hence, oxidation is a major setback due to the reaction between oxygen and these constituent elements. The microstructure of the superalloys are primarily made up of single phase of gamma and the weld zone created by fusion welding process is vulnerable to various hot cracking phenomena, e.g., solidification cracking, reheat cracking, ductility dip cracking and liquation cracking [79]. In the case of single crystal superalloys, there are three (3) major problems associated with fusion welding of these alloys which are loss of nature of single crystal superalloys, solidification cracking, and strain-age cracking [75] and they are discussed further below [75]:

i. Solidification cracking: This is also referred to as hot cracking and considered as the most common fusion zone defect in welding. In a fusion welding process, the region in the parent metal ahead of the weld pool is heated and melted such that stress (compressive) is built-up, thereby resulting into expansion. However, the region behind the weld pool is undergoing an alternate process of solidification and contraction.

Therefore, the interactions among the parent metal, weld pool, and the solidified weld region cause strength variation and tensile stresses to be developed. The cracking is said to occur if the developed thermal tensile stress is more than the yield strength of the parent metal in a region of low ductility. Such cracking, during the process of welding, is known as solidification cracking (or hot cracking). Based on weld pool theory, there is direct variation between the speed of welding and the rate of cooling of the region behind the weld pool. Thus, reduction in the size of the weld pool and increase in speed lead to a corresponding increase in the rate of cooling. If the rate of cooling is high, the thermal residual stresses formed would be high, and the joint is structurally deformed by the resulting cracks.

ii. Loss of nature of single crystal superalloys: During the process of solidification, some broken-off tips of dendrites grow into the mushy zones and the tips of these dendrites function as nuclei for the group of equiaxed grains. These grains become stray grains if they become misorientated and have grain boundary with a high angle. Formation of stray grains can impair the effectiveness of creep behavior of superalloys as a result of the formation of solidification cracking. Since single crystal superalloys are without grain boundary, there is no need for elements (such as hafnium) to promote strengthening of the boundary. This makes it very important that stray grains are not formed in single crystal superalloys due to their deleterious nature.

iii. Strain-ageing cracking: This is also called re-heat cracking [21], and it is caused by thermal stresses resulting from the combined effect of elevated temperature of service conditions and heat-treatment procedures [21]. Heat-treatment procedures can be used to remove residual stresses so as to restore the functional properties of single crystal superalloys by the precipitate strengthening. During the fusion welding, this precipitated phase can be formed in the regions within the heat affected zone (HAZ)

adjacent to the parent metal to be welded and can lead to different areas between the weld zone and the HAZ to have different strengths. Supposing fracture stress is less than the residual stress in certain areas in the course of aging; there is a high possibility that strain-age cracking will occur. This is known as heat treatment cracking after welding.

2.8.2 Soldering

Soldering is a low-strength joining technique for metals in which the heat input required is low relative to welding and the filler, known as solder, is melted at low temperature of 840° F. Similarly, the soldering technique is carried out at a lower temperature compared to the melting point of the metals intended to be joined. There are two grades of solder which are soft and hard types. Tin, lead, etc. are examples of soft solder while hard solders are copper and zinc. Surface cleaning is a pre-soldering action whereby a flux is used to get rid of unwanted oxides, scales, oil, grease, etc. from the surface of the metals to be joined. The flux could be either acidic fluxes (such as ZnCl and HCl) or non-acidic fluxes (resin). A major advantage of this process is that it can be applied to materials that are considered to have weldability that is relatively poor, which includes composite, ceramics, and plastics [10].

2.8.3 Brazing

The practice of the inhabitants of summers in Western Asia (present-day Iraq) by soldering silver and gold materials as early as 4000 B.C. [80] introduced the concept of brazing in which the filler alloy is used in the course of joining. A brazing technique is said to be effective if there is adequate heat transfer to the site of filler and the assembled joint. The process parameters that influence brazing are the rate of heating, cooling and production, heating cycle, and dimensions of materials prepared for brazing, etc.

Since the liquidus of the metals to be joined is usually higher than that of the filler metal [81],

the filler metal is rapidly heated to a temperature that is higher than 840 °F. The process is done in this manner because the brazing temperature should be greater than the melting point for the filler metal, but less than that for the metals to be joined. The common sources of heat suitable for brazing are from torch, induction heating coils, furnace to mention but few. In this process, a capillary force draws the liquid filler into the joint while heat is applied to the assembled joint. The melted parts of the joint then form a metallurgical bond through cooling to room temperature so as to complete the bonding process.

Usually, a large number of filler metals are made of pure materials or the alloys of Aluminium, Silver, Gold, Cobalt, Copper, and Magnesium and they could be in powdered form or may be fabricated as foil, tape or wire. Based on the specifications, a brazed joint can be configured as desired into a lap joint, butt joints, butt-lap joint, scarf joint or tee joint. The filler materials are required as a necessity to be cleaned with flux before brazing to guard against oxidation, and the flux helps to moisten the metal surfaces by dissolving the oxides on them. As a result of this, it creates a coating over the heated metal surfaces which would not allow oxygen to permeate. Fluxing agents can be found as a natural lime, charcoal, soda, or alkali [80].

2.8.3.1 Merits of Brazing

Brazing has a good number of benefits, which are stated below [80], [82]:

i. It is a harmless process with no melting of the materials to be joined.
ii. It retains the metallurgical integrity of the materials being joined.
iii. It is easily adapted to a variety of materials such as dissimilar, similar, metal, and non-metals for joining purposes.
iv. It produces high-quality joints with component tolerances that are greatly maintained, unlike in welding.
v. Welding associated problem such as HAZ is reduced to a minimum.

vi. It can be used for delicate thin sections that are hard to weld.

vii. There are relatively low heat input and power requirement.

2.8.3.2 Demerits of brazing

There are certain downsides to brazing as a method. These are:

i. The brazed joint has low strength when compared to welded joints.

ii. The brazed joint has low strength with respect to the metals to be joined.

iii. The joints made by brazing are not suitable for high-temperature applications

iv. The aesthetic disadvantage is a major challenge due to the color difference between the joints and the parent materials.

2.8.3.3 Methods of Brazing

Based on the source of heat applied, there are six popular brazing methods, namely [80], [83]:

- Dip method
- Infrared method
- Resistance method
- Induction method
- Torch method
- Furnace method

Moreso, there are four uncommon methods. These are:

- Microwave method
- Braze-welding method
- Exothermic method
- Laser method

2.8.3.3.1 Dip Method

Certain pre-brazing operations, which are crucial in dip brazing are cleaning, preheating, fluxing and assembling of the joint. The faying surfaces of the materials to be joined are cleaned firstly (to get rid of contaminants such as dirt, oil/grease, rust, and scales), preheated and dipped in a flux bath (chemical compound) to complete these pre-brazing operations. There is a possibility that oxides could be formed during the preheating due to chemical interactions between the surfaces and the air in the presence of heat. However, but the flux coating completely intercepts the oxide film formation and remove any unwanted oxides on the faying surfaces. The joint can now be assembled to commence brazing. By ramping the temperature to a suitable brazing temperature without melting the faying contact surfaces, the filler metal is heated and fills the gap provided. This results in a durable joint being formed through the solidification-cooling process. The process is time-efficient and applicable to electronics [80].

2.8.3.3.2 Infrared Method

The use of infrared waves has found applications in different fields/industries, including its use as a source of heat in brazing techniques. The infrared heating process is known to be faster with respect to the conventional furnace brazing [84] due to energy range for the infrared to be between 0.001eV[1] and 0.7eV [85] with respect to the electromagnetic spectrum. The heating rate and cooling rate are faster, and the evolution of the joint can be achieved in the order of seconds [86]. Infrared brazing is a joining technique whereby heating is achieved by the quartz lamps that can produce and discharge invisible infrared radiations at very high power levels and reflectors are used to focus the energy released on the joint area. It is a flexible method in such a way that the brazing atmosphere may be vacuum or inert gas under a pressure that is lower than atmospheric pressure, and the cooling of the system is done with the aid of platens

[1] eV is electron-volts

[87]. The benefits of this method are comparatively low energy requirement, rapid heating cycle, and absence of damage to the metallurgical characteristics of the materials to be bonded.

2.8.3.3.3 Resistance Method

In resistance brazing, the parts to be joined are arranged to form an electric circuit, and the required heat is generated by resistive opposition to the flow of applied current through water-cooled electrodes attached to a transformer. The resulting local heat is a measure of individual or collective resistivity of both the electrodes and materials to be joined and thereby flows into the joint, melts the filler metal and create a high-quality joint. Unlike in the conventional brazing, the necessity for the capillary drawing of the filler into the joint is eliminated in resistance brazing method since the surfaces of the materials to be joined must touch each other by employing suitable pressure between the electrodes and the assembly. Fluxes are applied in wet condition or as slurry on the parts of the joint, which must be free to move, especially during the heating stage. This method can be upgraded by incorporating a spot-welder into its application. Resistance method is faster, and there is a reduction of grain growth [80], [87].

2.8.3.3.4 Induction Method

This method uses the principle of electromagnetic induction developed by Faraday to cause local heating of the joint area in close proximity to the induction heating system, usually electric coils that converts an AC[2] into electric-magnetic fields which cut the ferromagnetic filler. This invariably induces eddy current, and corresponding heating of the filler metal occurs. The liquid filler melts and flows so as to braze the joint region. Unlike in the infrared heating, the parts to be joined are not included in the electric circuit. In order to prevent oxidation, inert gas

[2] AC is alternating current

cloud or flux is used. The heating cycle can take just seconds if the primary induction coils are very effective. The major benefits of this brazing technique are reduced distortion of component materials, faster precise heating, and durable joint [80], [88], [89].

2.8.3.3.5 Torch Method

Torch brazing is also known as a flame or oxyfuel brazing because heating is done by direct combustion of a fuel in the presence of oxygen. Torch brazing is a frequently used brazing technique due to its low-cost implications, simplicity, and adaptability for a small number of production batches, hard-to-reach applications as well as specially-designed operations. A torch that is equipped with hot gas is used to heat the joint area so as to melt the filler metal which is fed by capillary drawing into the gaps within the joint area. The most commonly used fuel gases are acetylene, natural gas, MAPP, butane, propane in air or oxygen (probably compressed). The brazing flame for torch brazing method is made up of at least two of these zones, namely: inner core, outer flame, and acetylene feathery. Based on these zones, there can be three types of flames, which are carburizing, oxidizing, and neutral flames. A very low gas-fuel ratio results into carburizing flames; otherwise, oxidizing flame is obtained. There is adequate protection against oxidation since the brazing temperature is actually below the oxidizing temperature of the brazed metals. The neutral flame (bluish/orange flame tip to prevent oxidation, white-bluish inner cone, and absence of acetylene feather) is regarded as the best flame during torch brazing, and it can raise the temperature of the joint area to the brazing temperature within 0.5 – 0.75 minutes. The modes of operation for torch brazing are manual, machine, and automated. In terms of productivity, an automatic torch brazing method is preferable to the manual or machine method [80], [87], [90], [91], [92].

2.8.3.3.6 Furnace Method

Furnace brazing method is identified as an economic means for processing numerous components at a time or joint production in intricate and large parts in various aerospace and nuclear applications/uses. This method reached the phase of commercialization in the 20th century with the development of three basic types of furnaces, which are vacuum, continuous, and retort/batch furnaces. The required heating for furnace brazing can be done by electric elements, especially. The gas or flame could be used in as much the flame does not impinge directly on the parts to be joined. The components to be brazed (which are self-jigging) are prepared by cleaning and properly positioned in the furnace while the braze is placed in close proximity to the joint or inside it. The braze takes the following forms, e.g., tape, wire, paste, foil, powder, slugs, fillings, etc. The use of flux is optional, and protective atmosphere can be used instead of flux, e.g., vacuum and gaseous atmosphere. The greatest benefit of furnace brazing is mass production brazing [80], [93], [94], [95], [96].

2.8.3.3.7 Microwave Method

The use of microwave energy has been in existence for more than 50 years for various purposes, but microwave brazing is a recent technique developed for brazing joints with ceramics especially in corrosion–resistant, high temperature, and high-performance applications. The use of microwave brazing for ceramics is at the developed stage while the joining of metals and ceramics is considered as newly developed technique. Unlike in the traditional heating, the microwave is directed unto the adjoining surfaces by high precision movements, which results into internally-generated heat by means of molecular interactions within the materials in conjunction with an electromagnetic field and thereby cause volumetric heating. During the brazing operation, the microwave reactor releases the microwave radiations so as to heat the joint assembly, and the filler material melts to cool afterward. The resulting energy is found

efficiently productive in brazing ceramics than metals, and microwave brazing is restricted to research and developments rather than industrial-commercial uses. Though the microwave brazing method is still being explored, it has proven effective in the production of blades, electronic devices, rotors, fuel cells to mention but few [80], [82], [97], [98], [99].

2.8.3.3.8 Braze-welding Method

Braze welding is referred to as bronze welding and mostly used for large castings applications. In braze welding, the melted filler is deposited into the joint and the metallurgical bond results from wetting actions as well as diffusion between the liquid and the base metal that does not melt by the applied heat via oxy-fuel flame. Though the principle of operation for fusion welding and braze welding are almost the same, the major differences are that materials to be brazed are not affected by heat unto melting and the filler is not drawn by capillary action unlike in fusion welding. The liquid braze fills the joint assembly by process of tinning. The strengths of the joints made by braze welding are generally considered commensurate to the fusion welded bonds without distorting the metallurgical characteristics of the materials to be bonded and can be suitably used for making metallic joints. Braze welding has a lot of benefits over welding by fusion such as room for joining dissimilar materials, the absence of residual stresses, reduced effect of heat distortion, and elimination of the need for prolonged preheating. However, the brazed joints are not suitable for service conditions involving elevated temperature and stresses [80], [82], [98], [100].

2.8.3.3.9 Exothermic Method

Exothermic brazing is a special brazing technique whereby the heat is liberated as free energy due to the solid-state exothermic chemical reaction such that the joint assembly is heated, the filler melts and wets the joint surfaces so as to produce the required bond. The major difference between the exothermic brazing and other methods of brazing is that it is of necessity that the

braze must be pre-placed before the actual brazing commenced. The process begins with chemical/mechanical cleaning of the base metal(s), then the joint is assembled and placed in an inert-gas equipped furnace. The furnace temperature is raised to the extent of causing ignition of the source of heat, and the end-products are removed by hot water to complete the brazing process. It is cheap and can be used for making hydraulic tubes [80], [82], [98].

2.8.3.3.10 Laser Method

A laser such as diode-types are used in laser brazing to locally melts the braze without causing any form of distortion in the base materials, wets the adjoining surfaces and joins the assembly. The major advantage of this method over welding is comparably low heat input and found applications in industries like aerospace, optical, automotive as chief of others. Similarly, problems of overheating, strong deformity, degradation, and damage to the joint parts make laser brazing to be preferred over the conventional brazing methods. The versatility of this method is the reason for being used in joining classes of materials including non-alloyed, high alloyed/galvanized steels, light-weight construction materials, and aluminum. The other benefits of this method are that deleterious secondary phases are absent after brazing, and there is high precision/surface finish of the joint [101], [102].

2.8.3.4 Selection and Forms of Filler Metals

The choice of filler metal and means of application play an essential role in ensuring effective brazing and dictate the outcome of whichever brazing technique employed. The factors to be considered while selecting the filler metal include the method of brazing, the degree of heating, joint configuration, the atmosphere, and the means of application of the filler material. Other considerations include the effectiveness in alloying the filler materials with the joint parts, the wettability of braze metal, the ease of flow by a capillary force, and vaporization of the constituent elements of the filler material. The measure of interactions occurring in the joint

region with regards to the braze and joint parts is very important too. These afore-mentioned factors are influenced by physical-state characteristics of the filler in the molten phase. Filler metals employed in brazing can be pure elements or alloys, and alloys are commonly used than pure elements. Filler metals are made and supplied in different forms. For instance, powdered fillers are made by gas atomization; filler foils by melt spinning; tapes by casting processes; filler paste by alloying a filler powder and a non-fluxing binder which can be organic or inorganic [80], [103].

2.8.3.5 Brazing Fluxes

Fluxes are oxidation-inhibitors. The brazing flux coats or shields the joint area from oxide formation and prevents the re-oxidation of the adjoining surfaces of the base metals. This is to ensure that oxidation by-products are adequately removed for brazing heat to get to the joint parts and molten filler readily flows to wet the cleaned surfaces of the joint. At the brazing temperature, the fluxes are either in the gaseous or liquid phase to function better, and the factor that determines the selection of fluxes are:

- ✓ Type of the base metal.
- ✓ Type of the braze material.
- ✓ The brazing conditions, e.g., time, temperature, etc.
- ✓ Cost.

The minimum and maximum working temperatures at which the flux is effective are determined by the solidus and liquidus of the filler alloy. It is expected that the filler should be completely liquid and actively stable throughout the duration of the wetting actions and cooling of the joint area. The effective working range for fluxes is about 310 K below the solidus of the braze and 366 K above the liquidus of the filler. This is influenced by the constituents of the parts being joined, nature and volume of the flux and brazing temperature. The duration of

the brazing must not be long so as to eliminate the occurrence of flux exhaustion. The constituents of a brazing flux are a mix of different chemical substances (such as chlorides, borates, boron, boric acids, alkalis, fluoroborates, fluorides, and water) and they must be thoroughly and adequately mixed to ensure a smooth process when the flux is applied. Some peculiar anti-oxides such as Ti/Mg may be added for the purpose of self-fluxing. The means of applying the fluxes is dictated by production volume, brazing technique, and configuration of the joint [80], [81], [100], [104].

2.8.3.6 Surface Cleaning and Preparation of Joints

Effective brazing process can be hindered when there are impurities (contaminants) on the joint surfaces because it will impede the flow of the braze as well as the wetting action. This necessitates that the filler materials and base metal parts are thoroughly cleaned prior to the brazing process since the flux can only remove the impurities in the form of tarnishes, and oxide films. Other impurities in the form of grease/oils, paints, lubricants, etc. are removed by the action of cleaning and preparation of the joint surfaces. The cleaning is done by chemical and mechanical cleaning, as discussed further below.

i. Chemical Cleaning

   The use of chemical solvents has long been tested efficiently in removing contaminants on metallic surfaces. The application of chemical cleaning is influenced by these factors, namely: type of impurity, the joint configurations, and the material to be cleaned. Colorless C_2HCl_3 and corrosive Na_3PO_4 are the most widely employed brazing cleaners.

ii. Mechanical Cleaning

   This cleaning encompasses a class of processes such as grinding, brushing, blowing or abrasive blasting. These processes aid capillary drawing and fluidity of the braze.

The first stage of cleaning is surface preparation. The end-products of the preparations are removed by an ultrasonic rinse, and brazing is expected to proceed, immediately the cleaning is done [80], [82].

2.8.3.7 Brazing Atmosphere

The presence of oxygen and moisture greatly impede the fluidity and spread area of the braze, which necessitate the need to control the brazing atmosphere so that the sole purpose of obtaining a joint that is of desired qualities will not be threatened. The atmosphere can interfere in the quality of the joint via the process of oxidation/reduction reactions, nitriding reactions, and carburization/decarburization reactions. These interactions between the joint parts and the constituents of the atmosphere should be avoided. The constituents can take two forms, namely: gaseous elements (O_2, H_2, N_2) and compound-mixture forms (CO, H_2, H_2O). The variety of constituents of the atmosphere are either chemically-reactive (H_2, CO, H_2O, CO_2, O_2, CO, hydrocarbons) or chemically-unreactive (Ar, He). It should be noted that the heat transfer rate is somehow dictated by gas varieties, constituents of the atmosphere, and kinetics of gas flows. To inhibit the net reaction between the atmospheric constituents and joint parts, the atmosphere for brazing can be divided into three, namely neutral, reducing, and vacuum [80], [105].

- Neutral atmosphere: This consists of noble elements found in the periodic table, e.g., helium (He) and argon (Ar). Nitrogen is added as well.
- Reducing atmosphere: This includes hydrogen (H) and carbon (C), which are capable of preventing any form of surface oxides during the early stages of heating as well as during the proper brazing process. Hydrogen is known to be the most reducing agent.
- Vacuum: This atmosphere is free from any form of gases or impurities such that the joint parts are not oxidized or being reacted with. Pumping method and dissociation are the means by which this atmosphere is controlled to avoid reaction with the joint parts.

2.8.4 Diffusion bonding

It is possible to achieve a microscopic bonding of metallic contact surfaces without necessarily melting them under the action of heat and pressure through a process called diffusion bonding. The bulk of the mass transport in this superplastic process is partly done by plastic deformation and completed by atomic diffusion. This is an advance joining technique via solid state diffusion to produce high-performance joints that have strength and microstructure comparable to the parent materials. Unlike in the traditional methods of joining whereby joints are made by plastic deformation alone, diffusion plays a vital role in strengthening this kind of bonds, and it is used where dissimilar/similar metals are to be joined. Critical features are required, including the microstructure of the parent metals being retained as well as the effect of degradation being eliminated. This method requires certain prominent conditions, which include mechanical intimacy and removal of asperities as well as contaminants. Prior to bonding, a conspicuous action that is required is the surface preparation by the effect of cold work in a bid to produce oxide-free, uniformly smooth and planar surfaces. This cold work induces recrystallization, which invariably increases the kinetics of the vacancy diffusion and alloying can increase the rates of diffusion too. The types of diffusion bonding are massive diffusion bonding and thin-sheet diffusion bonding. The parameters that greatly influence the process are temperature, cycle duration, perpendicularly-applied pressure to the bond area, and pre-bonding nature of the surfaces being joined [106], [107].

The various benefits of diffusion bonding are:

- ✓ Addition weights to the joints are eliminated relative to mechanical joining by fasteners.
- ✓ Comparable microstructures and features just like the base metals
- ✓ Cost efficiency
- ✓ Elimination of welding defects
- ✓ Alloys that are not easy to weld can be joined

- ✓ No need for further machining operation due to a low degree of distortion.

The hindrances to the application of this method are:

- ✓ Relatively long processing time.
- ✓ High set-up cost
- ✓ The non-adaptability to high productions
- ✓ Greater care in the preparation of samples
- ✓ Explicit control of the process parameters
- ✓ Application of heat as well as high pressure in an unreactive atmospheric covering

Regarding the hindrances encountered in the course of using diffusion bonding, then TLP bonding serves as a potential alternative. This will be discussed further in the next sub-section [10], [107].

2.8.5 Transient liquid phase (TLP) bonding

The crude method of joining materials was developed with the aid of interlayers upon the advent of Etruscans civilization in ancient Rome. This is called granulation whereby decorative beads were joined unto golden vessels using copper as a befitting interlayer. This method forms the premise on which the modern-day transient liquid phase (TLP) bonding is based. The granulation process is renamed as TLP upon critical reviews/modifications conducted in 1971 by Paulonis et al [80], [108], [109], [110], [111], [112].

TLP is a joining method that combines the principle of diffusion bonding and brazing [113]. Just as in conventional brazing, the assemblage consists of the base metal and the filler alloy. The filler is a special type because it contains melting point depressants (MPDs). The assemblage is heated to cause phase changes resulting in the formation of molten filler. This chemically reacts, by the wetting process, to form a liquated mixture of constituents of filler and base metal. There are microstructural changes in the joint region as the MPDs undergo

atomic movement into the substrate by solid-state vacancy diffusion while the joint is retained at a constant temperature. This is simultaneously complemented by isothermal solidification in which the liquid width shrinks towards the mid-line of the joint so as to permit the growth of the solid-solution phase within the joint region. Adequate time is required for isothermal solidification to be completed. Finally, a near-ideal non-heterogeneous bond, with metallurgical features comparable to the substrates, is formed [80], [109], [110], [111].

2.8.5.1 Applications of TLP Bonding

Over time, a good number of materials based on these elements Aluminium, Titanium, Cobalt, Iron, and Nickel have been effectively joined with TLP bonding. Similarly, it can be used for non-metals like ceramics, special composites, and microelectronics. It has solved the problem of joining materials that are prone to heat with minimum distortion. It is also easily employed where materials of either similar or different metallurgical properties are involved, especially when other joining techniques had proved abortive. It can be used in the manufacture of parts of combustion chambers and structures as well as in repairing parts of turbine engines [10], [80], [112].

2.8.5.2 Merits of TLP

TLP bonding can be so beneficial in the following ways [111]:

i. There is no difference in the properties of both the pairs of the base metal and the joint.
ii. The interface is completely removed after the bonding operation.
iii. The joint undergoes self-homogenization.
iv. Relatively low clamping forces are required.
v. There is a great chance to avoid the formation of intermetallics.
vi. It requires a minimum sample preparation.
vii. It can be used for bulk and intricate shapes simultaneously.

2.8.5.3 Demerits of TLP

The disadvantages of TLP bonding are stated below [111]:

i. There is a tendency for longer processing times.
ii. It is restrained to elevated temperatures of at least 0.6 T_m
iii. It requires fast-moving diffusing elements
iv. The heat-up stage must be rapid enough.
v. It requires heat-treatment procedures after bonding for age-hardening materials, especially.

TLP bonding is a brilliant joining technique, though imperfect with its disadvantages. Measures to forestall these limitations lie in leveraging on its benefits and complying with the requirements for a successful bonding process.

2.8.5.4 Description of TLP

The peculiarity of TLP bonding makes it being referred to as diffusion brazing. In TLP, there must be an appropriate arrangement of bonding materials to make the assembly that is subjected to high bonding temperature in order to melt the filler alloy (or interlayer). Then, the rapidly diffusing solute elements initiate the isothermal solidification so that a joint with equable composition profile is formed [114]. The interlayer is located between the pairs of materials to be joined and takes various forms like powder, foil, paste, or an electrolytic coating on the surfaces of the materials. One of the important things to ensure during bonding is close contact between the interlayer and the materials to be joined which is realized as long as the constant pressure on the assembly is not too much to cause spillage. TLP bonding can be carried out in a pressurized chemically unreactive atmosphere or a controlled atmosphere which is within a confined chamber while heating is done in a furnace. The furnace cools down, and the bonded sample is retrieved for post-bonding operations [80], [112].

2.8.5.5 Bonding Kinetics of TLP Process

In the course of making TLP bonding easy to understand, certain models have been developed. These TLP models presumed that there is concentration equilibrium at the solid/liquid interface, and the stages of TLP are occurring sequentially [80], [112], [115]. The sequential arrangement of the four stages of the TLP bonding process is melting of the interlayer, dissolution of the parent metal and widening, isothermal solidification, and homogenization of the bonded joint at solid state.

2.8.5.5.1 Melting Stage

A successful bonding starts with the heating of the assemblage to a suitable temperature that is usually above the eutectic temperature and thereby leads to the dissolution of the interlayer. The liquid interlayer moisturizes the closely fitted surfaces of the base materials due to its wettability. This wettability depends on the viscidity of the liquid and the surface energy of the parent metals [80], [112].

2.8.5.5.2 Dissolution Stage

This stage is appropriately known as the dissolution and widening stage and occurs after the melting of the filler alloy while the bond zone is continuously heated to the required bonding temperature. This dissolution results in a change in the composition of the interfacial elements via diffusion between the molten interlayer and the mating surfaces. Owing to this compositional imbalance, the surfaces of the base metal begin to melt-back, and the resulting liquated joint starts to widen. This widening continues until there is an equilibrium in both liquid and solid concentrations at maximum joint width. The measure of the dissolution depends on the initial joint width, the concentrations of MPDs in the interlayer, and the solubility of the solutes in the base materials [80], [112].

2.8.5.5.3 Solidification Stage

The dissolution stage terminates into this stage for bonding to continue at a constant predetermined temperature. The isothermal solidification stage may take several hours, and its kinetics greatly determines the kinetics of the entire TLP bonding process [116]**.** Then, the MPDs in the liquated joint diffuse into the adjacent substrates which, in turn, makes the width of the liquid inside the joint area to reduce steadily until it vanishes given that there is enough holding time. It is important to note that the rate at which the interface is displaced is directly proportional to the rapid movement of the MPDs [80], [117].

Local equilibrium is maintained at the joint interface such that the compositions of the phases (solid and liquid) remain constant for this stage to proceed accordingly till completion. The isothermal solidification stage has been proven essential due to its prominent role in the resulting metallurgical features of the bonded joint. However, it is slower and time-consuming as it is governed by the solid-state diffusion [10], [80], [115].

2.8.5.5.4 Homogenization Stage

Homogenization as a solid-state process removes the solute peaks from the stage of isothermal solidification so as to ensure a bonded joint with unvarying concentration profile and metallurgical features comparable to the substrates. The temperature for the homogenization stage is influenced by the degree of sensitivity of the joint microstructure, and this could be either higher or lower than the temperature at which the joint is made [10], [80], [118].

2.8.5.6 Selection of the Parameters of TLP Bonding Process

It is essential to control the bonding parameters for TLP bonding by optimization. This is to save time, cost of bonding, and enhance the attributes of the bonded joint. The factors

controlling TLP bonding include the bonding temperature, the holding time, gap width, type of base metal, and filler alloy used. These parameters will be discussed below.

- **Bonding temperature**

  The rate at which the liquated joint during TLP process solidifies is largely dependent on the selected bonding temperature. Hence, the influence of bonding temperature is crucial to TLP bonding. Moreover, the determination of appropriate temperature to be used can be obtained either directly from the phase diagram for the system or using already existing experimental data. The data should illustrate the diffusion mechanisms for the system under consideration [10], [80].

  Arrhenius equation already shows the relationship between temperature and diffusion coefficient that they both vary directly with each other. It is easy to draw a conclusion that the isothermal solidification becomes faster for every increase in bonding temperature since it is determined by the rate of atomic diffusion of the MPDs into the materials being joined. This invariably leads to a reduction in bonding time to complete isothermal solidification and supported by works reported by Norouzi et al. [119], Arafin et al. [120] to mention but few. Some studies [121], [11] reported otherwise that there is an inverse relationship between temperature and isothermal solidification, which implies a longer time for the liquid to entirely solidifies.

- **Filler Alloy Composition**

  The constituent elements that make up the filler alloy affect the joint quality during TLP bonding. The vitality of the filler is to ensure a good property in terms of fluidity and wettability for effective bonding. It should also be able to react with the substrate to provide the best solid solution with an optimum concentration profile of the solutes. The solubility of the MPD's is another paramount property to note while considering the selection of suitable filler [10].

- **Gap Width of the filler**

  The gap width is a potential process parameter that dictates the time to complete isothermal solidification because it quantifies the amount of liquid available at the end of the heating stage. This is in the sense that the larger the gap width, the more the liquid needed to solidify. In the case of using foil as the interlayer, the thickness of the foil should not be very small as it can be destroyed before reaching the isothermal solidification stage. This implies that there is a minimum thickness of the interlayer below which the bond would be damaged.

- **Nature of Base Metal**

  The quality of the bonded joint is influenced by the geometric dimensions of the base metal and MPD solubility in the base metal. Thus implies that the proportion of the MPD that makes up the composition of the base metal determines the quantity of MPD that can diffuse into it during the isothermal solidification stage. This means that a high fraction of solute diffuse into the base metal if the fraction of the MPD in the base metal prior to bonding is low provided that the maximum solubility is not yet reached and vice-versa. A very good characteristic feature of the base metal is to enable passage of the diffusing solutes and absorb adequate solutes into its matrix in such a manner that formation of brittle phases is avoided around the joint region. This is because they pose a danger to the structural integrity of the joint.

- **Holding time**

  The holding time is applicable to just one out of the four stages of TLP bonding, which is the isothermal solidification stage. It plays an essential role in the course of getting rid of the residual liquid found within the joint area, and there is direct variation between the fraction of the liquated joint that solidifies isothermally and the holding time. Therefore, abundant time must be set to hold the joint during isothermal solidification

stage to get rid of the residual liquid which does not offer any benefit to the microstructure of the bonded joint.

2.9 Research Scope

Having reviewed various methods of joining metals, the concept of welding is known to be universal or mostly used among them all. However, there are limitations to the use of welding in joining some materials such as single crystal Nickel-based superalloys. Hence, they are not easy to weld. The recently developed methods of joining are as a result of several modifications adopted, which makes TLP bonding as an attractive alternative for joining such materials since it addresses the challenges associated with welding. So, the main objective of this study is to investigate the effect of various process parameters related to TLP bonding on the microstructural transformations that may occur while bonding SX Rene-N5 superalloy with the aid of filler, NB-150.

In the purview of this work, characterization of the base materials is done. Then, bonding operations were conducted at some temperatures for certain holding times with the aim of identifying corresponding effects of each process parameters on the joint microstructure. The selected process parameters are holding time, bonding temperature, and filler material compositions.

CHAPTER 3 - MATERIALS AND METHODS

The materials needed and bonding parameters to achieve the aim of this study were carefully selected. This was followed by TLP bonding of the selected base material which is taken as the experimental work, and the bonded joints are examined using different microscopic equipment.

3.1 Materials Selection for TLP Bonding

3.1.1 Base-Materials

The samples of aerospace single crystal Rene-N5 were used for analysis during the experiment. The respective percentage compositions of each constituent elements are stated in Table 3.1.

3.1.2 Filler Alloy

The filler used for the major portion of the experiment is Nicrobraz 150. Table 3.1 presents the three constituent elements of this filler and their respective percentage weight compositions. Just like the base material, the chief element in this filler is Nickel. The filler is in powder form, and the boron atoms present are serving as the MPDs. It has liquidus temperatures of 1323K. The bonding temperatures selected for this work are ensured to be above this liquidus. To compare the effect of filler alloys on joint microstructure, IN-738 (see Table 3.1) is used as the additive powder.

3.1.3 Gap-width Spacer

Pairs of molybdenum wire are used in the course of bonding. They are used to maintain a uniform joint width at the setup stage and heating stage during the TLP bonding operations. The diameter, as obtained from micrometer screw gauge, is 200 μm. The 200 μm spacers are used for all the bonding operations except while quantifying the amount of reduction in processing time. To quantify the reduction, 75 μm spacers are used.

Table 3.1: Weight (%) of Rene-N5, IN-738 additive, and NB-150 filler [10], [122]

Elements	**Rene-N5**	**IN-738**	**NB-150**
Al	5.47	3.47	-
Co	7.39	8.50	-
Cr	6.94	15.84	**15.00**
Hf	0.55	-	-
Mo	1.80	1.88	-
Ni	62.23	balance	**balance**
Re	2.76	-	-
Ta	6.78	1.69	-
W	6.08	2.48	-
C	-	0.11	**0.06**
Ti	-	3.47	-
Fe	-	0.07	-
Zr	-	0.04	-
Mn	-	0.01	-
Nb	-	0.92	-
B	-	0.012	**3.5**

3.2 Experimental Work

3.2.1 Pre-bonding Sample Preparation

Since the materials are hard to cut using saws, computer numerically controlled (CNC) electro-discharge machine (EDM) was used to cut the samples into the desired shapes and dimensions. The dimensions used are 3 mm x 8.5 mm x 10 mm. For proper grinding operations, 600 graded Si-C papers were used to remove unwanted oxide layers and make smoothened/flattened sample surfaces. Then, they were transferred into beakers filled with acetone for ultrasonic cleaning for 15 minutes. The prepared samples were coated either partially or fully on the edges so as to guard against the spillage of molten filler in the course of bonding.

3.2.2 Bonding Procedure

3.2.2.1 Jig assembly

To carry out the TLP bonding in the furnace, the jig assembly must be set-up first. A typical jig assembly is shown in Figure 3.1. This set-up includes basic operations of pre-heating the bolts, proper coating of the samples and jigs, and arrangement of the materials into the jig assembly. Bolts, with 6mm diameter, are heat-treated under conditions of 950^{o}C and 45 minutes. Then, the machined jigs are coated inside with ceramic paste and allowed to dry. This coat constrained the flow of the liquid filler within the joint region and disallowed any escape in the form of spillage. The treated bolts are withdrawn from the furnace, cooled and fixed in their respective positions on the jigs. There are three bolts to hold down any jig assembly. A pair of dried coated samples are gently placed inside the jig in such a way that the cleaned surfaces are facing each other. Then, the spacers are used to create the required gap width, and the assembly is held down by the bolts carefully and firmly. The foils are coated, allowed to dry and used to cover all the edges of the jigs so as to serve as additional constraints to the

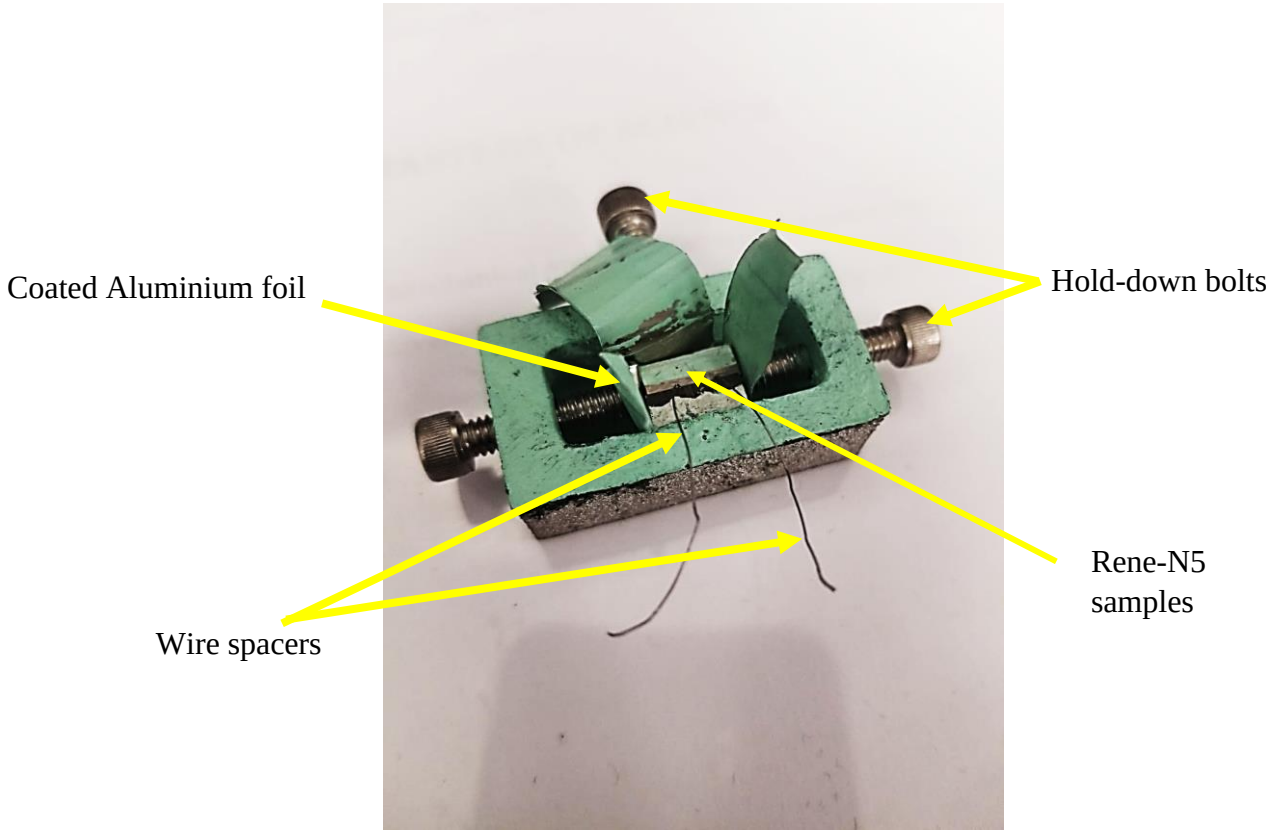

Figure 3.1: Joint assembly in a jig

liquid filler. The hand wrench is used to lock up the assembly without destroying the spacers (molybdenum wires). The filler is carefully located inside the clearance provided in the joint area.

3.2.2.2 TLP Bonding

The prepared assembly is placed inside a LABVAC II vacuum furnace under a vacuum pressure of approximately 5×10^{-5} torr to prevent oxidation. The furnace is operated to conduct the brazing operation through the earlier-stated first three stages of TLP bonding in section 2.9.7. Figure 3.2 represents the cycle of TLP bonding. Thus, the assembly is heated to the bonding temperature, retained at this condition for some predetermined time and finally cooled.

3.2.3 Post-bonding Sample Preparation

The assembly is later withdrawn from the furnace and dismantled for further post-bonding examinations. The bonded samples are sectioned, grounded, polished, and electro-etched. The sectioning is done perpendicularly relative to the bond line of the joint. The reagent used for the etching contains 40ml nitric acid, 12ml phosphoric acid, and 48ml sulphuric acid. Then, the prepared bonded samples are taken for microstructural examinations.

3.3 Microscopic Examinations

These examinations are done on two major equipment, namely:

i. An inverted -reflected optical microscope (OM).
ii. A JEOL 5900 scanning electron microscope (SEM).

The OM is equipped with a CLEMEX Vision 3.0 image analyzer. The microstructure examined on the OM is done at lower magnification relative to SEM. The SEM is equipped with an ultra-thin window Oxford energy dispersive spectrometer (EDS) and INCA analysis software. For a

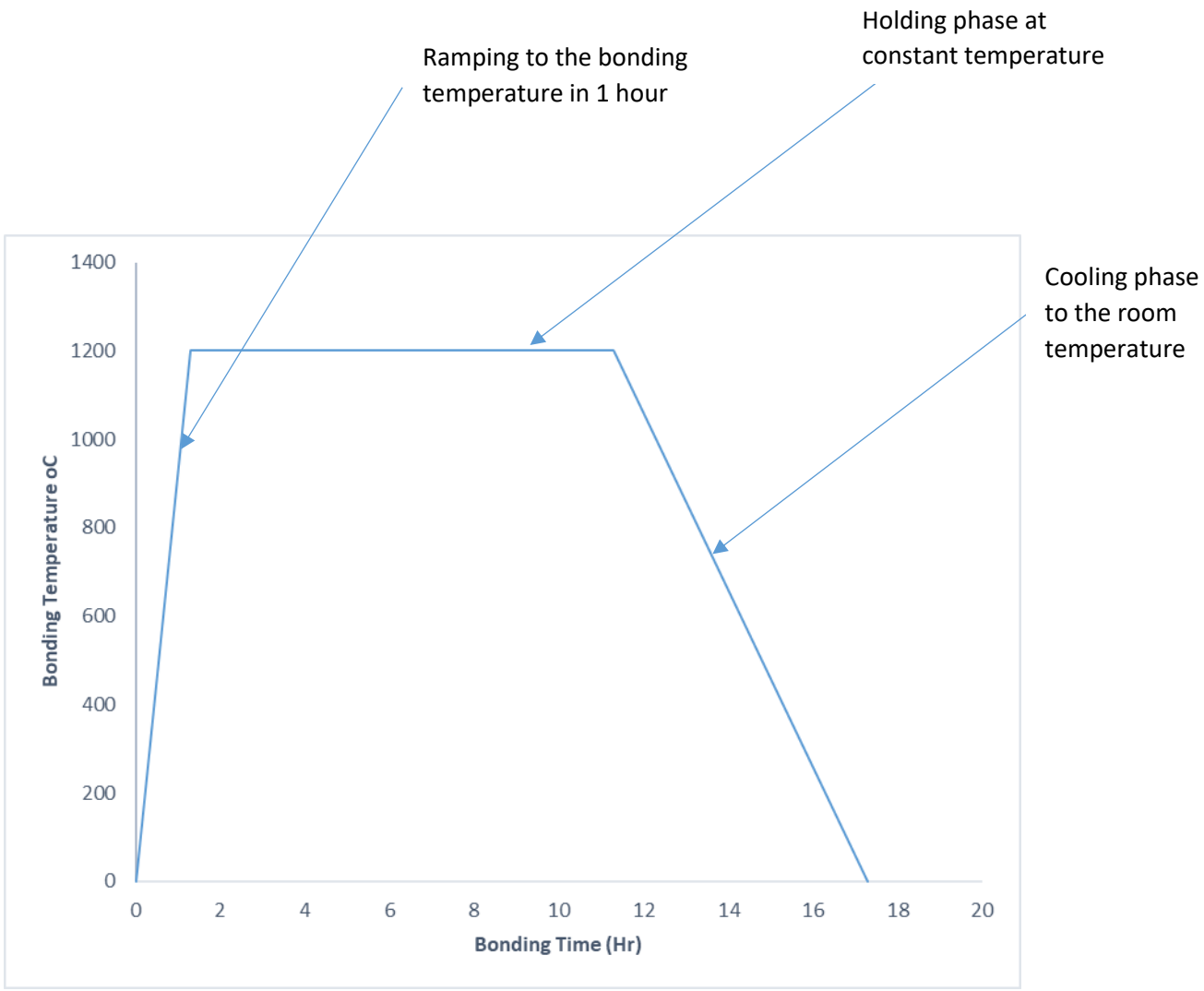

Figure 3.2: The schematic cycle of TLP bonding

higher magnification of the images and compositional characterizing, the SEM/EDS is used. The modes at which the SEM images are taken are; the secondary mode (SEI) and back-scattered mode (BES). The values recorded for the joint widths, isothermal zone widths and eutectic widths are computed by the arithmetic mean of the measured data of about twenty (20) readings.

CHAPTER 4 - RESULTS AND DISCUSSION

This chapter provides a discussion on the microstructure in the as-received Rene-N5 prior to TLP bonding. Also, the results of the effect of process parameters on microstructural changes in the TLP bonded joints, are presented and discussed.

4.1 Microstructure of Rene-N5 Prior TLP Bonding

The optical micrograph of the as-received Rene-N5 is presented in Figure 4.1. The microstructure is predominantly dendritic solidification microstructure. Some particles can be observed along the interdendritic region, as shown in Figure 4.1.

Low magnification SEM image shows some irregular particles along the interdendritic region, as shown in Figure 4.2. The summary of the results of EDS compositional analysis of these phases is given in Table 4.1. The EDS result suggests that these particles are based on carbides, which are secondary particles that are rich in carbon element. This is in agreement with some previous studies on this alloy [41], [123], [124]. It is observed that these carbides are rich in Ta and Hf.

Further microstructural analysis by using the SEM at high magnification showed another precipitate within the matrix of the alloy, see Figure 4.3. Some studies [123], [124] have identified these phases as gamma prime. Figure 4.3 shows the distribution of the γ' phases in the FCC γ matrix of the as-received Rene-N5. The relatively light-gray structures are the gamma prime (γ'). The γ' observed at different regions in the microstructure of the as-received Rene-N5 takes the form of a cube except that those found at the interdendritic region are a bit longer. The segregation of γ' forming elements could be the reason for the variation in the morphology of these particles [41], [125], [126], [127]. The γ' particles in the dendritic region are seen to spread uniformly within the γ-matrix with the length scale in the range of 2 μm. The volume fraction of γ' is estimated by the point-counting method and direct measurement [128].

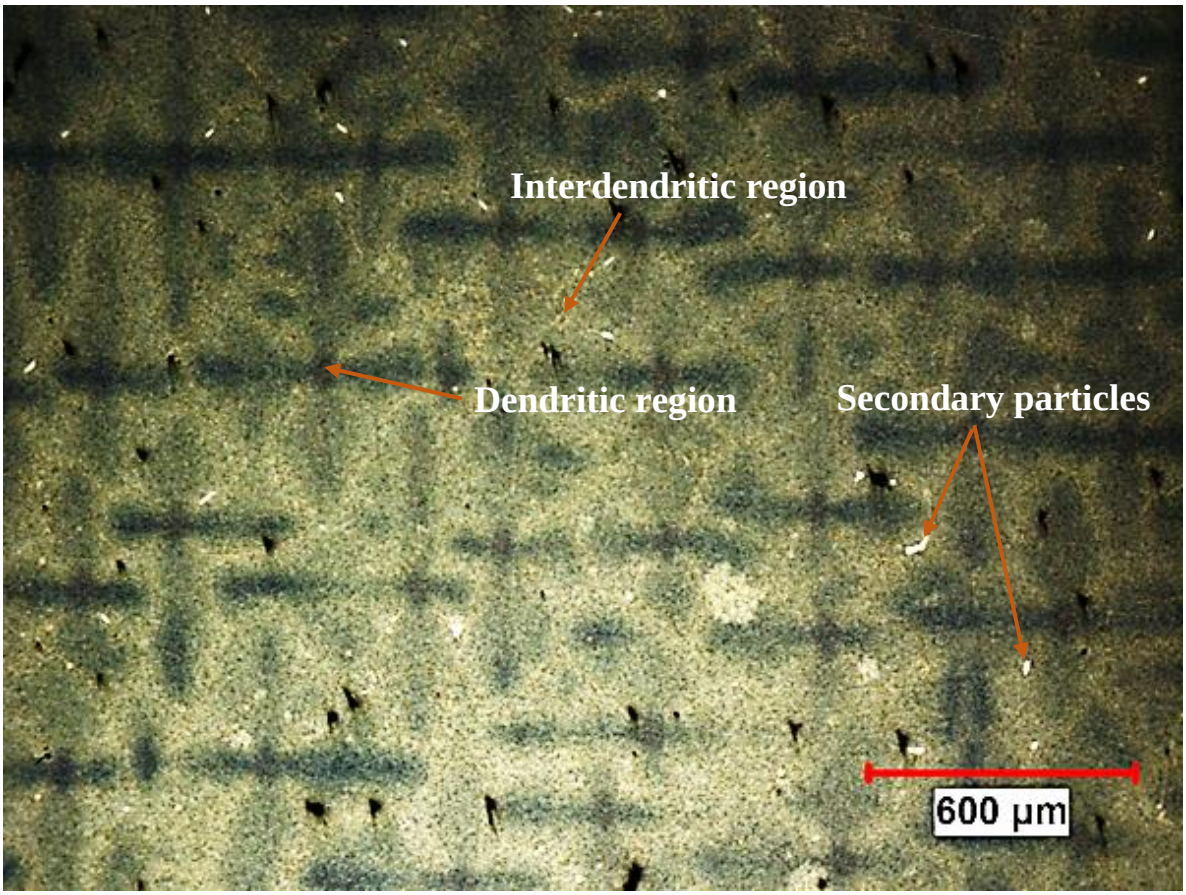

Figure 4.1: Optical micrograph of as-received Rene-N5 showing dendritic segregation structure

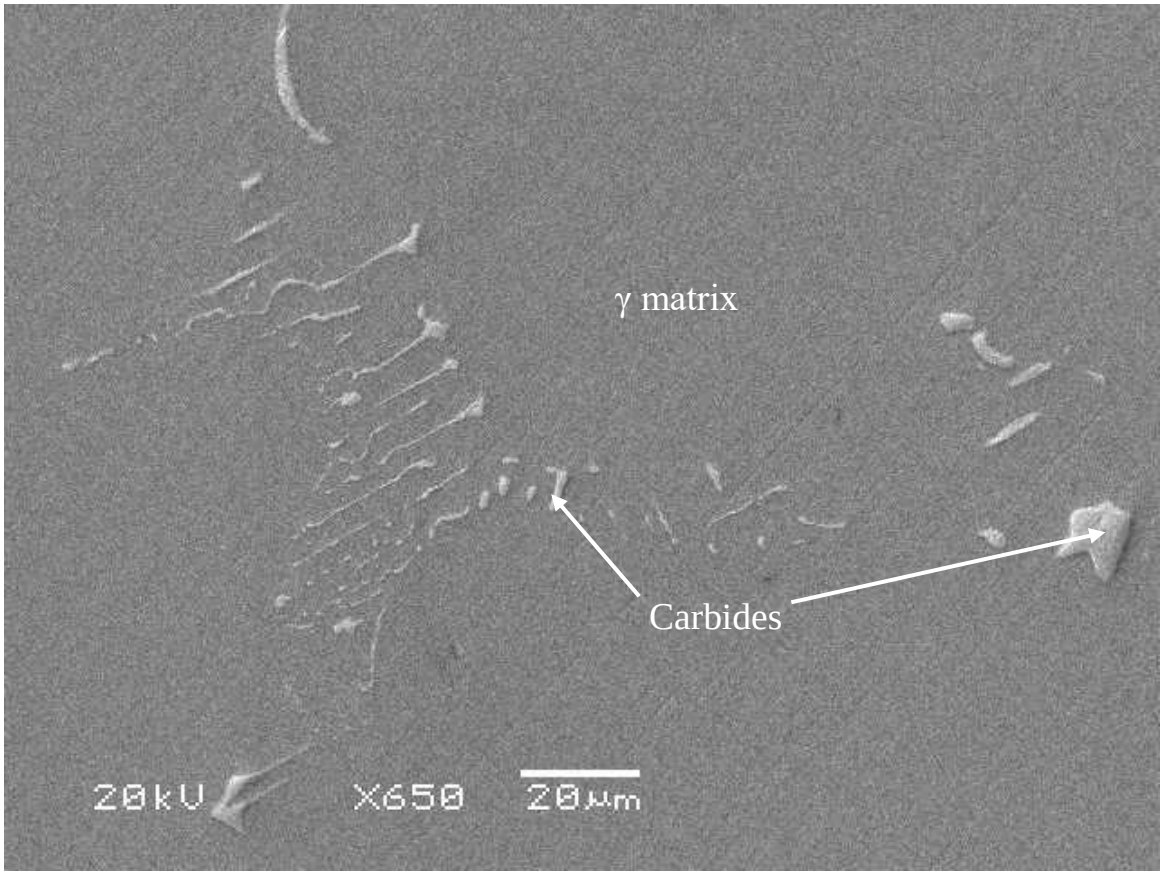

Figure 4.2: SEM image of the carbides found in as-received sample

Table 4.1: Typical composition of carbide formed at the interdendritic region

Elements	Al	Cr	Co	Ni	Mo	Hf	Ta	W	Re
Wt (%)	0.0	0.0	0.0	**4.3**	0.0	**21.7**	**74.0**	0.0	0.0

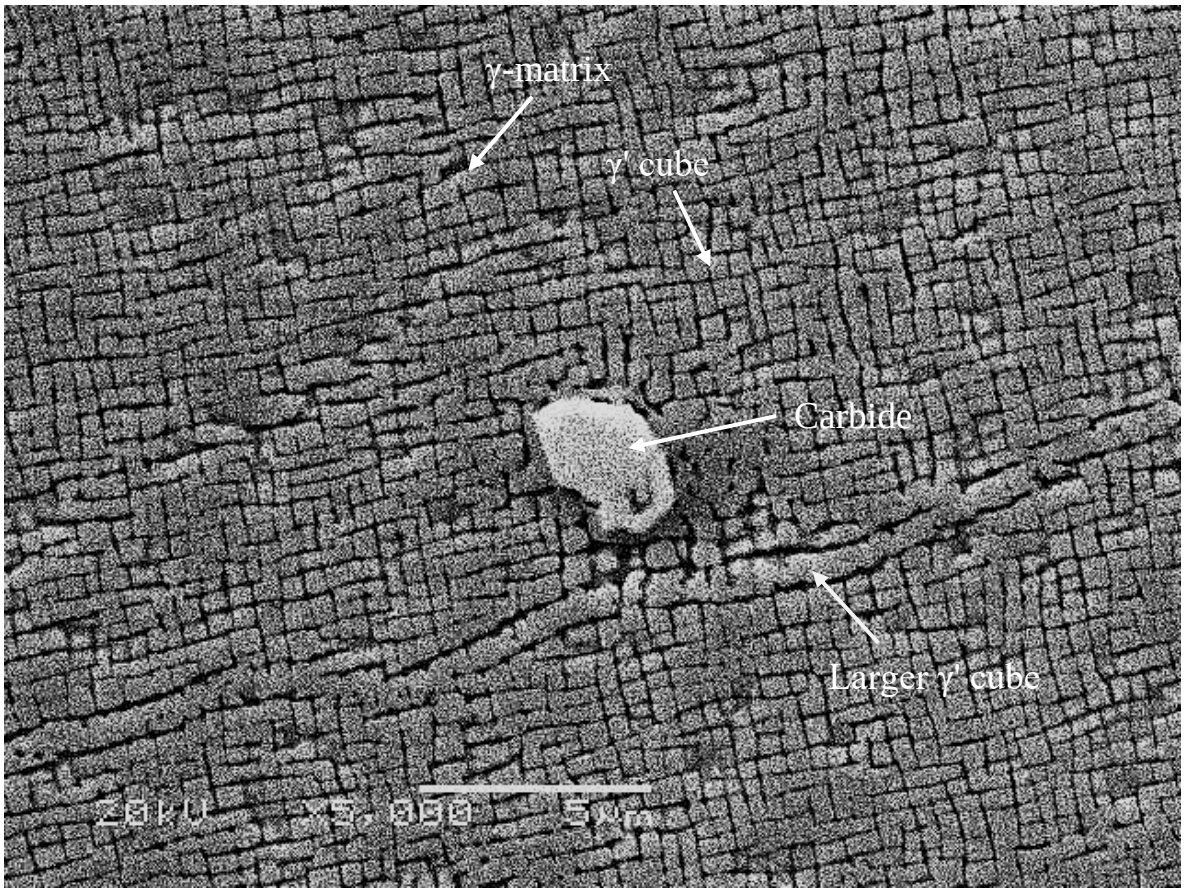

Figure 4.3: SEM image showing the distribution of γ' in the γ-matrix.

The average volume fraction is calculated to be about 70% using both methods [122], [129].

4.2 Microstructure of the Brazed Joint

The as-received Rene-N5 samples are bonded at 1090^{o}C for 15 hours, and the SEM image of the bonded joint is presented in Figure 4.4. Figure 4.4 illustrates that there are three (3) distinct regions within the joint zone with regards to their respective morphology, and they are denoted as A, B, and C for Diffusion Affected Zone (DAZ), Isothermally Solidified Zone (ISZ), and On-cooling Solidified Zone (OSZ), respectively. In this work, eutectic is observed within the OSZ as a result of inadequate time for complete isothermal solidification of the joint [10]. The details on the different regions are given in the subsections below.

4.2.1 Isothermal solidification zone

Figure 4.5 (a) shows a SEM image of the ISZ. The EDS quantitative data of this region is presented in the table attached to Figure 4.5 (b). The data analysis corresponding to ISZ in Figure 4.5 (b) reveals that the region is Ni-rich (FCC) solid solution. Elements including Al, Co, Mo, Hf, Ta, W and Re which were not originally included in the filler composition seem to have actually diffused into ISZ region as a result of dissolution-diffusion reactions between the filler and base metal. The ISZ is formed as a result of induced compositional changes by substrate-liquid filler interdiffusion during the holding time at a constant bonding temperature.

4.2.2 On-cooling solidified zone

In this work, the section of the bonded joint occupied by the eutectic which solidified from the bonding temperature through the process of cooling to the room temperature is referred to as the on-cooling solidified zone (OSZ). Microstructural analysis by using the SEM at higher magnification showed the microconstituents that made up this region, as demonstrated in Figure 4.6. Three (3) phases are noticeable in Figure 4.6. To understand the nature of these

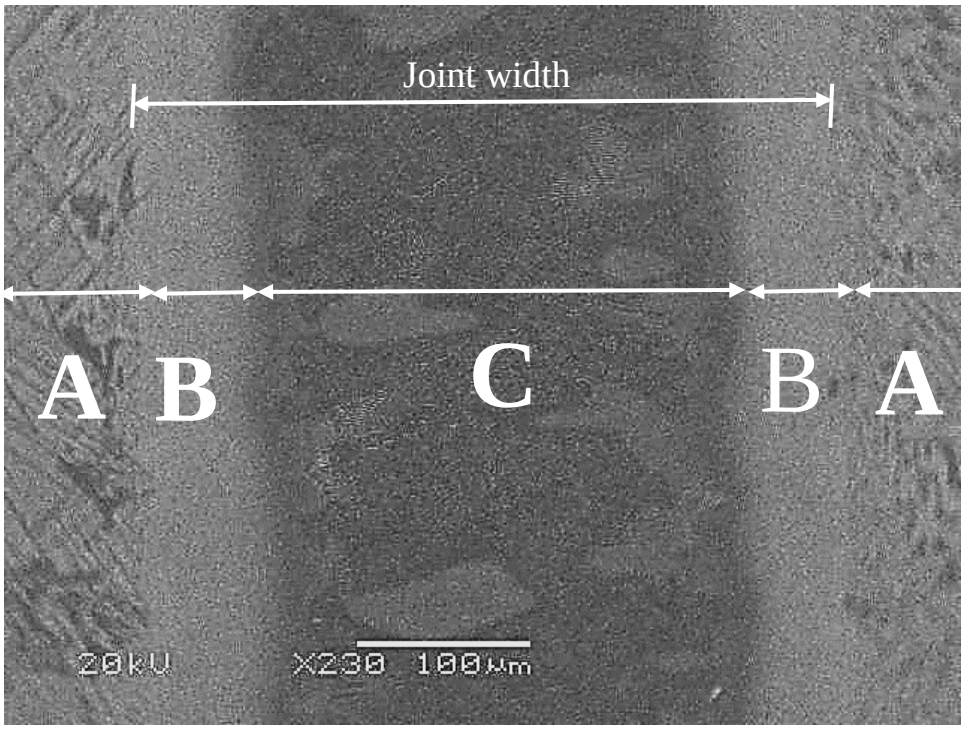

Figure 4.4: SEM micrograph of the bonded Rene-N5: where A is the DAZ; B is the ISZ and C is the ASZ (Eutectic)

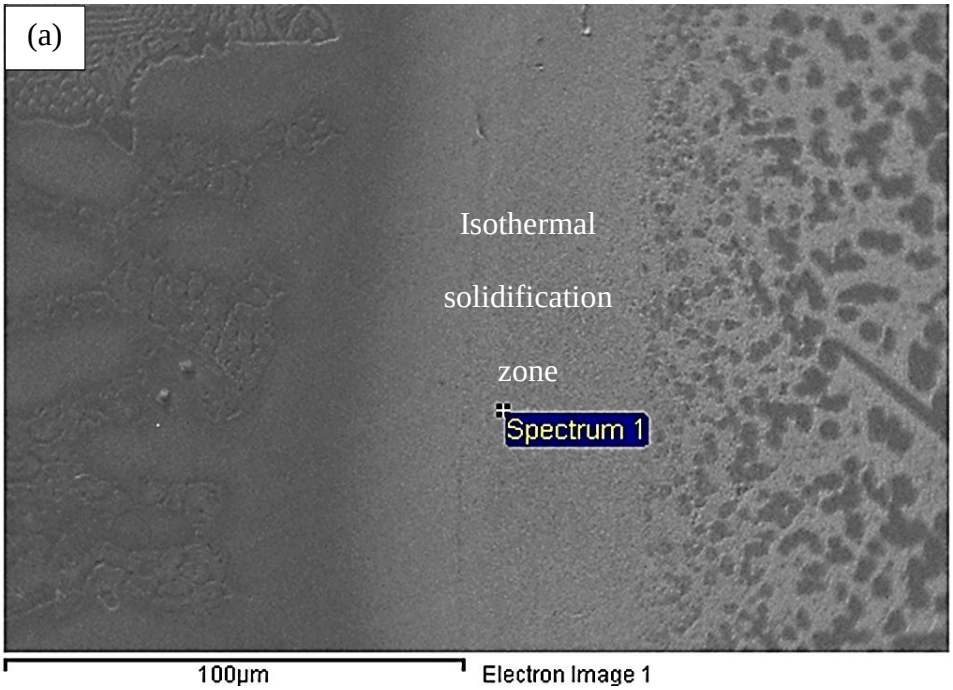

Element	Weight%	Atomic%
Al K	4.1	9.3
Cr K	8.2	9.7
Co K	6.0	6.3
Ni K	66.7	69.4
Mo L	1.4	0.9
Ta M	4.1	1.4
W M	6.4	2.1
Re M	3.1	1.0
Totals	100.00	

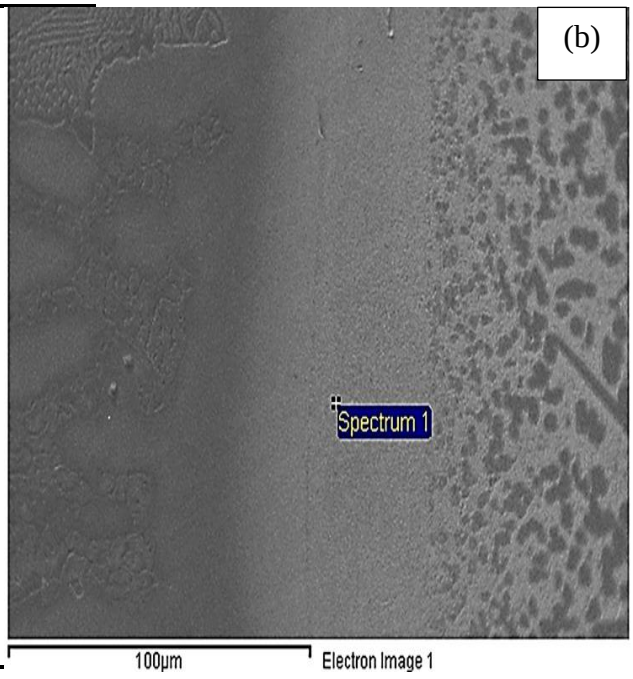

Figure 4.5: The SEM-EDS compositional analysis showing: (a) point scan image (b) composition of each element

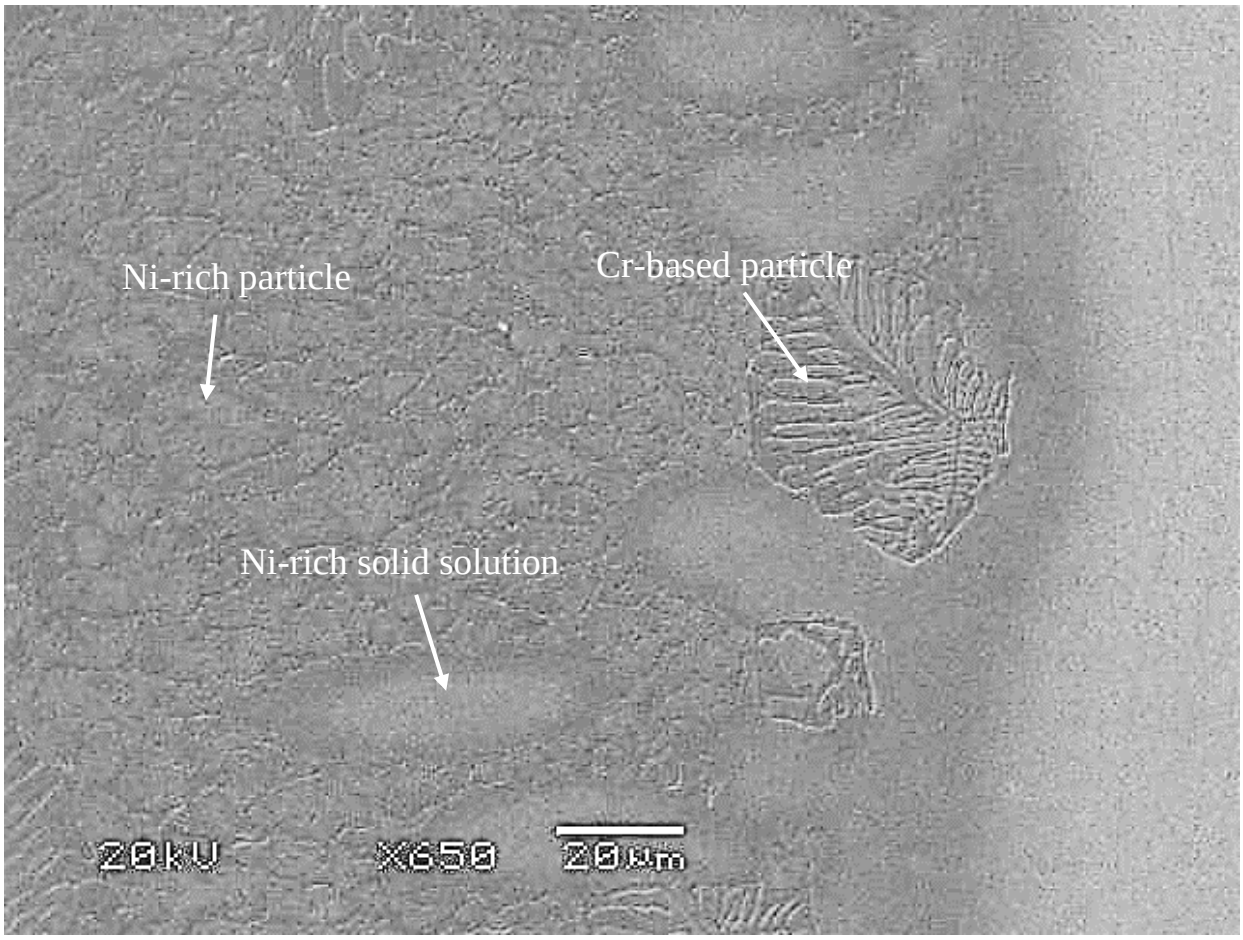

Figure 4.6: SEM micrograph of phases found in the ASZ.

eutectic microconstituents, the solidification sequence during TLP bonding reported by some researchers was reviewed.

A collective work by Tung et al. [130] was conducted on the use of BNi-4, as filler, to bond pure Nickel. This filler comprises Ni, B, and Si. The sequence of solidification behavior reported, in their work, is that γ-Ni single phase is formed first and followed by the formation of two phases: Ni-Boride and Ni-Silicide. In the earlier reported work by Ohsasa et al. [131], modelling work was performed on TLP bonding of Ni-blocks using Ni-Cr-B filler alloy. They employed Scheil simulation to study the solidification mechanisms during the cooling of the residual liquid. Following the sequence of transformations, a single Ni-rich phase was observed to form as a primary phase by isothermal solidification at a bonding temperature of 1110^{o}C. Then, an eutectic reaction which is represented as L => γ (FCC) + Ni_3B occurred at 1042^{o}C during cooling. Finally, the cooling process was fully completed by the ternary eutectic reaction: L => γ (FCC) + Ni_3B + CrB at a bonding temperature of 997^{o}C. Similarly, three different phases are reported during the TLP bonding of other Ni-base superalloys. These are: γ (FCC), Ni-boride and Cr-boride [14], [15], [25], [115].

In the current work, the phases seen at the center of the bonded joint (see Figure 4.4 and Figure 4.6) are considered to be results of eutectic reaction during cooling. SEM-EDS data from these phases are listed in Table 4.2. Based on the results, it is likely that these phases are Ni-solid solution, Ni boride, and Cr-Mo boride.

Table 4.2: Percentage weight composition of the phases in the OSZ

Elements	Weight (%)		
	Ni-rich solid solution	**Ni-rich boride**	**Cr-based boride**
Al	3.5	1.8	0.0
Cr	11.4	8.4	42.0
Co	2.2	2.5	1.5
Ni	76.4	82.5	13.1
Mo	2.5	0.0	24.5
Ta	0.0	4.9	0.0
W	4.1	0.0	10.3
Re	0.0	0.0	8.6

4.2.3 Diffusion affected zone

SEM micrograph of the microstructure of DAZ is represented in Figure 4.7. The secondary precipitates observed are needle-shaped particles and blocky particles within the DAZ. These needle-shaped particles are formed in arrays of parallel, intersecting, and combined parallel-intersecting forms. The amount of blocky phases is significantly more than the precipitated needle-like phases. The data for the chemical compositions of these particles acquired by EDS method are provided in Table 4.3. The DAZ is predominantly made up of Ni-based precipitates, which are presumably borides formed due to diffusion of boron into the solid substrate during bonding [12], [15], [132].

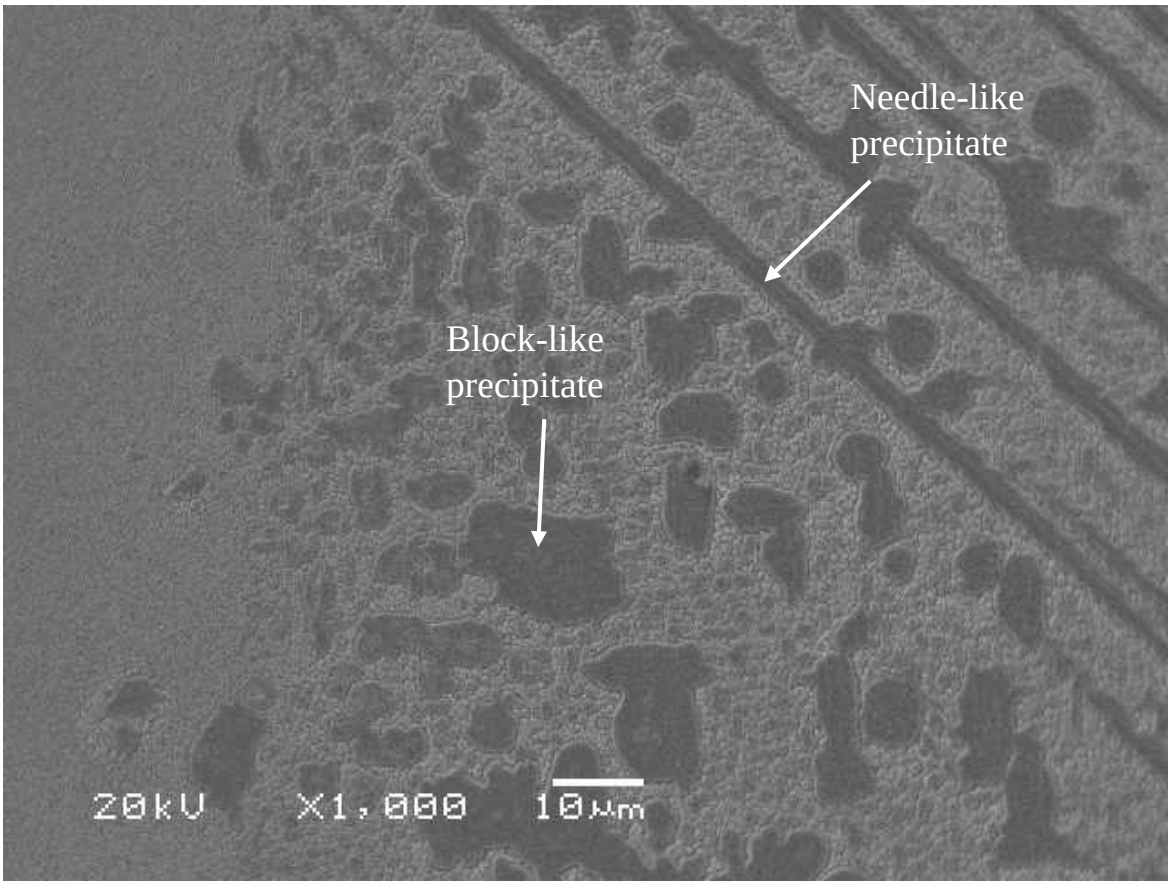

Figure 4.7: SEM micrograph of the phases found in the DAZ

Table 4.3: Percentage weight composition of the phases in the DAZ

Elements	Weight (%)	
	Blocky precipitates	**Needle-shaped precipitates**
Al	7.0	5.7
Cr	6.2	8.2
Co	5.4	4.7
Ni	59.0	49.0
Mo	1.9	5.5
Ta	9.0	8.8
W	8.2	13.2
Re	3.3	5.0

4.3 Effect of Bonding Parameters on the TLP Bonded Rene-N5

4.3.1 Effect of bonding time on the microstructure of the joint

To study the effect of time on the joint microstructure, bonding experiments were performed at 1090^{o}C for 1 hour, 5 hours, 10 hours, 15 hours, 25 hours, and 50 hours. The width of the bonded joints basically comprises of ISZ and OSZ. The plot of the average joint width against the holding time is shown in Figure 4.8. It can be seen that the average joint width stays within the experimental error range as the bonding time increased from 1 hour to 50 hours. This shows that the average joint width did not change significantly over the period of time used. This observation is expected since similar materials are bonded and the system actually undergoes dissolution in order to achieve equilibrium in TLP bonding. During the dissolution, the system attains a maximum joint width and maintains it for the duration of the process.

Figure 4.9 shows the plot of the isothermal solidification zone width (ISW) against the square root of holding time. A linear relationship between the width of the isothermally solidified zone and the square root of holding time is observed between 1 hour and 25 hours. This indicates that isothermal solidification is controlled, basically, by atomic diffusion. This observation is in a close agreement with some previously reported works [10], [118], in which Ni-based superalloys were bonded using the conventional filler, NB-150. Standard analytical models have been developed to explain the influence of time on the microstructure of TLP bonded joints. Based on the models, it has been found that there is a linear relationship between the width of isothermal solidified zone (ISW) and the square root of holding time. The governing equation for this relationship is given below [133],[134], [135]:

$$Y = \emptyset * \sqrt{t} \quad (1)$$

Where Y is the isothermal solidification zone width; $\emptyset$ is the isothermal solidification rate constant, t is the holding time.

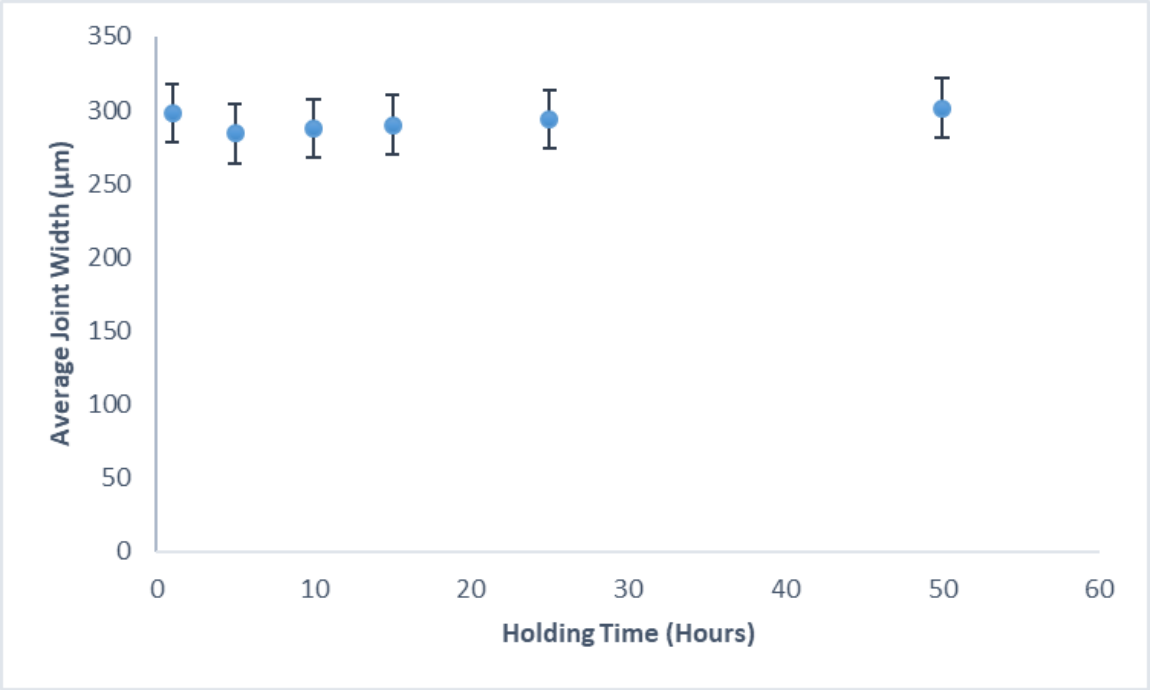

Figure 4.8: A plot of average N5/N5 joint width against holding time at 1090ºC

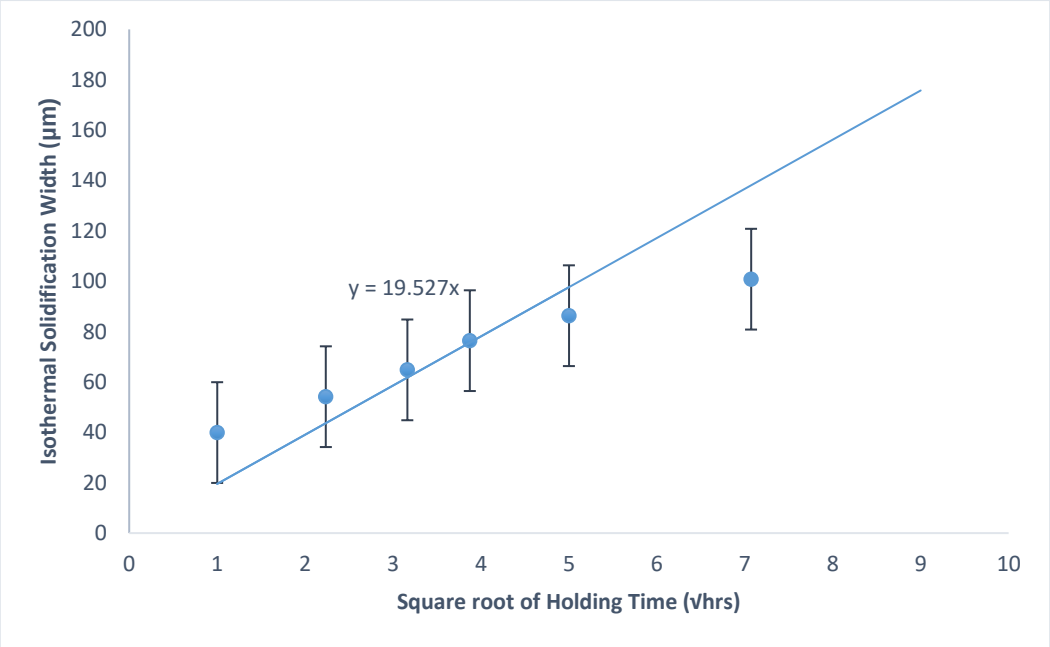

Figure 4.9: A plot of the average width of ISZ in N5/N5 joint against the square root of holding time at 1090^{o}C.

The isothermal solidification rate constant, Ø is the slope of the linear region (parabolic regime) between the ISW and the square root of holding time (Figure 4.9). It is also given by equation [136]:

$$Ø = 2 * K * \sqrt{D} \quad (2)$$

Where D is the diffusion coefficient; K is a constant for the system, and it is obtained by numerically solving the equation [134]:

$$\frac{C_{\propto l} - C_o}{C_{l\propto} - C_{\alpha l}} = \frac{\sqrt{\pi} * K * [1 + \mathrm{erf}(K)]}{e^{-k^2}} \quad (3)$$

Where $C_{l\propto}$ and $C_{\alpha l}$ are solidus and liquidus concentration respectively obtained from the Ni-B phase diagram, and C_o is the initial concentration of the MPD.

Also, the value of D in equation 2 can be calculated from equation [132]:

$$D = D_o e^{-\frac{Q}{RT}} \quad (4)$$

Where R and D_o are constants; Q is the activation energy (kJ/mol); T is the absolute temperature (Kelvin). The detailed algorithm used to solve for K, D, Ø, and Q is shown in the Appendix.

The apparent activation energy for the boron diffusion during the TLP bonding of single crystal Rene-N5 using NB-150 is computed to be 244.35kJ/mol. Table 4.4 presents the activation energy for different Ni-based superalloys. Regarding Table 4.4, the calculated Q for Rene-N5 is relatively large compared to the conventional Ni-based polycrystal superalloys. This high activation energy, Q implies that diffusion of boron into Rene-N5 during bonding will be slower than in the other superalloy and this will result in prolonged processing. However, the linear relationship observed in Figure 4.9, as well as established in equation 1, is not maintained throughout the bonding test. A deviation from the linear trend can be seen beyond 25 hours of bonding time. This deviation is a reduction change in the isothermal solidification rate constant. Based on the literature, the suggested possible causes for this deviation are highlighted below:

Table 4.4: Reported apparent activation energy for the diffusion of boron during the TLP bonding of some selected superalloys [23], [139].

Materials		Filler	Bonding Temperature (°C)	Activation Energy kJ/mol
Single crystal	**Rene-N5**	**NB-150**	**1120 - 1200**	**244**
Polycrystals	MM 007	MBF-80	1100 - 1180	219
	IN 713	MBF-80	1100 - 1200	211
	IN 600	MBF-80	1100 - 1180	209
	Mar-M 247	MBF-80	1100 - 1180	199

Firstly, the presence of more than one melting point depressant (MPD) solute diffusing from the filler alloy into the base metal, and thereby slowing down the isothermal solidification rate constant such that the processing time is prolonged [115].

Secondly, the formation of the second-phase precipitates(borides) in the base metal at the DAZ slows down the rate constant of the solidification process as well as prolonging the processing time [137].

Thirdly, the occurrence of the grain growth within the ISZ is claimed to cause reduction in the rate constant of isothermal solidification [138].

These afore-mentioned suggestions, however, do not explain the occurrence of the phenomenon in all systems because the phenomenon has been observed in systems:

i. that do not contain more than one MPD solute [80].
ii. in which second-phase precipitates (borides) are not formed within the DAZ [80].
iii. involving single crystals alloys in which there are no grain boundaries, let alone grain growth during the TLP bonding [80].

However, a recent numerical work undertaken by Amin et al. [135] has identified a possible cause of the deviation phenomenon, which is applicable to all systems. They found that the deviation from the linear relationship is due to the diffusion coefficient that is actually varying with concentration and time.

Lastly, the eutectic width reduces as the ISZ increases since the joint width is fixed. The trend in the width of isothermal solidified zone is essentially the same in eutectic width except that it is in reverse order, as shown in Figure 4.10. This is because the reduction in eutectic width is brought about by the epitaxial growth of the ISZ towards the centre of the joint.

4.3.2 Effect of bonding temperature

The changes in the joint microstructure due to the effect of bonding temperature were studied at the temperatures; 1090^{o}C, 1120^{o}C, 1150^{o}C, 1180^{o}C, and 1200^{o}C for maximum bonding time of 50 hours. The absence of significant changes in the joint width over the period of time used for bonding at 1090^{o}C (section 4.3.1) is also observed at other temperatures considered in this section. The variation in average joint width with respect to bonding temperature is shown in Table 4.5 and Figure 4.11. The joint width is 301.5 μm at a bonding temperature of 1090 ^{o}C. The increase of the bonding temperature to 1120^{o}C resulted into joint width being increased to 310.88 μm. Further increase in bonding temperature to 1150^{o}C, 1180^{o}C, and 1200^{o}C resulted in the joint width being increased to 334.88 μm, 354.27 μm, and 364.52 μm respectively. So, the trend in the data obtained demonstrates a gradual increase in the joint width as the bonding temperature is varied between 1090^{o}C and 1200^{o}C. During TLP bonding, the system undergoes dissolution so as to dilute the solute concentration to the solidus and liquidus compositions in order to achieve equilibration. As the temperature increases, the extent of dissolution required increases, thereby causing the maximum joint width reached to increase.

In addition, it is stated in section 4.3.1, that there is a linear relationship between the isothermal solidified zone width and the square root of holding time at 1090°C. A similar trend is also observed at the other bonding temperatures between 1120°C and 1200°C. This linear relationship is terminated by the occurrence of deviation at all these temperatures considered. The region of the linear trend is termed parabolic regime, and the deviation region is termed non-parabolic regime. The summary of the slopes of the parabolic regions at different bonding temperatures is given in Table 4.6. In Figure 4.12, it is observed that the slope initially increases between 1090°C and 1120°C. However, the slope generally reduces with further increase in bonding temperature from 1120°C up to 1200°C. Recall that the relationship between the slope (of the plot of the width of ISZ against the square root of holding time for a Ni-B system), the

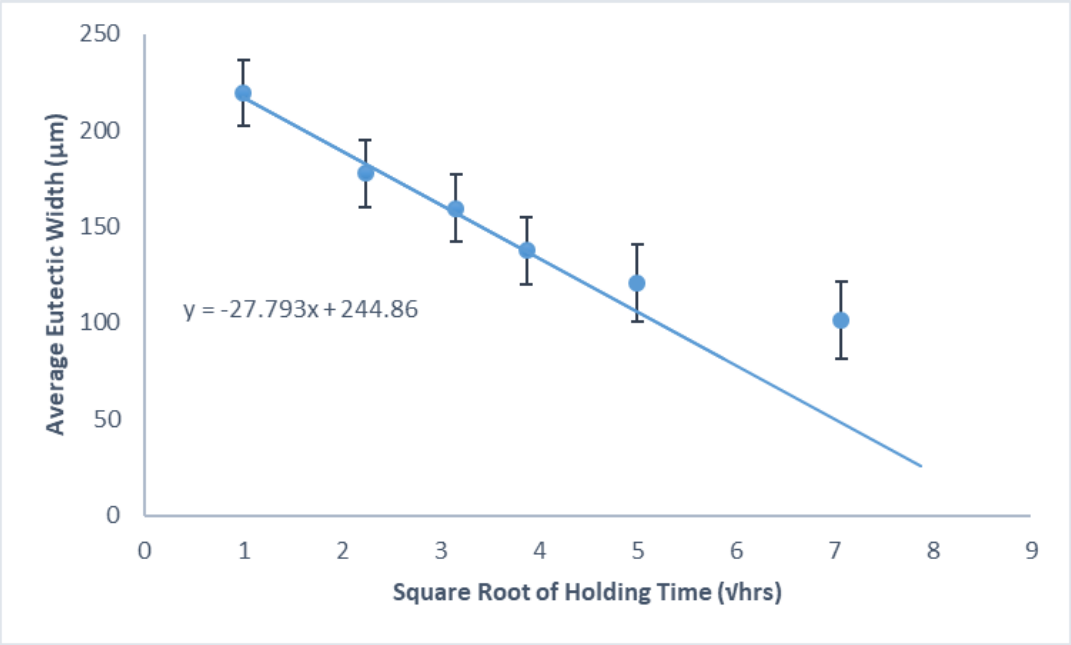

Figure 4.10: A plot of average eutectic width in N5/N5 joint against square root of holding time at 1090^{o}C.

Table 4.5: The average joint data for N5/N5 bonded between 1090°C and 1200°C

Temperatures (°C)	Average joint widths (μm)
1090	301.5
1120	310.9
1150	334.9
1180	354.3
1200	364.5

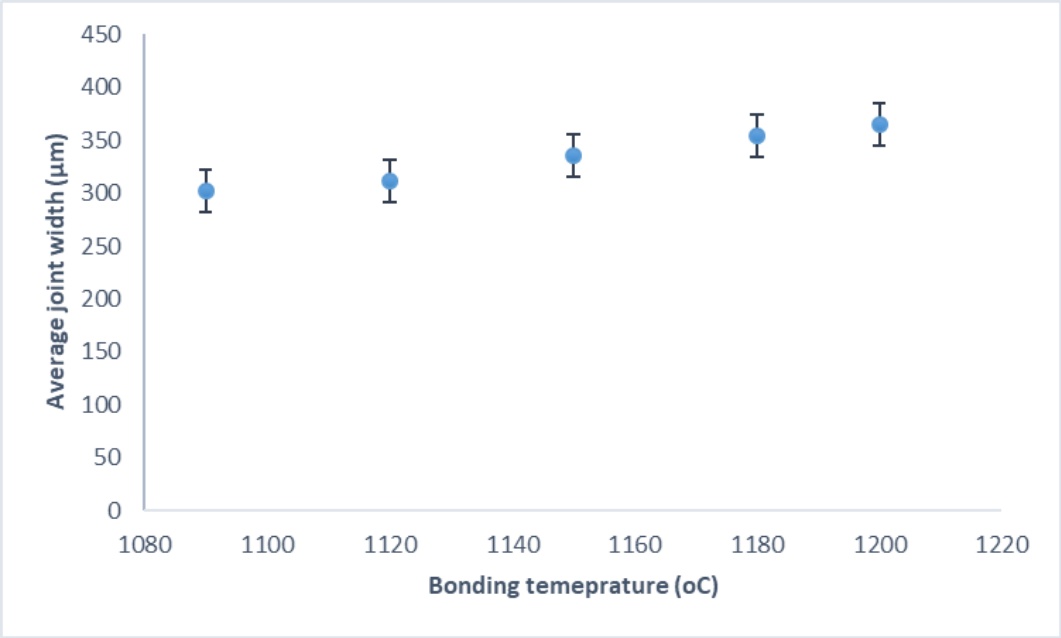

Figure 4.11: The plot of the average joint width against the corresponding bonding temperature

Table 4.6: The slopes of the parabolic regions at each bonding temperature.

Temperatures (ºC)	**Experimental slopes**
1090	21.4
1120	28.9
1150	22.7
1180	17.9
1200	15.8

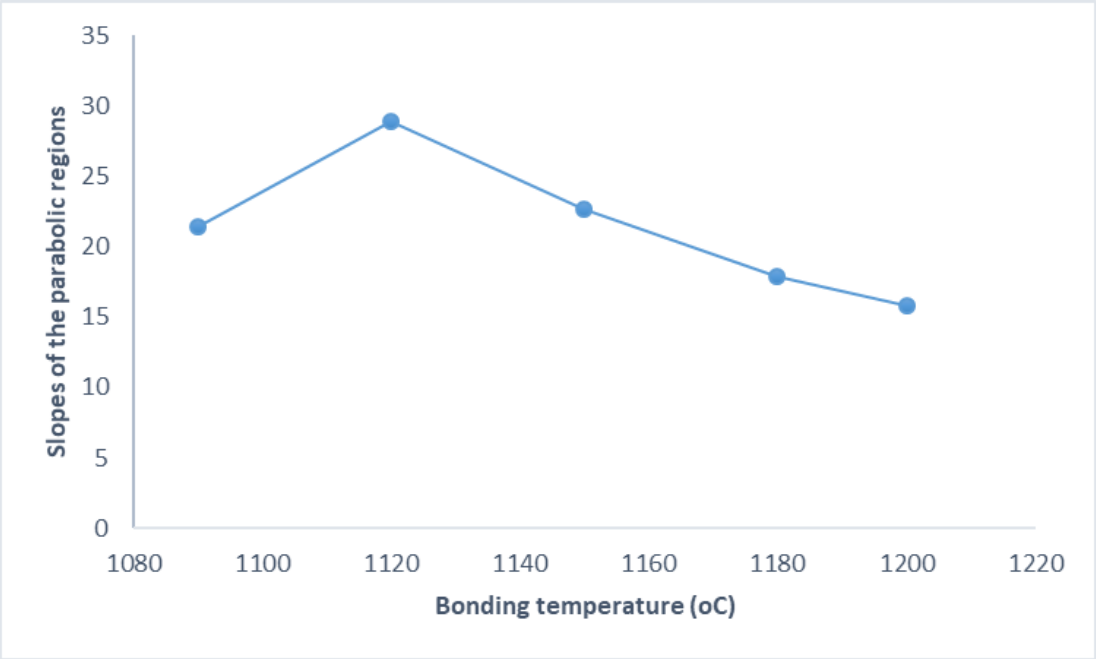

Figure 4.12: The plot of slopes of the parabolic regions and bonding temperature

constant (K), and the diffusion coefficient (D) is governed by equation 2. This equation shows that the slope is controlled by two important parameters, namely: diffusion coefficient, D and the constant, K. The influence of these parameters on the slope is on competitive basis.

Generally, diffusivity increases as temperature increases in any system, whereas the constant, K is dependent on the phase relationship at any temperature. At various values of the constant, K and diffusion coefficient, D (see appendix), the theoretical slopes (see Table 4.7) are calculated for each bonding temperature, based on the Ni-B binary system. In a binary system, it is found that the slope should increase with increase in temperature (see Figure 4.13) because the diffusion coefficient, D is large to the extent that it overcomes the effect of low constant, K. Moreover, the trend in the slope obtained by plotting the experimental data is consistent with the theoretically-predicted behavior between the bonding temperatures of 1090°C and 1120°C. However, the trend later deviates by a gradual decrease with further increase in bonding temperature between 1120°C and 1200°C. This observation seems not to be due to diffusivity in a multicomponent system such as Rene-N5. Rather, it is the constant, K that appears to control the slope between 1120°C and 1200°C. This may be explained using the phase relationship stated in equation 3.

In equation 3, the constant, K, is well known to be a function of three important parameters, namely: solidus concentration, liquidus concentrations and initial concentration of the MPD. The values of the solidus and liquidus concentrations for binary systems is probably different from that of multicomponent systems. Thus, a difference in phase relationship may be related to why a multicomponent Rene-N5 alloy system is behaving differently (reduction in ISZ rate constant at higher temperatures) in comparison to the expected increase in ISZ rate constant in simple Ni-B binary system. This reduction in the ISZ rate constant results into longer time to eliminate eutectic present within the bonded joint. Consequently, this reduction prolongs the processing time to achieve complete isothermal solidification of the bonded joint.

Table 4.7: The calculated slopes for a constant D in Ni-B systems.

Temperatures (°C)	Calculated slopes
1090	13.7
1120	16.4
1150	20.6
1180	26.3
1200	30.5

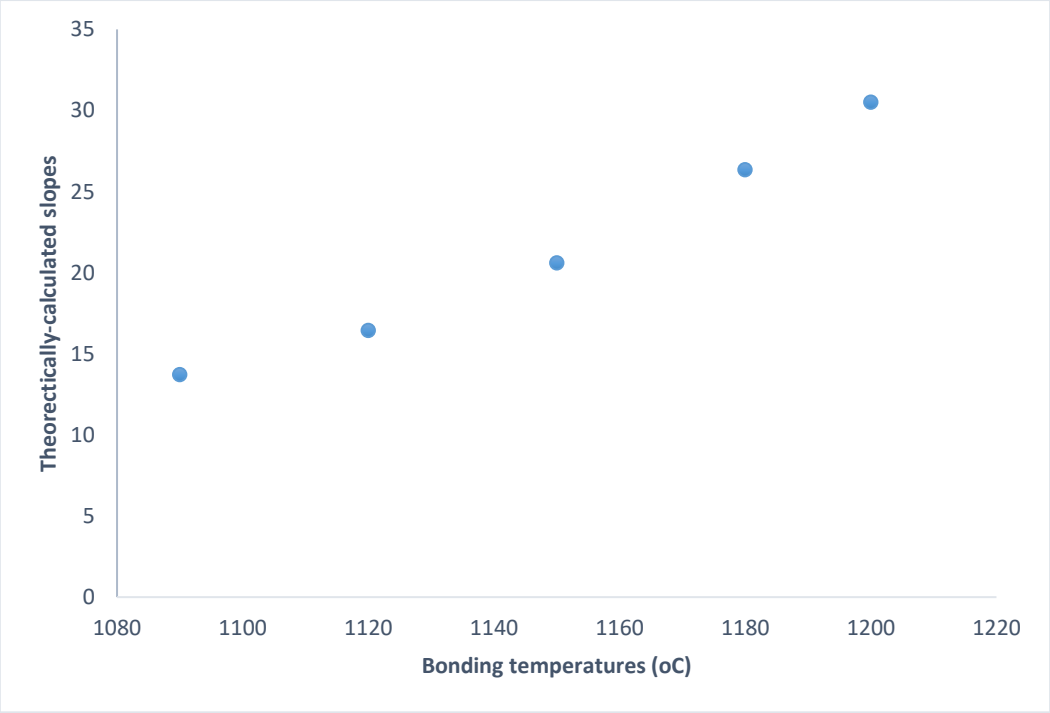

Figure 4.13: The relation between the calculated slopes and bonding temperatures for constant D

4.3.3 Effect of filler alloy composition on the microstructure of the joint

The type of filler is another important parameter that can affect the microstructure of the joint. The investigations described in the previous sections have shown that the processing time during TLP bonding of single crystal Rene-N5 superalloy is relatively long. A suggested means to reduce processing time, from the literature, is the use of a mixture of conventional filler and additive powder rather than using 100% conventional filler [118], [141]. An additive powder could be a pure metal or an alloy [142] and do not contain MPD solutes. Moreover, it is necessary that the additive should melt completely to avoid the formation of stray grains whenever it is used for brazing single crystal alloys. In this section of the current work, an experimental study is carried out to investigate the influence of process parameters, specifically mix ratio, powder size, temperature, and filler alloy composition on complete melting of the additive. The details of this experimental investigation are provided in the following discussions.

4.3.3.1 Identification of the criteria for complete melting of the filler mixture

Figure 4.14 reveals the microstructure of surface deposition of 100% NB-150 on Rene-N5 carried out at 1180^{o}C for 1 hour. This OM image shows a dendritic solidified micrograph. The formation of this microstructure can be attributed to the solidification of the liquid filler resulting from complete melting and cooling to room temperature since the experiment was conducted at a temperature above the liquidus of the filler, NB-150.

4.3.3.2 Effect of mix ratio on the extent of melting of the filler mixture

The OM images of the samples bonded at 1180^{o}C for 1 hour at different mix-ratios (70%, 50%, and 20%) using Ni-additive powder with coarse powder sizes of 100 µm are presented in Figure 4.15 (a) - (c) respectively. Figure 4.15a shows the OM image of deposit of mix-ratio of 70%

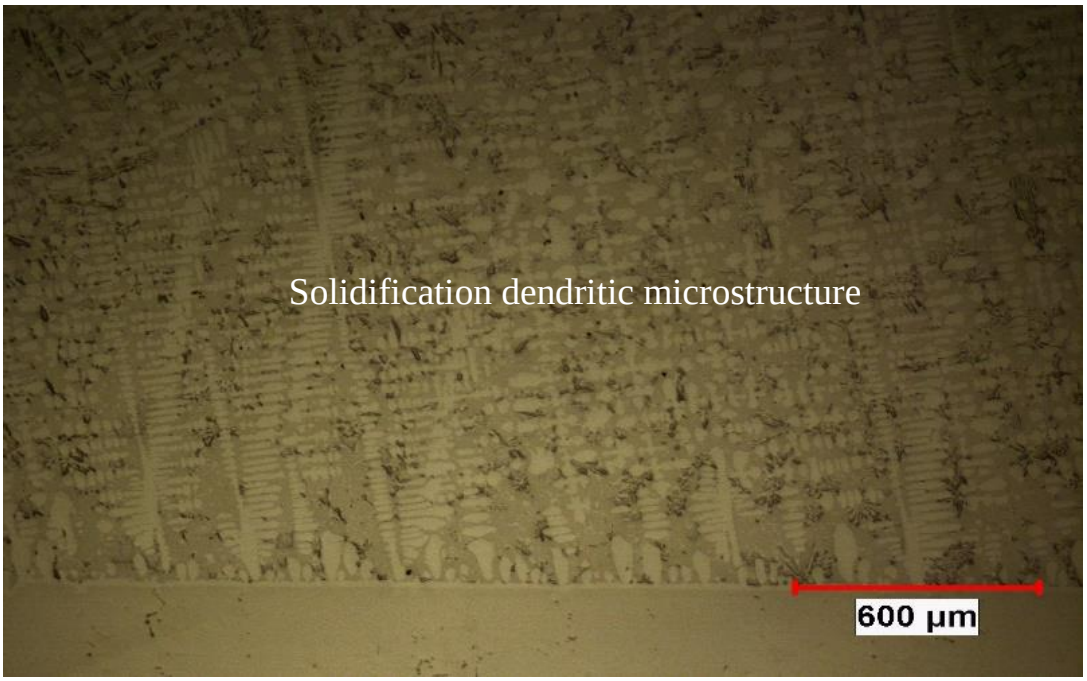

Figure 4.14: Optical images from the microscope of the completely melted 100% NB-150 filler at 1180^{o}C for 1hour

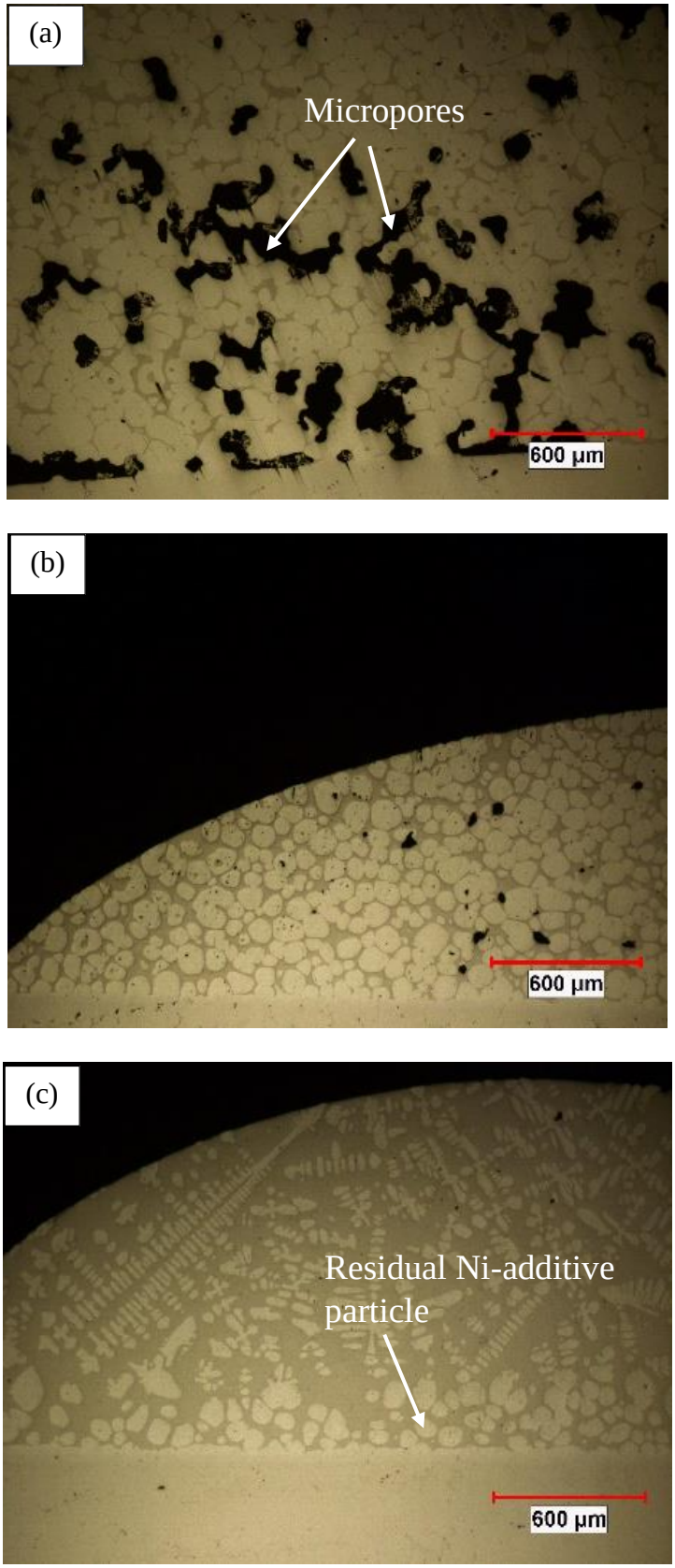

Figure 4.15: OM of the bonded samples of coarse Ni-additive powder at 1180ºC for 1 hour using different mix ratio of (a.) 70% (b.) 50% (c.) 20%

Ni-additive powder and 30% NB-150 filler on Rene-N5. This micrograph shows the appearance of randomly distributed solidification defects known as micropores and agglomerated Ni-additive powder embedded within the eutectic, solidified liquid filler. Similarly, these distinct particles of Ni-additive powder can still be seen when the mix-ratio of the additive powder was reduced to 50%, but the void volume at this condition is lower compared to 70% mix ratio (Figure 4.15b). The notably observed porosity at these mix ratios may be due to solidification shrinkage caused by limited melting of the additive powder. However, using 20% additive powder to conduct surface deposition, no micropores are observed in the micrograph (Figure 4.15c). The micrograph consists of two apparent zones; upper and lower zones. dendritic solidification microstructure is observed in the upper portion of the micrograph with complete melting of the powder while the incompletely melted Ni-additive powders are seen in the bottom zone. In general, the extent of melting increases as the fraction volume of the additive powder reduces

The effect of mix ratio was further investigated by another set of experiments conducted at 1180^{o}C for 1 hour at different mix ratios (60%, 30%, and 20%) using fine Ni-additive powder with powder size of 2-3 μm (Figure 4.16 a-c). As seen in Figure 4.16a, Rene-N5 at 60% mix ratio of Ni-additive powder shows the presence of micropores, similar to the previous experiments. Also, incompletely-melted Ni-additive powders are located within the dendritic solidification microstructure. The amount of the distinct Ni-additive powders is reduced by reducing the mix ratio of the additive powder to 30% as observed in Figure 4.16b. Furthermore, the dendritic solidification structure is noticeable at the top part of the micrograph, and very scanty micropores are present as well. The micrograph of 20% mix ratio (Figure 4.16c) demonstrates a completely-melted filler mixture since only dendritic solidification structure is observed in the entire OM image. Similar to the previous experiments, the extent of melting of the additive powder increases as the mix ratio of the additive powder reduces.

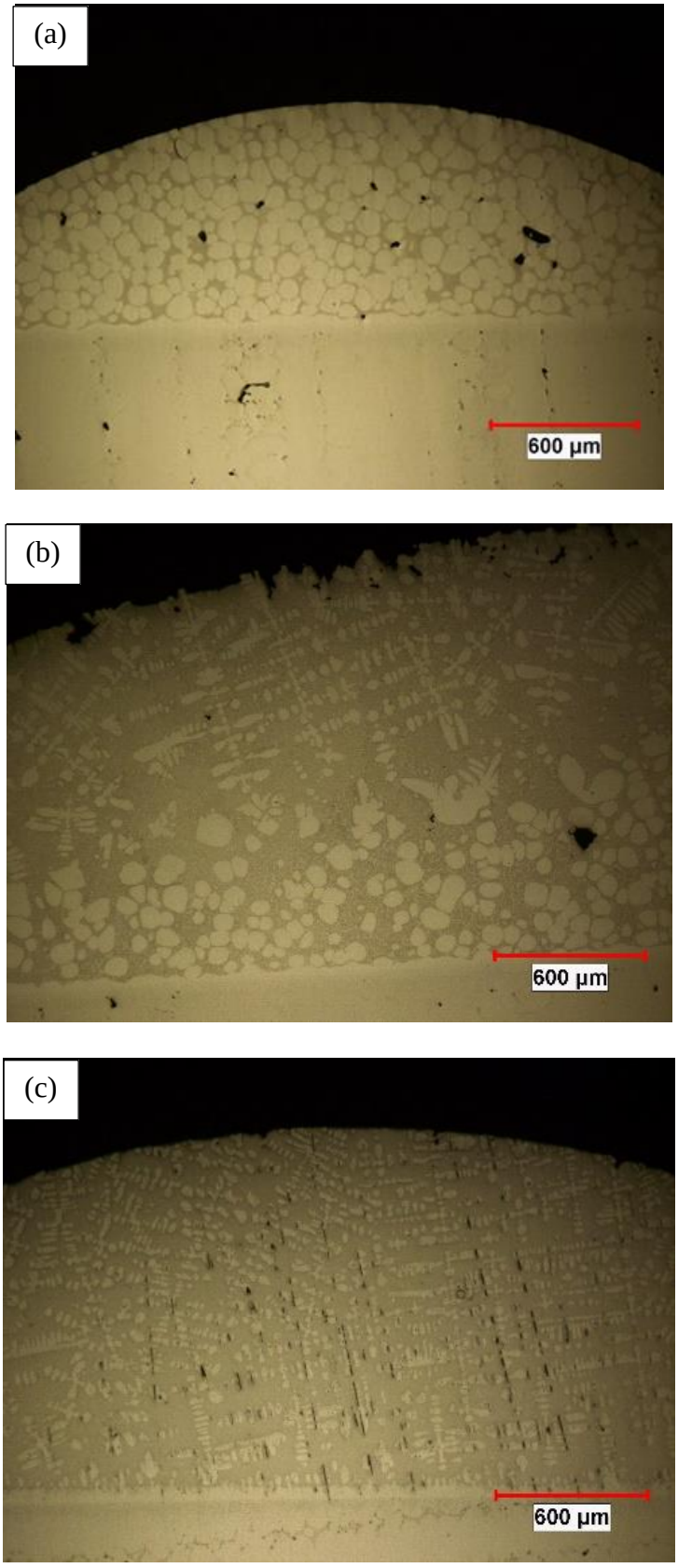

Figure 4.16: OM of the bonded samples of fine Ni-additive powder at 1180^{o}C for 1 hour using different mix ratio of (a) 60% (b) 30% (c) 20%

4.3.3.3 Effect of powder size on the extent of melting of the filler mixture

To evaluate the effect of powder size on the extent of melting of the filler mixture, 20% mix ratio of Ni-additive powder with powder sizes of fine (2-3 μm) and coarse (100 μm) at 1180^{o}C are compared (Figure 4.17 (a) and (b)). Although all the bonding conditions are the same except the powder sizes, there is a difference between the microstructures obtained. The micrograph in Figure 4.17a shows incompletely melted coarse Ni-additive powder. In contrast, there is complete melting of fine Ni-additive powders (Figure 4.17b).

4.3.3.4 Effect of temperature on the extent of melting of the filler mixture

To assess the effect of temperature on the extent of melting of the filler mixture, 30% mix ratio of fine Ni-additive powders was deposited on the Rene-N5 at 1180^{o}C and 1200^{o}C as presented in Figures 4.18 (a)-(b). The OM image provided in Figure 4.18a shows the presence of incompletely-melted Ni-additive powders in the filler mixture at 1180^{o}C. However, when the bonding temperature was increased to 1200^{o}C, the microstructure shows complete melting of the additive powder (Figure 4.18b). This observation could be explained from the understanding of mechanism of TLP bonding in conjunction with Ni-B phase diagram. Fundamentally, dissolution occurs in order to achieve equilibration through dilution of solute (MPDs) concentration from the initial filler composition to the liquidus concentration. In Ni-B binary system, as the temperature increases, liquidus concentration reduces, as shown in Figure 4.19. This will cause the extent of dissolution to increase. Hence, large amount of additive powder is expected to be dissolved at 1200^{o}C than at 1180^{o}C.

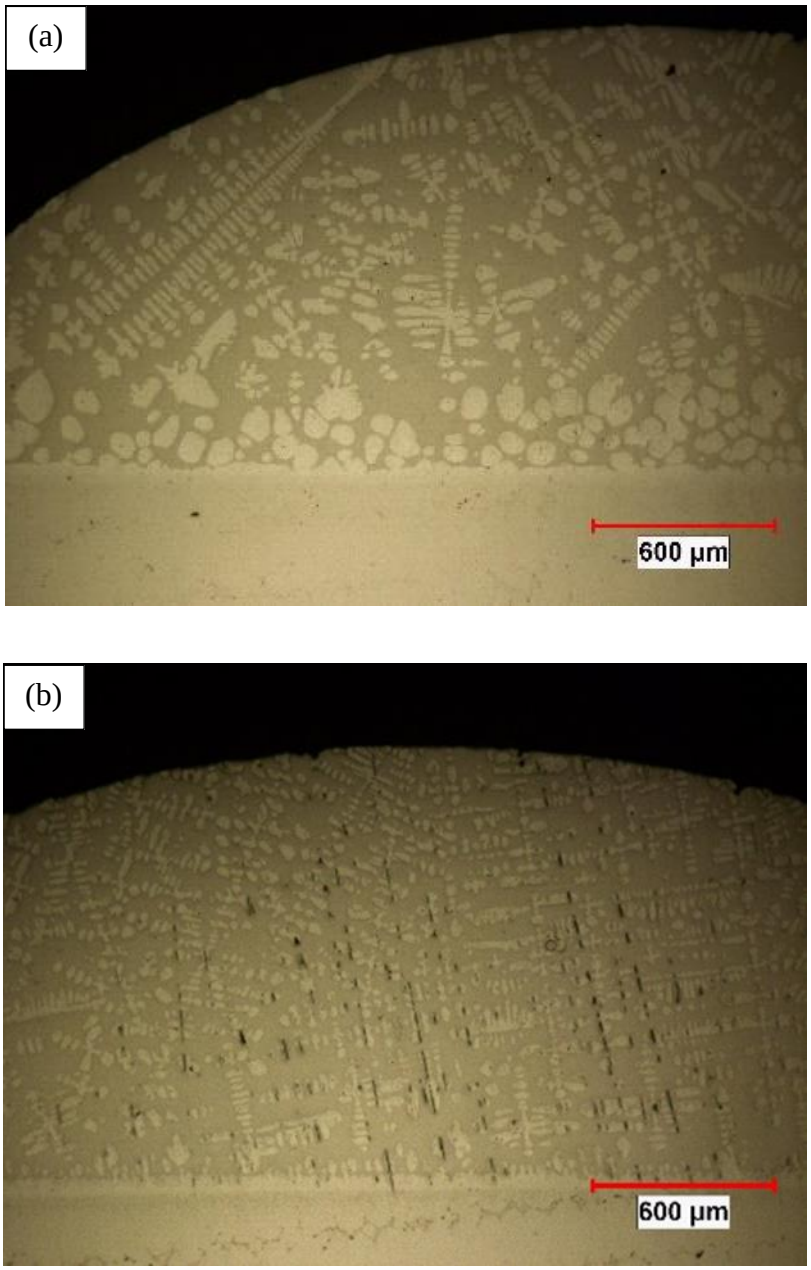

Figure 4.17: OM of the bonded samples of 20% mix ratio of Ni-additive powder at 1180^{o}C for 1 hour using different powder sizes of (a) 100 µm (b) 2-3 µm

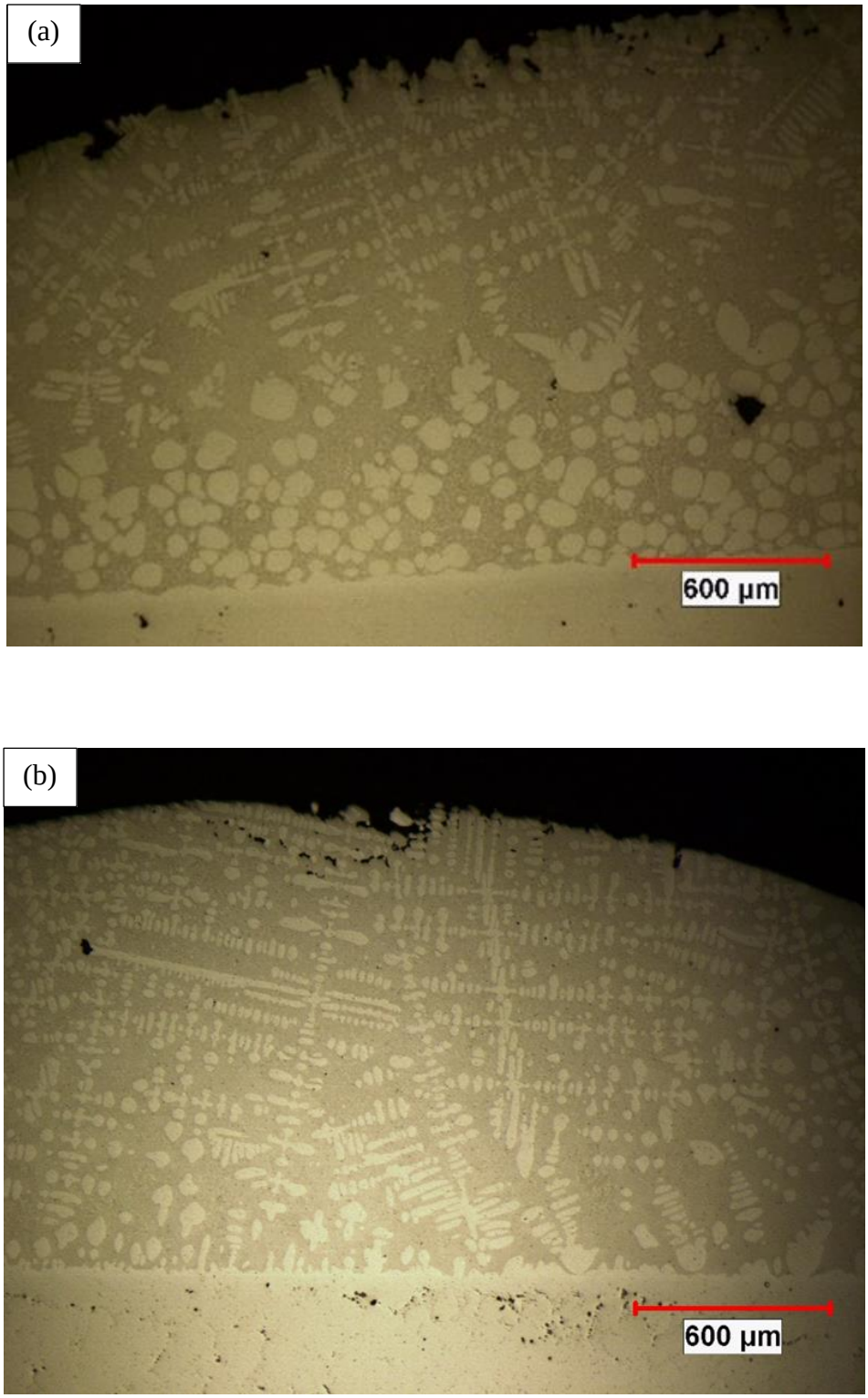

Figure 4.18: OM of the bonded samples of 30% mix ratio of fine Ni-additive powder bonded at (a) 1180^{o}C (b) 1200^{o}C

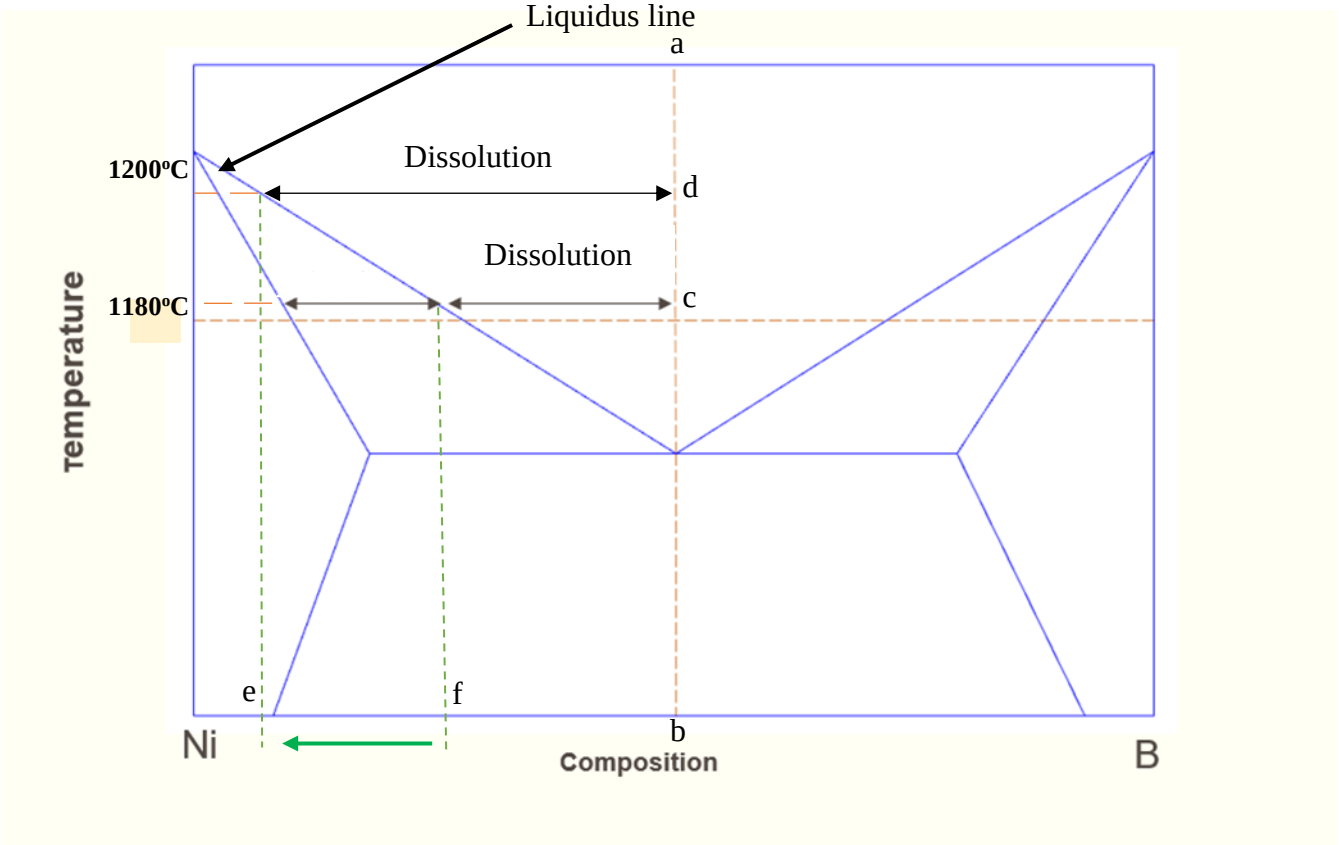

Figure 4.19: The Schematic of Ni-B phase diagram

4.3.3.5 Effect of filler mixture composition on the extent of melting of the filler mixture

Two types of additive powders, namely: pure Nickel and Nickel-based alloy, IN738 are used to study the effect of powder composition on the melting behaviour of the filler alloy. Surface deposition was carried out at 1200^{o}C for 1 hour by using 30% mix ratio of fine powder of both Nickel and IN-738 (Figure 4.20 (a)-(b)). It can be seen that both powder melted completely. Further investigation is carried out by increasing the mix ratio from 30% to 40% while other bonding conditions remain constant, as shown in Figure 4.21 (a) – (b). Figure 4.20a shows the micrograph of 40% mix ratio of Ni-additive deposit at 1200^{o}C for 1 hour. It can be seen that incomplete melting occurred. However, the micrograph obtained when 40% IN-738 is used is found to have complete melting of the additive powder. This implies that chemical composition can affect the melting behavior of the filler mixture. Hence, the reason the IN-738 powder melted more than Nickel powder may be attributed to the fact that alloying elements in IN-738 reduces the melting point of Nickel.

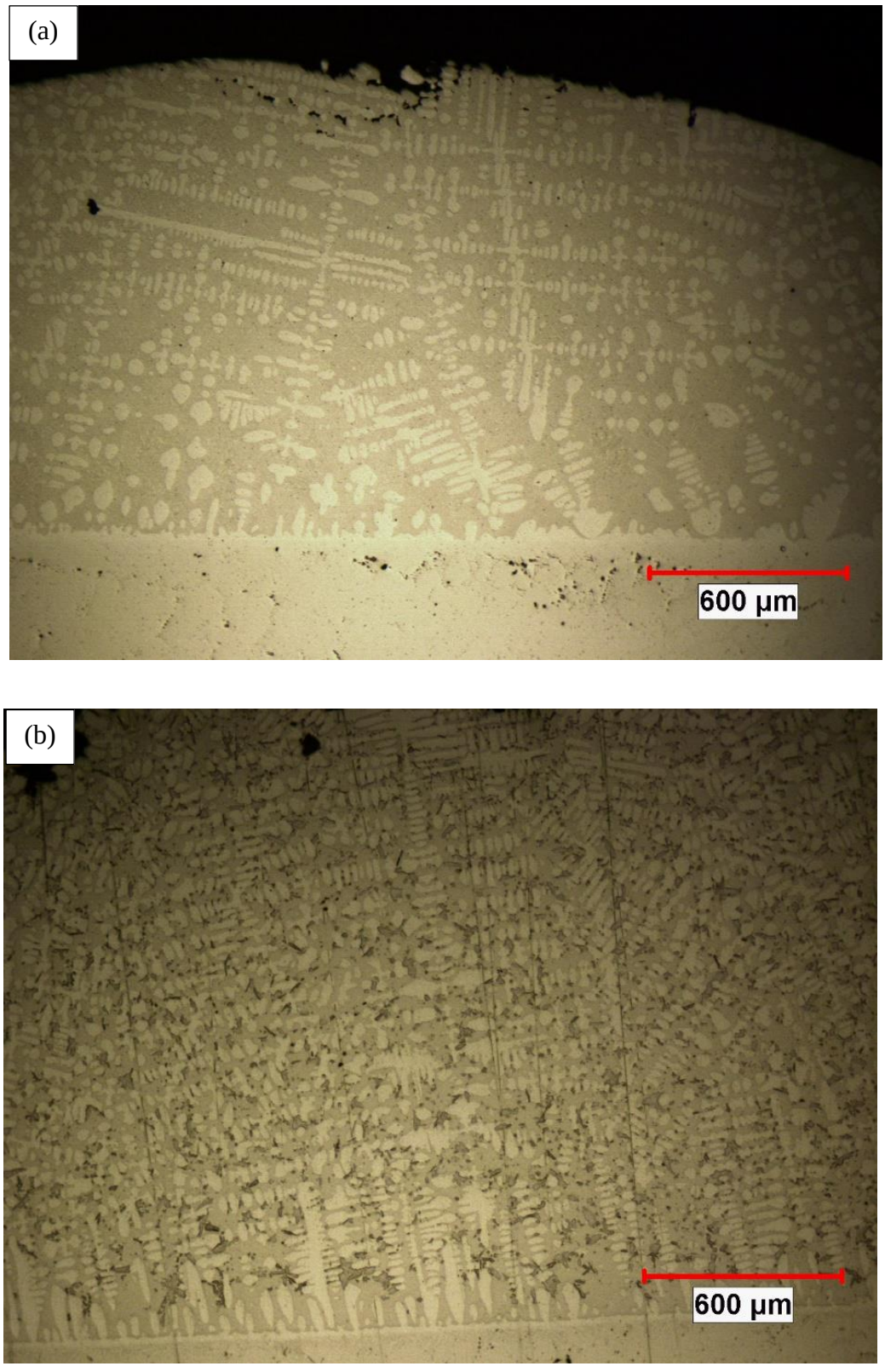

Figure 4.20: Processed images after bonding at 1200^{o}C for 1 hour using 30% mix ratio of: (a) Ni-additive (b) IN-738

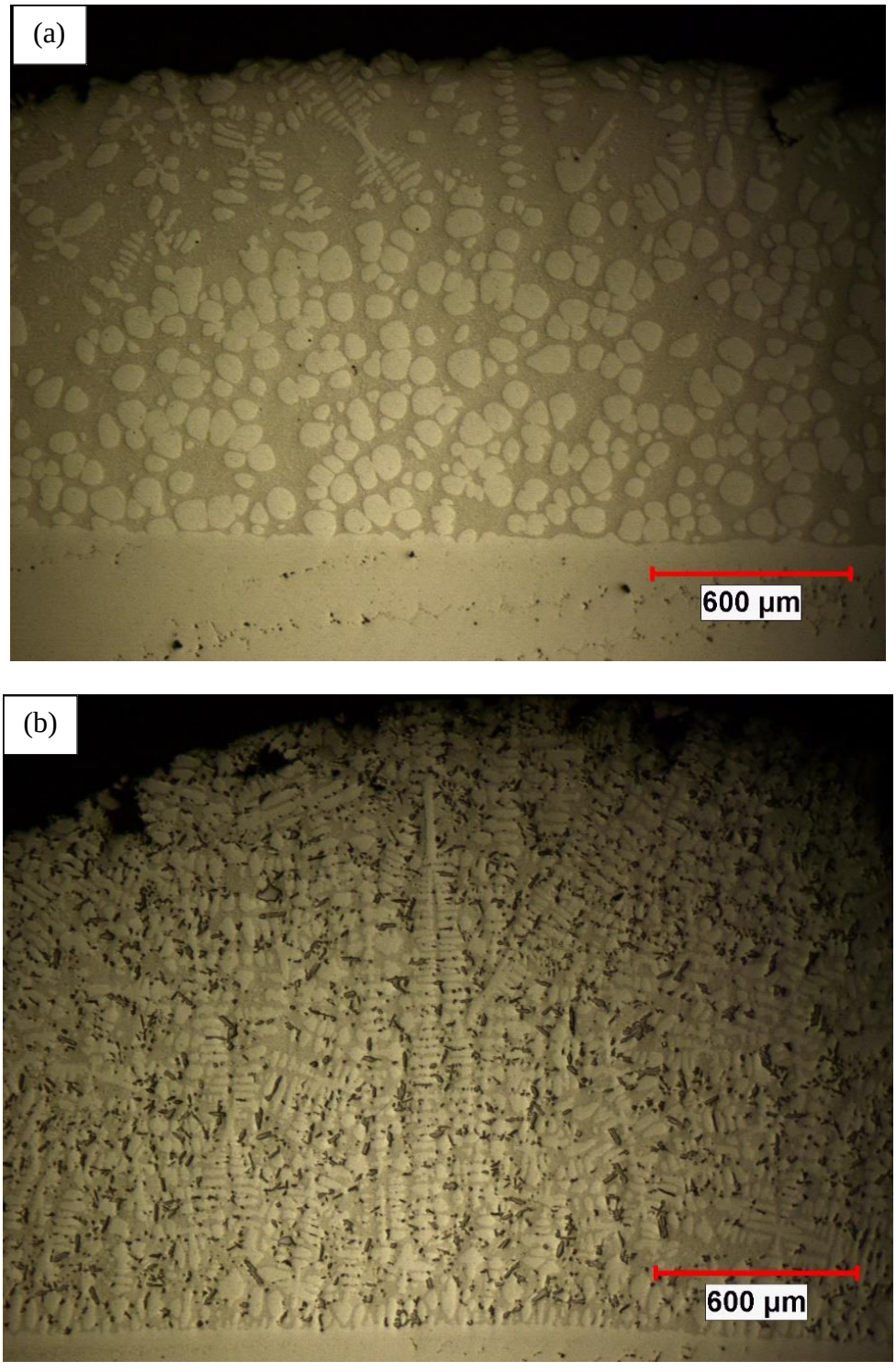

Figure 4.21: Processed images after bonding at 1200^{o}C for 1 hour using 40% mix ratio of: (a) Ni-additive (b) IN-738

4.3.3.6 Quantitative analysis of the reduction of processing time during TLP bonding

The results of the bonding experiments show that the system appears to be slow. This prolongs the required processing time to achieve complete isothermal solidification. A suggested means that can help, from the literature, is the use of additive powder and must melt completely. 40% mix ratio of fine IN-738 is selected because there is complete melting with this condition at a bonding temperature of 1200^{o}C. To investigate the reduction in processing times, TLP bonding of Rene-N5 was conducted at 1200^{o}C for bonding times between 1 hour to 50 hours using 100% NB-150 and 40% mix ratio of fine IN738-additive powder. The plot of the average eutectic width (AEW) against the square root of holding time is presented in Figure 4.22. By comparing AEW for both systems, it is observed that the use of filler mixture containing additive holds the benefit of producing smaller widths of eutectic compared to 100% conventional filler. This invariably implies that the processing time to achieve complete isothermal solidification would be lesser by the use of filler alloy and additive instead of conventional filler alloy only. The reason is attributed to the reduced amount of MPD solutes within the joint prior to TLP bonding. During the TLP bonding, the system undergoes dissolution of the substrate to achieve equilibration. The extent of this dissolution is fundamentally controlled by the amount of MPD present in the joint. By using additive powder, the amount of MPD solutes is reduced and thus the extent of dissolution is reduced, which results in less amount of liquid within the joint and hence, shorter time to achieve complete isothermal solidification.

The variation between the width of ISZ and the square root of time is shown in Figure 4.23. In Figure 4.23, the extrapolated time to complete isothermal solidification for 100% filler and 40% IN-738 are 531.72 hours and 457.099 hours, respectively. Since the times are very long, initial joint width, W_o was reduced from 200 µm to 75 µm. The experimental results obtained by bonding Rene-N5 using 75 µm gap-width at 1200^{o}C for 12 hours are presented in Figure

4.24 (a) and (b). These results show that almost complete isothermal solidification occurred after 12 hours in the 40% additive sample due to only isolated thin eutectic found along the joint. However, in the 100% filler sample, a thick and continuous eutectic with an average width of 43.72 μm is formed along the whole joint. Therefore, there is 23.16% reduction in the processing time using 40% mix ratio of fine IN-738 relative to NB-150 filler.

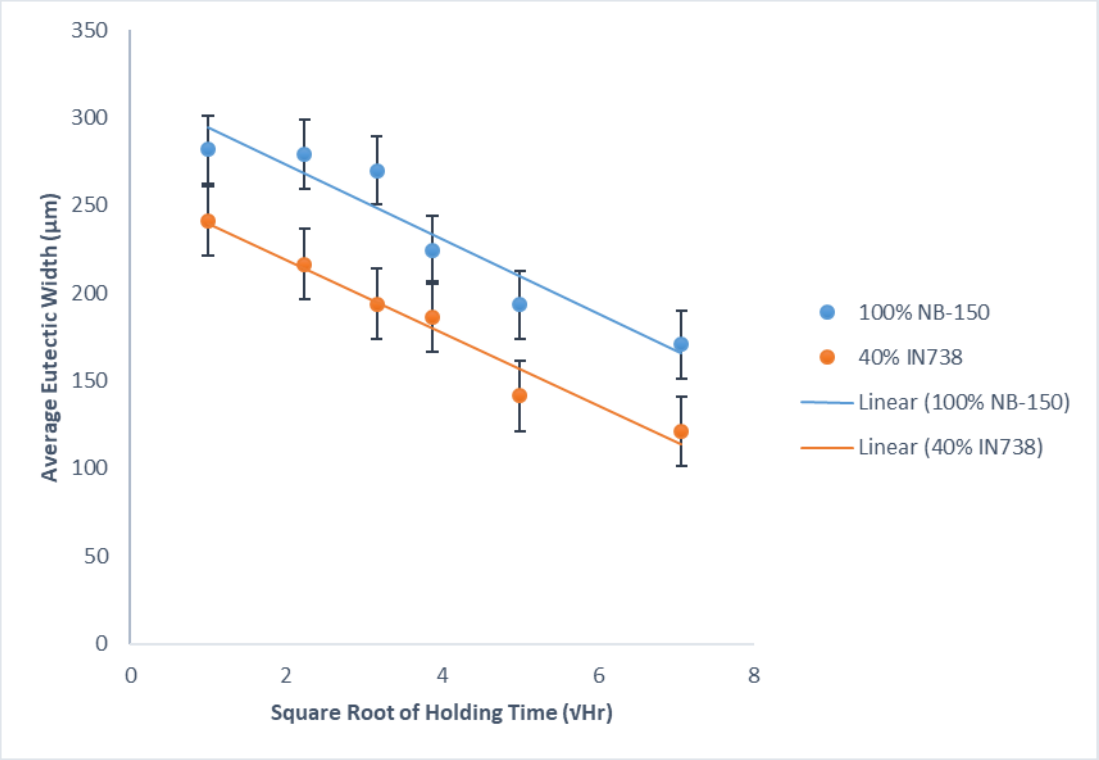

Figure 4.22: The plot of average eutectic width with the square root of bonding time for Rene-N5 at 1200ºC by using the 100% filler and filler mixture containing 40% IN738.

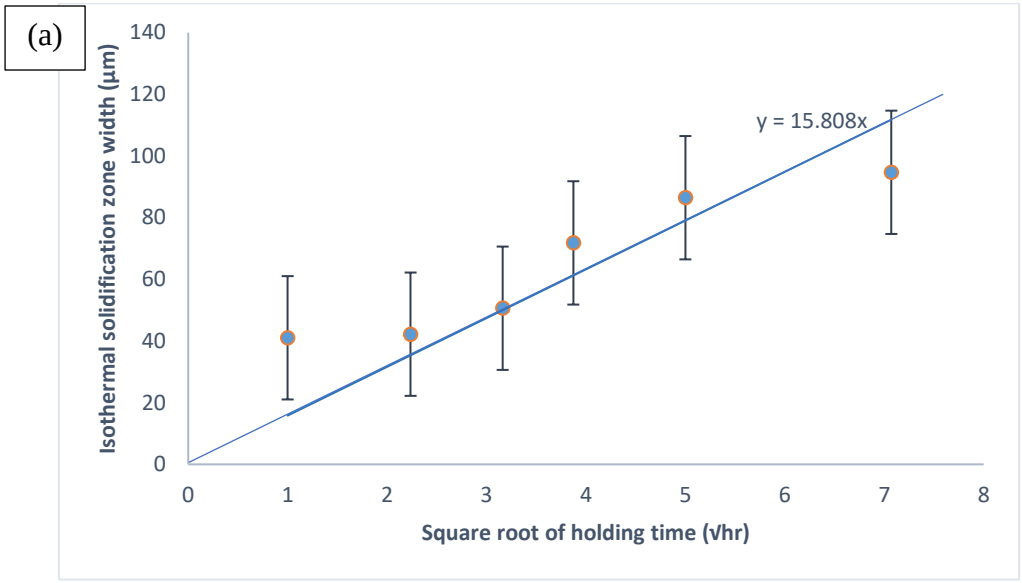

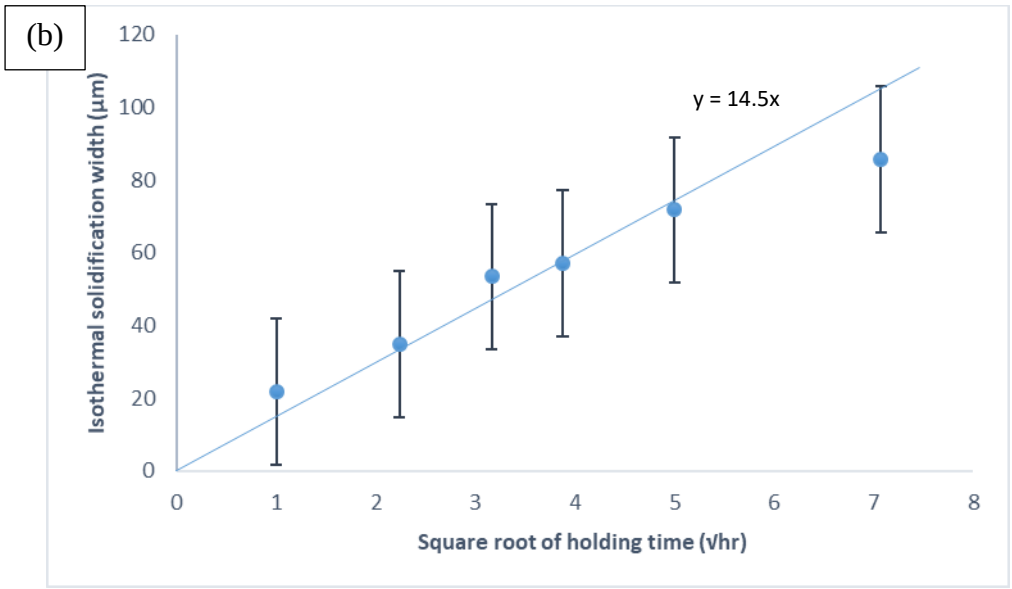

Figure 4.23: The graph of ISZ against the square root of time at 1200°C for (a) NB (b) IN-738 additive

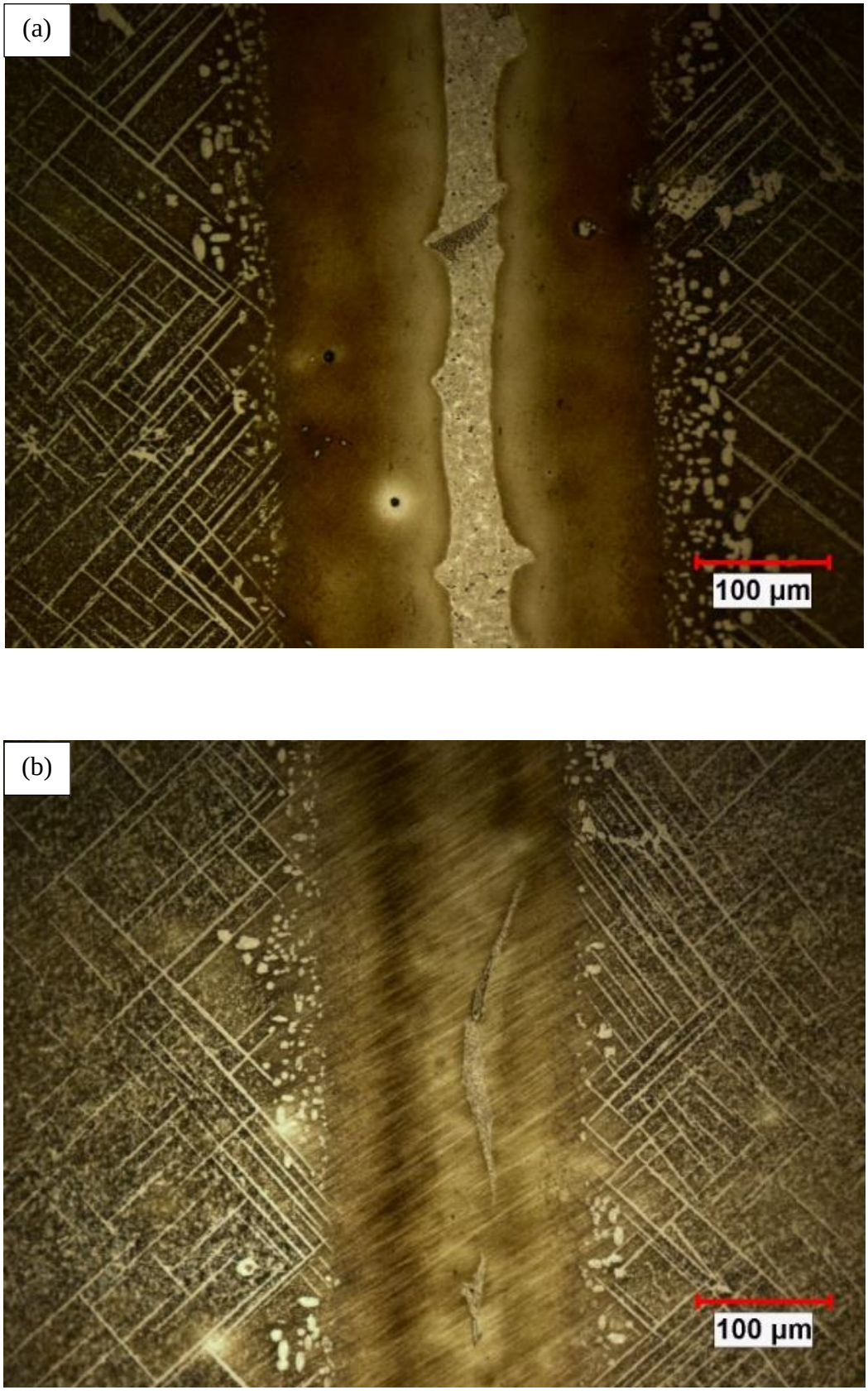

Figure 4.24: OM of the bonded Rene-N5 using an initial gap of 75 µm at 1200°C for (a) NB (b) 40% fine IN-738

CHAPTER 5 – SUMMARY, CONCLUSIONS, AND SUGGESTIONS FOR FUTURE WORK

5.1 Summary and Conclusions

In this study, single crystal Rene-N5 has been successfully bonded using transient liquid phase bonding process with the aid of NB-150 filler. The following conclusions are drawn:

1. Generally, the microstructural analysis of the bonded samples reveals three regions of the joint, namely: Isothermal Solidified Zone, On-cooling Solidified Zone, and Diffusion Affected Zone.
2. There is formation of eutectic along the bonded joints owing to insufficient holding time to achieve complete isothermal solidification. The width of the eutectic is observed to reduce with the increase in holding time.
3. Rather than a linear relationship between the isothermal solidified zone width and the square root of the holding time, based on standard TLP bonding models, deviation from this linear relationship is observed. This could be due to variation of the diffusion coefficient with concentration and time.
4. The activation energy for diffusion computed in this work suggests that the TLP bonding of single crystal Rene-N5 will take a longer processing time compared to conventional polycrystalline superalloys like IN 738 etc.
5. Contrary to theoretical expectations based on binary alloy system, the experimental results show that the rate constant of isothermal solidification reduces with the increase in the bonding temperature between the 1120 ^{o}C and 1200 ^{o}C.
6. Therefore, the reduction in isothermal solidification rate constant with temperature may be attributed to phase relationship in a multicomponent system, such as Rene-N5,

between 1120 ^{o}C and 1200 ^{o}C to be in a form that the constant, K which is a function of liquidus concentration, solidus concentration and initial concentration to outweigh diffusivity, thereby reducing slope as temperature increases.

7. Some parameters are found to influence the extent of melting of the additive powder. These include: temperature, powder size, mix ratio and filler alloy composition. It is observed that the extent of melting increases as powder size and mix ratio reduces and as temperature increases. In addition, the use of IN-738 alloy instead of pure Nickel as an additive material was found to aid complete melting of the filler mixture due to the fact that alloying elements in IN-738 reduces the melting point of Nickel.
8. The use of filler mixture that contains 40% fine IN-738 additive powder and 60% conventional filler resulted into complete melting at 1200^{o}C and caused a considerable reduction (23.16%) in the processing time of a single crystal joint when compared to the use of 100% conventional filler, NB-150. This can enhance the effectiveness of the bonding process for commercial application.

5.2 Suggestions for Future Works

1. Further study can be performed with the use of other filler alloys to study how the effect of process parameters on the joint microstructure are influenced by different MPD solutes during TLP bonding of single crystal superalloys.
2. Experimental investigation is recommended to be carried out to study the effect of filler materials that contains completely melted additive powder on mechanical properties of the joints of TLP bonded single crystal superalloys.
3. Experimental study can be conducted to evaluate the hot-corrosion properties of single crystal joints produced by TLP bonding using different filler alloys that contains completely melted additive powder.

REFERENCES

[1] L. Cao, Y. Zhou, T. Jin, and X. Sun, “Effects of Re on surface eutectic formation for Ni-base single crystal superalloys during directional solidification,” *J. Mater. Sci. Technol.*, vol. 33, 2017, pp. 1308–1313.

[2] R. Hashizume, A. Yoshinari, T. Kiyono, Y. Murata, and M. Morinaga, “Development of Ni-based single crystal superalloys for power-generation gas turbines,” in *Superalloys 2004*, 2004, pp. 53–62.

[3] M. Konter, E. Kats, and N. Hofmann, “A Novel casting process for single crystal gas turbine components,” in *Superalloys 2000*, 2000, pp. 189–200.

[4] J.L. Caron and J.W. Sowards, “Weldability of Nickel-base alloys,” in *Comprehensive materials processing*, 2014, p. 171.

[5] A. Mottura and R. C. Reed, “What is the role of rhenium in single crystal superalloys?,” in *EUROSUPERALLOYS 2014 – 2nd European Symposium on Superalloys and their Applications*, vol. 14, 2014, p. 01001.

[6] G. Wang *et al.*, “Microstructure evolution and mechanical behavior of Ni-based single crystal superalloy joint brazed with mixed powder at elevated temperature,” *J. Mater. Sci. Technol.*, vol. 33, 2017, pp. 1219–1226.

[7] L. Chai, L. Wang, J. Huang, J. Hou, B. Lang, and H. Yang, “Microstructure and property of N5 single crystal superalloy joints bonded by transient liquid phase diffusion bonding,” *Appl. Mech. Mater.*, vol. 751, 2015, pp. 77–81.

[8] A. Basak and S. Das, “Carbide formation in Nickel-base superalloy MAR-M247 processed through scanning laser epitaxy (SLE),” in *Solid Freeform Fabrication 2016: Proceedings of the 27th Annual International Solid Freeform Fabrication Symposium*

– *An Additive Manufacturing Conference*, 2016, pp. 460–468.

[9] M. Pouranvari, A. Ekrami, A. H. Kokabi, and H. N. Han, "Microstructural characteristics of a cast IN718 superalloy bonded by isothermal solidification," *Met. Mater. Int.*, vol. 19, no. 5, 2013, pp. 1091–1099.

[10] O. Aina, "Effects of process parameters on the transient liquid phase bonding of dissimilar materials: IN 738 superalloy and cobalt," University of Manitoba, 2018.

[11] B. Binesh and A. J. Gharehbagh, "Transient liquid phase bonding of IN738LC / MBF-15 / IN738LC : Solidification behavior and mechanical properties," *J. Mater. Sci. Technol.*, vol. 32, 2016, pp. 1137–1151.

[12] A. Y. Shamsabadi, R. Bakhtiari, and G. Eisaabadi B., "TLP bonding of IN738/MBF20/IN718 system," *J. Alloys Compd.*, vol. 685, 2016, pp. 896–904.

[13] B. K. Lee, W. Y. Song, D. U. Kim, I. S. Woo, and C. Y. Kang, "Effect of bonding temperatures on the transient liquid phase bonding of a directionally solidified Ni-based superalloy, GTD-111," *Met. Mater. Int.*, vol. 13, no. 1, 2007, pp. 59–65.

[14] M. Khakian, S. Nategh, and S. Mirdamadi, "Effect of bonding time on the microstructure and isothermal solidification completion during transient liquid phase bonding of dissimilar nickel-based superalloys IN738LC and Nimonic 75," *J. Alloys Compd.*, vol. 653, 2015, pp. 386–394.

[15] L. X. Zhang, Z. Sun, Q. Xue, M. Lei, and X. Y. Tian, "Transient liquid phase bonding of IC10 single crystal with GH3039 superalloy using BNi2 interlayer: Microstructure and mechanical properties," *Mater. Des.*, vol. 90, 2016, pp. 949–957.

[16] G. M. M.B. Henderson , D. Arrell , M. Heobel, R. Larsson, "Nickel-Based Superalloy Welding Practices for Industrial Gas Turbine Applications M.B. Henderson , D. Arrell,

M. Heobel*, R. Larsson and G. Marchant + +," *Sci. Technol. Weld. Join.*, vol. 9, no. 1, 2004, pp. 1–14.

[17] X. Wu, R. S. Chandel, and H. Li, "Evaluation of transient liquid phase bonding between nickel-based superalloys," *J. Mater. Sci.*, vol. 36, 2001, pp. 1539–1546.

[18] V. Jalilvand, H. Omidvar, H. R. Shakeri, and M. R. Rahimipour, "Microstructural evolution during transient liquid phase bonding of Inconel 738LC using AMS 4777 filler alloy," *Mater. Charact.*, vol. 75, 2013, 2013, pp. 20–28.

[19] M. Segersäll, "Nickel-Based single-crystal superalloys temperature properties," Linköping University, 2013.

[20] E. Akca and A. Gürsel, "A review on superalloys and IN718 Nickel-based INCONEL superalloy," *Period. Eng. Nat. Sci.*, vol. 3, no. 1, 2015, pp. 15–27.

[21] M.B. Henderson, D. Arrell, R. Larsson, M. Heobel and G. Marchant, "Nickel-based superalloy welding practices for industrial gas turbine applications," *Sci. Technol. Weld. Join.*, vol. 9, no. 1, 2004, pp. 13–21.

[22] J. farouk Hunedy, "Influence of base alloy composition on processing time during TLP bonding of Nickel-base superalloys," University of Manitoba, 2013.

[23] D. Kim and K. Nishimoto, "Bonding phenomena of transient liquid phase bonded joints of a Ni-base single crystal superalloy," *Met. Mater. Int.*, vol. 8, no. 4, 2002, pp. 403–410.

[24] K. Nishimoto, K. Saida, D. Kim and Y. Nakao, "Transient liquid phase bonding of Ni-base single crystal, CMSX-2," *ISIJ Int.*, vol. 35, no. 10, 1995, pp. 1298–1306.

[25] W. Guo, H. Wang, Q. Jia, P. Peng, and Y. Zhu, "Transient Liquid Phase Bonding of Nickel-Base Single Crystal Alloy with a Novel Ni-Cr-Co-Mo-W-Ta-Re-B Amorphous

Interlayer," *High Temp. Mater. Process.*, vol. 36, no. 7, 2017, pp. 677–682.

[26] L. Chai, J. Huang, J. Hou, B. Lang, and L. Wang, "Effect of holding time on microstructure and properties of transient liquid-phase-bonded joints of a single crystal alloy," *J. Mater. Eng. Perform.*, vol. 24, no. 6, 2015, pp. 2287–2293.

[27] A. Kracke, "Superalloys, the most successful alloy system of modern times - past, present, and future," in *a 7th international symposium on superalloy 718 and derivatives*, 2010, pp. 13–50.

[28] G. R. Thellaputta, P. S. Chandra, and C. S. P. Rao, "Machinability of Nickel-Based Superalloys : A Review," *Proceedings*, vol. 4, no. 2, 2017, pp. 3712–3721.

[29] M. J. Donachie and S. J. Donachie, *Superalloys: a technical guide*, 2nd ed. Ohio: ASM International, 2002.

[30] R. N. Ghosh, "Superalloy: Processing and performance," *Adv. Mater. Proc. Indo-Malaysian Jt. Work.*, 2002, pp. 97–106.

[31] A. Nowotnik, "Nickel-Based Superalloys," *Ref. Modul. Mater. Sci. Mater. Eng.*, 2017, pp. 1–7.

[32] S. Liu *et al.*, "Effect of interactions between elements on the diffusion of solutes in Ni-X-Y systems and γ′-coarsening in model Ni-based superalloys," *Scr. Mater.*, vol. 138, 2017, pp. 100–104.

[33] R. Sowa, S. Arabasz, and M. Parlinska-wojtan, "Classification and microstructural stability of high generation single crystal nickel-based superalloys," *Zast. Mater.*, vol. 57, no. 2, 2016, pp. 274–281.

[34] R.C. Reed, *The superalloys: Fundamentals and applications*, 1st ed. Cambridge: Cambridge University Press, 2006.

[35] H. A. Kishawy and A. Hosseini, “superalloys,” in *Machining Difficult-to-Cut Materials, Materials Forming, Machining and Tribology*, USA: Springer International Publishing, 2019, pp. 94–135.

[36] J.L. Smialek and G.H. Meier, *Superalloys II: High temperature oxidation*. USA: John Wiley and Sons, Inc, 2016.

[37] A. F. Giamei, “A Brief History,” *Adv. Mater. Process.*, 2016, pp. 26–30.

[38] M. Durand-Charre, *The Microstructure of Superalloys*, 1st ed. London: CRC Press, 1997.

[39] Y. Huang, Z. Mao, R. D. Noebe, and D. N. Seidman, “The effects of refractory elements on Ni-excesses and Ni-depletions at (f.c.c.)/(L12) interfaces in model Ni-based superalloys: Atom-probe tomographic experiments and first-principles calculations,” *Acta Mater.*, vol. 121, 2016, pp. 288–298.

[40] P. A. J. Bagot *et al.*, “An Atom Probe Tomography study of site preference and partitioning in a nickel-based superalloy,” *Acta Mater.*, vol. 125, 2017, pp. 156–165.

[41] T. M. Pollock and S. Tin, “Nickel-based superalloys for advanced turbine engines : Chemistry, microstructure, and properties,” *J. Propuls. power*, vol. 22, no. 2, 2006, pp. 361–374.

[42] M. Gebura, “Chemical composition and classification of single crystal nickel base superalloys,” *Mater. Inz.*, 2008, pp. 1–4.

[43] T. M. Pollock, and A. S. Argon, “Creep resistance of CMSX-3 nickel base superalloy single crystals,” *Acta Metall. Mater.*, vol. 40, no. 95, 1992, pp. 1–30.

[44] A. F. Giamei and D. L. Anton, “Rhenium additions to a Ni-base superalloy : Effects on microstructure,” *Metall. Trans. A*, vol. 16A, 1997, pp. 1997–1998.

[45] K. Harris, G. L. Erickson, and S. L. Sikkenga, “Development of the rhenium-containing superalloys CMSX-4 and CM 186 LC for single crystal blade and directionally solidified vane applications in advanced turbine engines,” *Superalloys*, 1992, pp. 297–306.

[46] A. K. Sinha, “Topologically close-packed structures of transition metal alloys,” *Prog. Mater. Sci.*, vol. 15, no. 2, 1972, pp. 81–185.

[47] J. S. Van Sluytman, A. La Fontaine, J.M. Cairney, and T.M. Pollock, “Elemental partitioning of platinum group metal-containing Ni-base superalloys using electron microprobe analysis and atom probe tomography,” *Acta Mater.*, vol. 58, no. 6, 2010, pp. 1952–1962.

[48] F. Pyczak, S. Neumeier, and M. Göken, “Temperature dependence of element partitioning in rhenium and ruthenium bearing nickel-base superalloys,” *Mater. Sci. Eng.*, vol. 527, no. 29–30, 2010, pp. 7939–7943.

[49] Z. Peng, I. Povstugar, K. Matuszewski, R. Rettig, R. Singer, and A. Kostka, “Effects of Ru on elemental partitioning and precipitation of topologically close-packed phases in Ni-based superalloys,” *Scr. Mater.*, vol. 101, 2015, pp. 44–47.

[50] A. Sato, H. Harada, A. Yeh and K. Kawagishi, “A 5th Generation SC superalloy with balanced high-temperature properties and processability,” in *Superalloys*, 2008, pp. 131–138.

[51] G.N. Haidemenopoulos, *Physical metallurgy: Principles and design*. Florida: CRC Press, 2018.

[52] F. Xu, Y. Lv, Y. Liu, F. Shu, P. He, and B. Xu, “Microstructural evolution and mechanical properties of Inconel 625 alloy during pulsed plasma arc deposition

process," *J. Mater. Sci. Technol.*, vol. 29, no. 5, 2013, pp. 480–488.

[53] A. Sato and M. Meshil, "Solid solution softening and solid solution hardening," *Acta Metall.*, vol. 21, no. 6, 1973, pp. 753–768.

[54] H. Kitaguchi, "Microstructure-property relationship in advanced Ni-based superalloys," in *Metallurgy – Advances in materials and processes interface.*, Uk: InTECHOPEN, 2012, pp. 1–42.

[55] H. Rehman, "Solid solution strengthening and diffusion in nickel- and cobalt-based superalloys," FAU university press, 2016.

[56] S.C.R. Aluru, "Microstructure – mechanical property relationships in transient liquid phase bonded nickel-based superalloys and iron-based ODS alloys," Auburn University, 2006.

[57] S. Singh, "Superalloy report," India, 2016.

[58] S. Meher, M.C. Carroll, T.M. Pollock, and L.J. Carroll, "Designing nickel base alloys for microstructural stability through low γ-γ′ interfacial energy and lattice misfit," *Mater. Des.*, vol. 140, 2018, pp. 249–256.

[59] M. Kamaraj, "Rafting in single crystal nickel-base superalloys – An overview," *Sadhana*, vol. 28, no. 1–2, 2003, pp. 115–128.

[60] A. Basak and S. Das, "Additive manufacturing of Nickel-base superalloy Rene N5 through scanning laser epitaxy (SLE) - Material processing, microstructures, and microhardness properties," *Adv. Eng. Mater.*, vol. 19, no. 3, 2017, pp. 1–10.

[61] W.S. Walston, K.S. O'Hara, E.W. Ross, T.M. Pollock and W.H. Murphy, "Rene N6: Third generation single crystal superalloy," *Miner. Met. Mater. Soc.*, 1996, pp. 27–34.

[62] D. H. and M. H. J.R. Li, Z.G. Zhong, D.Z. Tang, S.Z. Liu, P. Wei, P.Y. Wei, Z.T. Wu, "A low-cost second generation single crystal superalloy DD6," in *Superalloys*, 2000, pp. 777–783.

[63] R. C. Reed, T. Tao, and N. Warnken, "Alloys-By-Design : Application to nickel-based single crystal superalloys," *Acta Mater.*, vol. 57, no. 19, 2009, pp. 5898–5913.

[64] C. Feng, J. M. Tannenbaum, B. S. Kang, and M. A. Alvin, "A load-based multiple-partial unloading micro-indentation technique for mechanical property evaluation," *Exp. Mech.*, vol. 50, 2010, pp. 737–743.

[65] R. I. Wu and J. H. Perepezko, "Liquidus temperature determination in multicomponent alloys by thermal analysis," *Metall. materals Trans.*, vol. 31, 2000, pp. 497–501.

[66] J. Cheng, E. H. Jordan, B. Barber, and M. Gell, "Thermal/residual stress in an electron beam physical vapor deposited thermal barrier coating system," *Acta Mater.*, vol. 46, no. 16, 1998, pp. 5839–5850.

[67] O.M. Barabash, R.I. Barabash, S.A. David, and G.E. Ice, "Residual stresses, thermomechanical behavior, and interfaces in the weld joint of Ni-based superalloys," *Adv. Eng. Mater.*, vol. 8, no. 3, 2006, pp. 202–205.

[68] O.J. Adebajo, "Effects of transient liquid phase bonding on corrosion performance of a single crystal aerospace superalloy," University of Manitoba, 2016.

[69] D.G. Brandon and W.D. Kaplan, *Joining processes: An introduction*, 1st ed. USA: Wiley and Sons, 1997.

[70] B.J. Moniz and R.T. Miller, *Welding skills*, 3rd ed. Illinois: American Technical Publishers, 2004.

[71] S. Kou, *Welding metallurgy*, 2nd ed. USA: John Wiley and Sons, Inc, 2003.

[72] A.A.Y. Al-Quenaei, “Fusion Welding Techniques,” *Int. J. Eng. Res. Appl.*, vol. 6, no. 3, 2016, pp. 78–83.

[73] M. Sokolov and A. Salminen, “Improving laser beam welding efficiency,” *Engineering*, vol. 6, 2014, pp. 559–571.

[74] T. DebRoy and S.A. David, “Physical processes in fusion-welding,” *Rev. Mod. Phys.*, vol. 67, no. 1, 1995, pp. 85–112.

[75] S. Wang, “Welding and repair of single crystal Ni-based superalloys,” Carleton University, 2005.

[76] K. Mundra, T. DebROY, S. S. Babu and S. A. David, “Weld metal microstructure calculations from fundamentals of transport phenomena in the arc welding of low-alloy steels,” *Weld. J.*, no. January 2016, 1997, pp. 163–171.

[77] Z. Yang and T. Debroy, “Weld metal microstructure prediction from fundamentals of transport phenomena and phase transformation theory,” *Sci. Technol. Weld. Join.*, vol. 2, no. 2, 1997, pp. 53–58.

[78] P. Lacki, K. Adamus, K. Wojsyk, M. Zawadzki and Z. Nitkiewicz, “Modeling of heat source based on parameters of electron beam welding process,” *Arch. Metall. Mater.*, vol. 56, no. 2, 2011, pp. 455–462.

[79] K. Shinozaki, “Welding and joining Fe and Ni-base superalloys,” *Weld. Int.*, vol. 15, no. 8, 2001, pp. 593–610.

[80] D. E. Michael, “Analyses of isothermal solidification kinetics during transient liquid phase bonding of silver with aluminum and copper filler metals,” University of Manitoba, 2018.

[81] V. Garg and A. Gupta, “Developing and easing the brazing method,” *Int. J. Sci. Res.*

Publ., vol. 3, no. 9, 2013, pp. 1–6.

[82] M. M. Schwartz, *Brazing*, 2nd ed. Ohio: ASM International, 2003.

[83] A. Sharma, S.H. Lee, H.O. Ban, Y.S. Shin, and J. Jung, "Effect of Various Factors on the Brazed Joint Properties in Al Brazing Technology," *J. Weld. Join.*, vol. 34, no. 2, 2016, pp. 30–35.

[84] R. K. Shiue, S. K. Wu and S.Y. Chen, "Infrared brazing of TiAl using Al-based braze alloys," *Intermetallics*, vol. 11, 2003, pp. 661–671.

[85] S. H. Nazari, "Impact of using infrared irradiation technology in food processing operations," Zanjan, 2017.

[86] Z. Y. Wu, T. Y. Yeh, and R. K. Shiue, "Infrared Heating Applied in Titanium Brazing," *Adv. Mater. Res.*, vol. 79–82, 2009, pp. 1379–138.

[87] E. E. Levi, "Brazing-heating methods," *Practical Welding Letter*, 2019. [Online]. Available: https://www.welding-advisers.com/Brazing-heating.html. [Accessed: 02-Apr-2019].

[88] UltraFlex power 2019, "Brazing," *Application Guide*, 2019. [Online]. Available: https://ultraflexpower.com/wp-content/uploads/2015/05/app-guide-brazing.pdf. [Accessed: 08-Mar-2019].

[89] V. I. Rudnev, "Joining components by induction heating - Part I," *Heat Treating Progress*, 2005. [Online]. Available: https://inductoheat.eu/wp-content/uploads/sites/15/2015/04/Joining_by_induction__part_1_Optimieren.pdf. [Accessed: 08-Mar-2019].

[90] R. Henson and G. David, "Oxyfuel brazing primer," *Practical Welding*, 2014. [Online]. Available: https://aus.harrisproductsgroup.com/~/media/Files/PDF/...

/Oxyfuel-brazing-primer.pdf. [Accessed: 08-Mar-2019].

[91] Precision Metal Industries, “Torch brazing,” *Welding and Brazing Services*, 2019. [Online]. Available: http://www.pmiquality.com/torch-brazing/. [Accessed: 08-Mar-2019].

[92] THESSCO, “Hand torch or flame brazing principles,” 2018. [Online]. Available: https://www.thesscogroup.com/wp-content/uploads/2018/02/THESSCO_handtorch v1feb2018.pdf. [Accessed: 08-Mar-2019].

[93] and A. H. K. M. M. Atabaki, H. R. M. Hosseini, “Influence of the furnace brazing process parameters on the chemical heterogeneity, mechanical and physical properties of copper-beryllium alloy joints,” in *4th International Brazing and Soldering Conference (IBSC)*, 2009.

[94] THESSCO, “Brazing principles,” 2018. [Online]. Available: https://www.thesscogroup.com/wp-content/uploads/2018/02/THESSCO_brazing principlesv1feb2018.pdf. [Accessed: 08-Mar-2019].

[95] Air Products, “Introduction to furnace brazing,” 2001. [Online]. Available: http://www.airproducts.com/~/media/downloads/white-papers/I/en-introduction-to-furnace-brazing-white-paper-330-0018.pdf?productType=Gases&productLevel1=Mixtures&productLevel2=Metals-Processing&productLevel3=Brazing-Gas-Atmospheres. [Accessed: 08-Mar-2019].

[96] Indian Institute of Technology, “Lecture 4: Design for brazing and soldering,” *Module 4: Design for Assembly*. [Online]. Available: https://nptel.ac.in/courses/112101005/downloads/Module_4_Lecture_4_final.pdf. [Accessed: 08-Mar-2019].

[97] D. Agrawal, “Microwave sintering, brazing, and melting of metallic,” in *Sohn*

International Symposium: Advanced Processing Of Metals And Materials - New, Improved And Existing Technologies: Non-Ferrous Materials Extraction And Processing, vol. 4, 2006, pp. 183–192.

[98] M. Schwartz, *Brazing for engineering technologists*, 1st ed. London: Chapman and Hall, 1995.

[99] M. Shukla, S. Ghosh, N. Dandapat, A. Kmandal, and V. K. Balla, "Microwave-assisted brazing of alumina ceramics for electron tube applications," *Bull. Mater. Sci.*, vol. 39, no. 2, 2016, pp. 587–591.

[100] United States Navy, "Soldering, brazing, braze welding, wearfacing," in *Steelworker, NAVEDTRA 14250,* 1st ed., vol. 1, USA: Naval Education And Training Professional Development and Technology Center, 1996, pp. 1–42.

[101] A. M. Nasiri, L. Li, S. H. Kim, Y. Zhou, D. C. Weckman, and T. C. Nguyen, "Microstructure and properties of laser brazed magnesium to coated steel," *Weld. J.*, vol. 90, 2011, pp. 211–219.

[102] S. Ernst, "Studies of laser brazing with regard to the quality influencing parameters," Loughborough University, 2015.

[103] M.F. Arenas, V.L. Acoff and R.G. Reddy, "Physical properties of selected brazing filler metals," *Sci. Technol. Weld. Join.*, vol. 9, no. 4, 2004, pp. 423–429.

[104] Y. Baskin, "How to select a brazing flux," *Superior Flux and MFG. Co. Publications*, 1992. [Online]. Available: http://www.superiorflux.com/papers/How_to_Select_a_ Brazing_Flux.pdf. [Accessed: 08-Mar-2019].

[105] R. Andersson, T. Holm, S. Wiberg, and A. Åstrom, "Furnace atmospheres," *Linde Gas Publication*, 2019. [Online]. Available: https://www.ferronova.com/International/Web

/LG/FER/likelgfer.nsf/repositorybyalias/lit_brazmet/$file/Furnace_Atmospheres_No_4_Brazing_of_Metals.pdf. [Accessed: 11-Mar-2019].

[106] H. Lee, J. Yoon, and Y. Yi, "Solid state diffusion bonding of titanium alloys," *Solid State Phenom.*, vol. 124–126, 2007, pp. 1429–1432.

[107] R. Rusnaldy, "Diffusion bonding: An advanced of material process," *ROTASI*, vol. 3, no. 1, 2001, pp. 23–27.

[108] J. Wolters, "The ancient craft of granulation," *Gold Bull*, vol. 14, no. 3, 1981, pp. 119–129.

[109] W. D. MacDonald and T. W. Eagar, "Transient liquid phase bonding," *Annu. Rev. Mater. Sci.*, vol. 22, 1992, pp. 23–46.

[110] W. F. Gale and D. A. Butt, "Transient liquid phase bonding," *Sci. Technol. Weld. Join.*, vol. 9, no. 4, 2004, pp. 283–300.

[111] W.D. Macdonald, and T.W. Eagar, "Transient liquid phase bonding processes," in *The Metal Science of Joining*, 1992, pp. 93–100.

[112] G. O. Cook and C. D. Sorensen, "Overview of the transient liquid phase and partial transient liquid phase bonding," *J. Mater Sci*, vol. 46, 2011, pp. 5305–5323.

[113] D.H. Jung, A. Sharma, M. Mayer, and J.P. Jung, "A review on recent advances in the transient liquid phase (TLP) bonding for thermoelectric power module," *Rev. Adv. Mater. Sci.*, vol. 53, 2018, pp. 147–160.

[114] M. A. Arafin, M. Medraj, D.P. Turner and P. Bocher, "Optimization of process variables during TLP bonding of nickel," in *45th Annual Conference of Metallurgists of CIM*, 2006, pp. 301–313.

[115] N. Sheng, J. Liu, T. Jin, X. Sun, and Z. Hu, “Isothermal solidification stage during transient liquid-phase bonding single-crystal superalloys,” *Philos. Mag.*, vol. 94, no. 11, 2014, pp. 1219–1234.

[116] S. C. Barman, T. K. Pal, and J. Maity, “Kinetics of transient liquid phase diffusion bonding process for joining aluminum metal matrix composite,” *Mater. Sci. Technol.*, vol. 27, no. 5, 2011, pp. 951–957.

[117] I. Tuah-poku, M. Dollar, and T. B. Massalski, “A Study of the transient liquid phase bonding process applied to an Ag/Cu/Ag sandwich joint,” *Metall. Trans.*, vol. 19, no. A, 1988, pp. 675–686.

[118] O. A. Olatunji, “Transient liquid phase bonding of dissimilar single crystal superalloys,” University of Manitoba, 2016.

[119] E. Norouzi, M. Atapour, M. Shamanian, and A. Allafchian, “Effect of bonding temperature on the microstructure and mechanical properties of Ti-6Al-4V to AISI 304 transient liquid phase bonded joint,” *Mater. Des.*, vol. 99, 2016, pp. 543–551, 2016.

[120] M.A. Arafin, M. Medraj, D.P. Turner, and P. Bocher, “Transient liquid phase bonding of Inconel 718 and Inconel 625 with BNi-2 : Modeling and experimental investigations,” *Mater. Sci. Eng. A*, 2007, pp. 125–133.

[121] V. Jalilvand, H. Omidvar, M.R. Rahimipour, and H.R. Shakeri, “Influence of bonding variables on transient liquid phase bonding behavior of nickel-based superalloy IN-738LC,” *Mater. Des.*, vol. 52, 2013, pp. 36–46.

[122] M. Walker, “Effect of pre-oxidation and thermal exposure on the microstructure of superalloys and thermal barrier coating systems,” Carleton University, 2016.

[123] Jonathan Durocher, “Thermo-Mechanical Fatigue Of Polycrystalline, Directionally

Solidified and Single Crystal Nickel Base Superalloys Repaired By Laser Beam Welding," University of Manitoba, 2013.

[124] A. Basak and S. Das, "An investigation of the Dendritic Segregation in SC Rene-N5 fabricated Through Scanning Laser Epitaxy," in *Proceedings of the 27th Annual International Solid Freeform Fabrication Symposium – An Additive Manufacturing Conference*, 2016, pp. 487–498.

[125] X. D. Yue, J. R. Li, and X. G. Wang, "The microstructure of a single crystal superalloy after different aging heat treatments," *Rare Met.*, vol. 37, no. 3, 2018, pp. 210–216.

[126] O. A. Ojo and M. C. Chaturvedi, "Liquation microfissuring in the weld heat-affected zone of an overaged precipitation-hardened nickel-base superalloy," *Metall. Mater. Trans. A Phys. Metall. Mater. Sci.*, vol. 38, no. 2, 2007, pp. 356–369.

[127] F. Masoumi, D. Shahriari, M. Jahazi, J. Cormier, and A. Devaux, "Kinetics and Mechanisms of γ′ Reprecipitation in a Ni-based Superalloy," *Sci. Rep.*, vol. 6, 2016, pp. 1–16.

[128] W.D. Ham, "Nickel-based superalloy operating temperature determination via analysis of gamma/gamma prime microstructure and coating/base material interdiffusion," Massachusetts Institute of Technology, 2005.

[129] H. D. M. Smart, "A Study of Directionally Solidified Rene 80 Subjected to Short-term Overtemperature," University of Manitoba, 2017.

[130] S.K. Tung, L.C. Lim, and M.O. Lai, "Microstructural evolution and control in BNi-4 brazed joints of nickel 270," *Scr. Metall. Mater.*, vol. 33, no. 8, 1995, pp. 1253–1259.

[131] K. Ohsasa, T. Shinmura, and T. Narita, "Numerical modeling of the transient liquid phase bonding process of ni using Ni-B-Cr ternary filler metal," *J. Phase Equilibria,*

vol. 20, no. 3, 1999, pp. 199–206.

[132] O.A. Ojo, N.L. Richards and M.C. Chaturvedi, “Isothermal solidification during transient liquid phase bonding of Inconel 738 superalloy,” *Sci. Technol. Weld. Join.*, vol. 9, no. 6, 2013, pp. 531–540.

[133] J. Ramirez and S. Liu, “Diffusion brazing in the nickel-boron system,” *Weld. J. WRS*, no. October, 1992, pp. 365–376.

[134] Y. Zhou, “Analytical modeling of isothermal solidification during transient liquid phase (TLP) bonding,” *J. Mater. Sci. Lett.*, vol. 20, 2001, pp. 841–844.

[135] A. Ghanbar, D. E. Michael, and O. A. Ojo, “Influence of variable diffusion coefficient on solid-liquid interface migration kinetics during transient liquid phase bonding,” *Philos. Mag.*, vol. 0, no. 0, 2019, pp. 1–16.

[136] A. Ghoneim, “Experimental and theoretical studies of transient liquid phase bonding of nickel-based materials,” University of Manitoba, 2008.

[137] C. W. Sinclair, G. R. Purdy, and J. E. Morral, “Transient liquid-phase bonding in two-phase ternary systems,” *Metall. Mater. Trans. A*, vol. 31, no. 4, 2008, pp. 1187–1192.

[138] J. F. Li, P. A. Agyakwa, and C. M. Johnson, “Kinetics of Ag3Sn growth in Ag-Sn-Ag system during transient liquid phase soldering process,” *Acta Mater.*, vol. 58, no. 9, 2010, pp. 3429–3443.

[139] O. A. Ojo, N. L. Richards, M. C. Chaturvedi, O. A. Ojo, N. L. Richards, and M. C. Chaturvedi, “Isothermal solidification during transient liquid phase bonding of Inconel 738 superalloy Isothermal solidification during transient liquid phase bonding of Inconel 738 superalloy,” vol. 1718, 2013.

[140] A. Ghanbar, “Numerical Simulation of Transient Liquid Phase Bonding with Variable

Diffusion Coefficient in Planar , Cylindrical and Spherical Systems," University of Manitoba, 2019.

[141] O. A. Ojo, A. Ghoneim, and J. Hunedy, "Transient liquid phase bonding of single crystal Ni3 Al-based intermetallic alloy eutectic microconstituents," no. April, 2012, pp. 1–6.

[142] A. Ghoneim, J. Hunedy, and O. A. Ojo, "An interface-enriched extended finite element-level set simulation of solutal melting of additive powder particles during transient liquid phase bonding," *Metall. Mater. Trans. A*, vol. 44, no. 2, 2013, pp. 1139–1151.

APPENDIX

ALGORITHM TO CALCULATE "K" NUMERICALLY

```
function [D,K,Q,Wmax] = Activation_function(T,S,W0,CF)
%UNTITLED15 Summary of this function goes here
%   Detailed explanation goes here
D0=0.0144;

 R=8.314/1000;
S1=S*(1/3600).^.5; %to convert from the square root of hours to seconds
S2=S1*10.^-6; %to convert from micron meters to meters
Tem=(T*9/5) + 32 ;% to convert from fari to celsius

C0=0;  % initial concentration in the base metal
 [ConL,ConS] = SolidusLiquidus(Tem);
syms K
E1=K*(1+erf(K))*sqrt(pi)/(exp(-K.^2))==(ConS-C0)/(ConL-ConS);
K=solve(E1,K) ;  %value of k

D=(S2/(2*K)).^2;  % diffusion coefficient m^2/sec

Q=R*(T+273)*(log(D0)-log(D));  % kj/mol/k

Wmax=2*W0*(CF/ConL);
End
```

ALGORITHM TO CALCULATE ACTIVATION ENERGY

```
clc

clear all


T=[1093 1120 1150 1180 1200]  % in celsius

S=[21.429 28.929 22.689 17.860 15.808] %slope in micro meters per square-root hour


CF=3.5  % initial conc. in filler

W0=200  % initial joint width

D0=0.0144; % m^2/s

R=8.314/1000; % kJ/K-mol


for i=1:length(T)


   [D(i),K(i),Q(i),Wmax(i)] = Activation_function(T(i),S(i),W0,CF);


end


Qaverage=mean(Q)


for i=1:length(T)


   Dsolved(i) = D0*exp(-Qaverage/(R*(273+T(i))));

   SlopeSolved(i)=2*K(i)*sqrt(Dsolved(i))/(1/3600).^.5/10.^-6;

end
```

```
 clc
 display('T S D K Q Wmax Dsolved SlopeSolved')
Values=vpa([T' S' D' K' Q' Wmax'  Dsolved' SlopeSolved'],6)

display('Average Q')
Qaverage=mean(Values(:,5))

figure(1), clf
plot(T,D,'r-*')
title('Diffusion Coefficient vs Temperature')
xlabel('Temperature (Celsius)')
ylabel('Diffusion Coefficient (m^2/s)')

figure(2), clf
plot(T,Q,'r-*')
title('Activation Energy vs Temperature')
xlabel('Temperature (Celsius)')
ylabel('Activation Energy (KJ/mol/K)')

Tx=T+273;
figure(3), clf
plot(Tx.^-1,log(D),'r-*')
title('Arrhenius plot')
xlabel('1/T (1/Kelvin)')
ylabel('ln(D)')
```

T S D K Q Wmax Dsolved SlopeSolved

Values =

[1093.0, 21.429, 1.98634e-11, 0.0400676, 231.700, 365.171, 8.14550e-12, 13.7225]

[1120.0, 28.929, 3.80942e-11, 0.0390591, 228.738, 371.793, 1.23072e-11, 16.4431]

[1150.0, 22.689, 2.31765e-11, 0.0392745, 239.543, 385.697, 1.91133e-11, 20.6044]

[1180.0, 17.860, 1.34050e-11, 0.0406506, 251.207, 406.040, 2.91487e-11, 26.3365]

[1200.0, 15.808, 1.02683e-11, 0.0411100, 257.929, 423.045, 3.82525e-11, 30.5111]